QUANTIFYING STANDING DEAD TREE VOLUME AND STRUCTURAL LOSS WITH VOXELIZED TERRESTRIAL LIDAR DATA

A Thesis

by

ERIC BRYAN PUTMAN

Submitted to the Office of Graduate and Professional Studies of
Texas A&M University
in partial fulfillment of the requirements for the degree of

MASTER OF SCIENCE

Chair of Committee,	Sorin Popescu
Committee Members,	Marian Eriksson
	Anthony Filippi
Head of Department,	Kathleen Kavanagh

August 2017

Major Subject: Ecosystem Science and Management

Copyright 2017 Eric Bryan Putman

ABSTRACT

Standing dead trees (SDTs) are an important forest component and impact a variety of ecosystem processes, yet the carbon pool dynamics of SDTs are poorly constrained in terrestrial carbon cycling models. The ability to model wood decay and carbon cycling in relation to detectable changes in tree structure and volume over time would greatly improve such models. The overall objective of this study was to provide automated aboveground volume estimates of SDTs and automated procedures to detect, quantify, and characterize structural losses over time with terrestrial lidar data. The specific objectives of this study were: 1) develop an automated SDT volume estimation algorithm providing accurate volume estimates for trees scanned in dense forests; 2) develop an automated change detection methodology to accurately detect and quantify SDT structural loss between subsequent terrestrial lidar observations; and 3) characterize the structural loss rates of pine and oak SDTs in southeastern Texas.

A voxel-based volume estimation algorithm, "TreeVolX", was developed and incorporates several methods designed to robustly process point clouds of varying quality levels. The algorithm operates on horizontal voxel slices by segmenting the slice into distinct branch or stem sections then applying an adaptive contour interpolation and interior filling process to create solid reconstructed tree models (RTMs). TreeVolX estimated large and small branch volume with an RMSE of 7.3% and 13.8%, respectively. A voxel-based change detection methodology was developed to accurately detect and quantify structural losses and incorporated several methods to mitigate the

challenges presented by shifting tree and branch positions as SDT decay progresses. The volume and structural loss of 29 SDTs, composed of *Pinus taeda* and *Quercus stellata*, were successfully estimated using multitemporal terrestrial lidar observations over elapsed times ranging from 71 – 753 days. Pine and oak structural loss rates were characterized by estimating the amount of volumetric loss occurring in 20 equal-interval height bins of each SDT. Results showed that large pine snags exhibited more rapid structural loss in comparison to medium-sized oak snags in this study.

ACKNOWLEDGEMENTS

I would like to thank my committee chair, Dr. Sorin Popescu, for his feedback, support, advice, and expertise throughout my time at Texas A&M University. I would also like to thank my committee members, Dr. Marian Eriksson and Dr. Anthony Filippi, for their feedback and support. I owe a debt of gratitude to Dr. Eriksson for piquing my interest in programming as an undergraduate student.

I would like to thank Ryan Sheridan, Nian-We Ku, Tan Zhou, and Paul Klockow for their assistance while collecting data as well as their friendship. Also, I would like to thank everyone in the LASERs lab and the department of Ecosystem Science and Management for their support and encouragement.

Finally, thanks to my mother, brother, and girlfriend for their continued love, support, and patience.

CONTRIBUTORS AND FUNDING SOURCES

Contributors

This work was supervised by a thesis committee consisting of Professor Sorin Popescu and Professor Marian Eriksson of the Department of Ecosystem Science and Management and Professor Anthony Filippi of Geography.

All work for the thesis was completed independently by the student.

Funding Sources

Graduate study was supported by a fellowship from Texas A&M University.

This work was made possible in part by the National Aeronautics and Space Administration Rapid Response and Novel Research in Earth Science program under Grant Number NNX14AN99G.

Its contents are solely the responsibility of the authors and do not necessarily represent the official views of the National Aeronautics and Space Administration.

NOMENCLATURE

ALS	Airborne laser scanning
C	Carbon
DBH	Diameter at breast height
DRF	Density reduction factor
GNSS	Global navigation satellite system
ICP	Iterative closest point
Lidar	Light detection and ranging
RTM	Reconstructed tree model
SDT	Standing dead tree
SLA	Structural loss adjustment
Slice	Horizontal cross section of one-voxel thickness
TLS	Terrestrial laser scanning
UTM	Universal Transverse Mercator
Voxel	Volumetric element
VPCR	Vertical point cloud resampling

TABLE OF CONTENTS

Page

LIST OF FIGURES

Page

LIST OF TABLES

Page

1. INTRODUCTION AND LITERATURE REVIEW

Standing dead trees (SDTs) are an integral component of forest ecosystems and impact a variety of processes of interest to forest managers and researchers, such as forest carbon stores, carbon cycling dynamics as aboveground woody debris transitions to atmospheric and soil C pools, nutrient cycling, species composition dynamics, fuel loading with respect to wildland fires, wildlife habitat, and structural diversity of forest stands (Russell et al., 2015). Generally, nondestructive individual tree volume estimates are derived via measurement of tree parameters (e.g., diameter at breast height (DBH) and tree height) which are then used as predictors in empirically-derived, species-specific allometric equations (Brown et al., 1989).

Current SDT aboveground volume estimates employed by the United States Forest Service (USFS) Forest Inventory and Analysis (FIA) program characterize only the volume, and thus carbon, of a tree's main stem in the case of timber species (i.e., from a one foot stump to a top diameter of four inches or the point where all limbs are smaller than a 4" diameter) or the stem, bark, and large branches in the case of woodland species (Woudenberg et al., 2010). These estimates are not derived from direct volume measurements, but from standard FIA field measurements which are input to the same allometric equations used on live trees to arrive at an aboveground volume estimate (Domke et al., 2011). Due to their focus on the tree's bole, these estimates neglect to characterize the volume of a SDT's entire stem and branches, especially when stem breakage and branch drop cannot be accurately accounted for. Recent studies have proposed methodologies which incorporate structural loss adjustments (SLAs) and

density reduction factors (DRFs) to account for the inherent morphological differences of SDTs vs. their live counterparts (Domke et al., 2011). These adaptations have resulted in more accurate estimates of SDT volume and carbon, yet are still based on allometric equations and qualitative decay class assignments, which may limit their overall accuracy in comparison to quantitative remote sensing-based methodologies. Currently, these SLAs and DRFs have yet to be developed and evaluated for a wide range of species and regions, leaving more generalized estimates as the pragmatic approach in most situations.

As observed density reductions fail to completely account for the total amount of biomass lost during the decay process (Fraver et al., 2013; Harmon et al., 1987; Næsset, 1999; Zell et al., 2009), it is important for studies to quantify and incorporate structural losses when modelling the decay rates of SDTs. Laiho and Prescott (2004) reviewed 34 wood decomposition studies and found that only five had considered mass loss as a component of decay, while the remaining studies were based on observed density reductions.

The extent to which decay rates, estimated by reductions in wood density over time, affect the structural loss rates of SDTs is not clearly defined. A number of studies have observed the longevity of standing dead trees or modelled their transition through qualitative decay classes in different regions (Aakala et al., 2008; Cain, 1996; Cline et al., 1980; Conner and Saenz, 2005; Corace et al., 2010; Garber et al., 2005; Landram et al., 2002; Vanderwel et al., 2006), but these approaches often are focused on stand-level observations and not able to quantify the different ways in which SDTs lose volume and

mass over time (i.e., fragmentation or structural loss vs. collapse), which could provide valuable contributions towards understanding the flux of woody debris from standing pools to downed pools among various species and regions. In a review of research concerning the decomposition and carbon storage of dead wood in various forms, Russell et al. (2015) conducted a sensitivity analysis and found that structural reductions had the greatest relative influence on the C content of standing dead trees, 59.1%, while wood density had a relative influence of 19.8%. This finding emphasizes the need for accurate volume estimations of SDTs, the increased development of SLAs for additional species and regions, and the development of methodologies which can precisely quantify structural losses of SDTs over time.

Light detection and ranging (lidar) is an active remote sensing system which utilizes laser pulses to precisely measure the distance from the lidar sensor to an object by measuring the elapsed time between the transmission and return, at the sensor's receiver, of a laser pulse which has been reflected off an object (Lefsky et al., 2002). The elapsed time measurement may be multiplied by the speed of light through air to obtain the total distance travelled by the laser pulse and subsequently divided by two to determine the distance from the lidar sensor to the object which reflected the pulse (Shan and Toth, 2008). Lidar sensors are broadly categorized into two groups with respect to how the sensor records returned signals: discrete return systems identify significant amplitude peaks in the returned pulse which correspond to the energy reflected by physical objects and are thus recorded as individual points; while full waveform systems characterize the entire duration of the laser pulse by recording the amplitude of the

received pulse as it varies with time, thus digitizing and recording the entire reflected waveform (Lefsky et al., 2002).

Modern lidar sensors are typically of the "scanning" variety, meaning they utilize rotating or oscillating mirrors, fiber optics, or rotating sensor heads to collect data in the across-track direction and may emit thousands of laser pulses per second, resulting in dense data sets which provide a detailed, three-dimensional characterization of an area (Wehr and Lohr, 1999). Lidar sensors are deployed on an assortment of platforms to meet a variety of research objectives at a broad range of spatial and temporal scales, each with unique acquisition challenges. Common lidar platforms include spaceborne (e.g., satellites), airborne (e.g., manned aircraft, unmanned aerial vehicles), terrestrial (e.g., mounted on a stationary tripod), and mobile platforms (e.g., handheld sensors, ground-based vehicles) (Van Leeuwen and Nieuwenhuis, 2010).

In the context of forestry studies, airborne laser scanning (ALS) has been used to estimate biomass or volume (Anderson et al., 2008; Drake et al., 2002; Hudak et al., 2012; Lefsky et al., 2005; Popescu et al., 2003; Sheridan et al., 2014) as has spaceborne lidar (Guo et al., 2010; Lefsky et al., 2005; Simard et al., 2011), but spaceborne systems are better-suited for regional or global estimates, respectively, and lack the precision required to reliably provide accurate individual tree estimates and change detection capabilities. While ALS can effectively characterize a forest canopy and has been used to observe individual trees (Hyyppä et al., 2001; Popescu, 2007), terrestrial laser scanning (TLS) has the potential to provide significantly more detailed observations at the individual tree level. Collecting data from a terrestrial vantage point, TLS has

several advantages over ALS when considering objectives at the individual tree level: (1) the ability to characterize intermediate, suppressed, and understory trees which would often be subjected to significant occlusion from dominant and codominant trees with ALS; (2) the ability to more-completely capture the complex morphological characteristics of the entire tree (e.g., fine branches, stem sections) which would not be apparent from the aerial perspective of ALS; (3) higher point density and reduced point spacing in comparison to ALS; and (4) collection procedures which are more conducive to repeated observations at desired temporal intervals. The general limitations of TLS in forest systems include: (1) occlusion (i.e., shadowing) caused by nearby vegetation or branches on the tree of interest; (2) fewer dedicated software packages and established methodologies for analyzing TLS data, particularly at the individual tree level; (3) potentially time-consuming data collection procedures; and (4) noise points caused by tree movement due to wind during scanning operations.

TLS has been used to estimate tree volume at both the plot level and individual tree level. Aboveground biomass is commonly estimated as well, which is closely related to carbon content in that 50% of a tree's biomass is commonly attributed to carbon (Penman et al., 2003), as is aboveground volume with the use of species-specific wood density estimates. One approach to estimating tree volume or biomass with TLS consists of scanning trees at the plot or individual tree level, extracting metrics (e.g., height percentiles, point densities, skewness) or measurements (e.g., DBH, tree height, crown area) from the resultant point clouds which serve as a proxy for traditional field measurements, and subsequently using these measurements as inputs to allometric

equations (or regression models based on allometric equations) to estimate volume or biomass (Hopkinson et al., 2004; Ku et al., 2012; Tansey et al., 2009; Yao et al., 2011). While these studies have shown that TLS-derived metrics and tree measurements can work reliably with allometric equations, the reliance on allometric equations for volume estimates, biomass estimates, or accuracy assessments neglects to characterize the variation present in trees with the same morphological parameters (e.g., DBH or height), particularly with respect to SDTs (Hosoi et al., 2013).

TLS-derived volume estimates through 3D reconstruction of individual trees provide a nondestructive methodology which functions without the need for allometric equations, structural loss adjustments, or detailed field measurements. Individual tree 3D reconstructions, with the objective of estimating a tree's total volume, may be broadly categorized into two, sometimes used in tandem, approaches: (1) fitting geometric primitives (e.g., cylinders, cones) to tree components; and (2) converting point clouds to voxels and creating voxel-based tree models. Côté et al. (2009) created approximated individual tree reconstructions of live trees, including foliage, by utilizing geometric primitives derived from tree skeletons and estimated convex hull volume with a mean root mean square error (RMSE) of 14.83%. Delagrange and Rochon (2011) estimated the crown volume of a single hybrid poplar sapling using tree skeletons and fitted cylinders, resulting in a volume estimate deviation of 14.5% from a reference volume estimated by treating each point in their point cloud as a 1 cm^3 voxel and summing their aggregate volumes. The use of the point cloud data, which was used to

generate the tree model, to estimate a reference volume leads to uncertainty with regards to the validity of the accuracy assessment.

Dassot et al. (2012) in a semi-automated procedure, used tree skeletons and fitted cylinders to estimate solid wood (i.e., branches or stems greater than 7 cm in diameter) volume for a variety of tree species, in leaf-off conditions, at the individual tree level. The authors estimated solid wood volume of main stems within 10% relative difference for 40/42 trees and total branch volume from 10% - 30% for 15/36 and 31/36 trees, respectively; and estimated the total solid wood volume within 10% relative difference for 40/42 trees. It should be noted that, in contrast to the two aforementioned studies, the authors used destructive sampling (i.e., felled the individual trees and used diameter measurements and taper equations to estimate the volume of stem and branch sections), resulting in a presumably more reliable accuracy assessment. Kaasalainen et al. (2014) used a methodology referred to as quantitative structure modeling (QSM) (Raumonen et al., 2013) which utilizes fitted circular cylinders applied to a point cloud in accordance with the morphological rules of tree structure (e.g., smaller branches attaching to larger branches, which are attached to the stem) to estimate the total volume of a large aspen branch, approximately 2 m in length, with multiple sub-branches. Using the QSM methodology, the authors estimated the branch's volume within approximately 12% of reference volumes which were calculated by weighing branch sections and calculating their density via water displacement.

Hackenberg et al. (2014) utilized a sphere-cutting routine to extract point clouds corresponding to cross sectional areas of stems and branches, which were fitted with

cylinders and then refined to produce a final model consisting of many connected cylinders. This method was assessed to have coverage values (i.e., the percentage of points within 3 cm of a cylinder in the final model) of approximately 99% when applied to two high quality point clouds and 84.45% when applied to 26 lower quality point clouds, all of which were scanned in an agroforestry system. Testing volume estimation accuracy on 14 branches, each consisting of multiple small and fine branches, the method had an RMSE of approximately 0.123 L.

Lefsky and McHale (2008), in one of the earliest studies to quantify wood volume with TLS voxels, utilized cylinders fitted to voxelized TLS data to estimate the volume of the main stem and large branches of individual trees in leaf-on condition. The authors used cubic voxels ranging in size from less than 3.1 cm to 20 cm, based on limitations of available computer memory with respect to the number of points present in the original TLS point clouds. As the authors did not model fine branches or compare their results to reference volume measurements, an accuracy assessment of their methodology is unavailable. Moskal and Zheng (2011) scanned individual trees, in leaf-on condition, from a single location with TLS and used voxels to estimate total aboveground volume by multiplying the total number of points in the original TLS point cloud by the volume of an individual voxel and adding a "volume adjustment" factor, derived from an estimate of the main stem's volume via the tree's DBH and height as measured in the TLS point cloud. The authors found their methodology to account for an average of 18% of an individual tree's volume and attributed the low accuracy to occlusion effects caused by the use of a single scan position during data collection,

suggesting that multiple scan positions or alternative processing methods designed to compensate for point cloud occlusion may be necessary to increase the accuracy of volume estimates in future studies.

Vonderach et al. (2012) used TLS to scan nine deciduous trees in leaf-off conditions and reconstruct the trees with 1 cm voxels to estimate the total volume of each tree. Each tree was scanned from three to five positions and filtering was conducted to remove spatially isolated voxels from the initial model. To fill interior sections of the stem and branches, horizontal layers of one voxel-thickness were processed by traversing each layer in four orthogonal directions, with respect to each voxel in the layer. Voxels which were counted four times during this process were considered to be interior voxels and thus added to the tree's voxel model. This interior filling process sometimes resulted in erroneously filled voxels, appearing between branch segments, which were then removed with a region growing algorithm implemented to segment individual branches from inadvertently filled voxels. The volume of each layer was calculated by averaging the area of the branches with and without the original surface voxels and multiplying this resultant area by the voxel height to determine the volume of that particular layer. The volume of each layer was then summed and a filtering process was carried out to remove sparsely populated voxels (i.e., voxels containing a small number of points) from the final model. The authors felled and weighed the nine trees, taking samples at a range of heights to arrive at a total reference volume; resulting in accuracies ranging from -5.1% to +14.3% for their final volume estimates.

Hosoi et al. (2013) used TLS to scan a Japanese zelkova (*Zelkova serrata*) tree in leaf-off conditions from six positions and performed a complete tree reconstruction using 0.5 cm voxels to estimate the tree's total volume. The authors presented an automated algorithm which converts the point cloud to voxels and processes horizontal layers of one voxel-thickness to create the model. Large branches and stem sections were first distinguished from small branches, under the premise that small branches would not require the contour and filling processing necessitated by the larger branches and stem. In each horizontal layer, an implementation of Moore's neighbor-tracing algorithm was used to segment voxels into discrete branches which were then processed with linear interpolation to form a closed contour model of each branch segment. The segments were then filled (i.e., voxels in the interior of the stem/branch were added to the model) by scanning the segment in the positive X and Y directions, such that voxels which were intersected twice during the scanning were considered to be interior voxels. Once each horizontal layer had been processed, the stem and large branches which had been filled were merged with the small branches, which were not filled, to form a completed reconstruction of the tree. The Hosoi et al. (2013) algorithm estimated small branch (diameter $\leq$ 1 cm) accuracy with a mean average percentage error (MAPE) of 34% and large branch and stem volume with a MAPE of 6.8%, determined by averaging the percentage errors of volume estimates, compared to direct volume measurements taken with clay molds of the target tree, among 0.3 meter height intervals along the main stem and a portion of the tree's large and small branches.

Bienert et al. (2014) scanned 13 young Norway maple (*Acer platanoides*) trees, in leaf-off conditions, from four positions each using TLS to estimate the total wood volume of each tree. The authors used an algorithm similar to that presented in Hosoi et al. (2013), but used axis-parallel bounding boxes, based on point distribution within voxels, to characterize the contour of large branch and stem sections to avoid volume overestimates. The authors felled the thirteen trees and measured their volume by cutting the trees into small segments and weighing the amount of water displaced by each individual tree, which is considered to be the most accurate method of measuring a tree's volume; resulting in an absolute error of 6.8% and an RMSE of 18.5% when comparing the summed reference volume to the estimated volume of the entire dataset of 13 trees. Small and fine branches, when considered separately from the trunk of each tree, were estimated with percentage errors ranging from -80.2% - 70.1%.

Despite the increasing interest in, and successful examples of, reconstructive tree modelling, the use of TLS to perform change detection analysis on individual trees, and structural loss in particular, has not been thoroughly tested in the literature. Kaasalainen et al. (2010) used TLS to quantify the defoliation of Scots pine (*Pinus sylvestris*) and Norway spruce (*Picea abies*) trees scanned in a laboratory environment. Three point cloud parameters were derived, for each tree, to estimate measured biomass changes after needles had been manually removed from the trees: (1) the total number of point cloud returns; (2) the ratio of tree returns to total returns; and (3) the number of ground returns. These parameters were used as predictors for biomass loss in linear regression models, resulting in Pearson correlation coefficients ranging from 0.929 to 0.977. A

similar methodology was carried out in a field setting, but visual assessments were used as reference data and quantified linear relationships were not reported. While this study shows the potential of TLS to quantify biomass changes, it is unclear how well this particular methodology would work under a variety of field conditions with varying tree species and significant reductions in tree biomass, such as branch drops or stem breakage.

Srinivasan et al. (2014) used single-position scans with a TLS to estimate the biomass change of 29 loblolly pine (*Pinus taeda*) trees in a forested environment. The authors used linear regression techniques to model biomass change at the individual tree level in comparison to reference biomass changes estimated with allometric equations over a three year period. Out of several different approaches, the most accurate estimate of biomass change was based on the direct changes in two point cloud parameters between observations, volume beneath top of canopy and 90th percentile height, resulting in an R-squared of 0.50 and an RMSE of 10.09 kg. Kaasalainen et al. (2014) applied the quantitative structure modelling (QSM) methodology to detecting biomass changes in laboratory and field environments, with an accuracy of 12% in estimating the volume of a small branch following the manual removal of branch sections and an unknown accuracy in the field with regards to a estimating the volume of a single live tree over time, which was estimated to be approximately +/- 10%. These estimates were the mean results of 10 modelling runs, which typically exhibited a standard deviation of 5 – 15 % for estimated branch volume due to the stochastic nature of the algorithm. The

accuracy of this study suggests that reconstructive tree modeling has the potential to reliably quantify biomass or volume loss in forest environments.

As current SDT volume, and thus carbon, estimates are derived primarily from field-based inventory measurements input into allometric equations which only account for a SDT's main stem volume, the development of accurate TLS-based volume estimates, which do not rely on field measurements or allometric equations and characterize the entire SDT, may potentially provide a more accurate and direct means of estimating individual SDT volume and carbon in forest ecosystems. By avoiding the generalizations of allometric equations and regression modelling, the proposed methodology facilitates non-destructive, detailed volume estimations of individual trees as well as the potential to evaluate and refine existing allometric equations or the development of new allometric equations without the constraints of laborious destructive sampling typically required for field measurements. This study presents a novel voxel-based SDT volume estimation technique which is designed to be robust with respect to mitigating the common error sources encountered in point clouds collected in dense forest systems. The volume estimation methodologies proposed in this study have the potential to be applied to a variety of tree species and field conditions, making them well-suited to filling current information gaps. Such volume estimation methodologies could serve as useful components to a variety of programs such as the U. S. Environmental Protection Agency (EPA) National Greenhouse Gas Inventory (NGHGI), FIA national inventory, and similar programs around the world when combined with regional sampling of SDTs. Additionally, these methodologies could be useful to a

variety of research interests such as regional carbon flux studies, tree morphology, tree structural loss and decay dynamics, nutrient cycling, species composition dynamics, wildlife habitat, and fuel loading with respect to wildland fires.

The change detection methodology described in this study presents a novel, voxel-based TLS approach to addressing the current knowledge gaps concerning the structural loss of standing dead trees by developing automated methods to detect, quantify, and characterize volumetric losses over time using solid, voxel-based reconstructed tree models. To the best of the author's knowledge, this study represents the first attempt to characterize the fragmentation of SDTs in a forest environment with the use of multitemporal TLS observations at the individual-tree level. The presented approach may be applied to future studies and has the potential to be applied to a variety of tree species in different forest systems. In the future, this technique, or similar approaches, may be used to provide quantitative structural loss data which could facilitate the development of SLAs for a variety of species in various regions to increase the accuracy of regional volume and carbon accounting with respect to SDTs.

2. AUTOMATED ESTIMATION OF STANDING DEAD TREE VOLUME USING VOXELIZED TERRESTRIAL LIDAR DATA

2.1 Introduction

Standing dead trees (SDTs) are an integral component of forest ecosystems and impact a variety of processes of interest to forest managers and researchers, such as forest carbon stores, carbon cycling dynamics as aboveground woody debris transitions to atmospheric and soil C pools, nutrient cycling, species composition dynamics, fuel loading with respect to wildland fires, wildlife habitat, and structural diversity of forest stands (Russell et al., 2015). Generally, nondestructive individual tree volume estimates are derived via measurement of tree parameters (e.g., diameter at breast height (DBH) and tree height) which are then used as predictors in empirically-derived, species-specific allometric equations (Brown et al., 1989).

Current SDT aboveground volume estimates employed by the United States Forest Service (USFS) Forest Inventory and Analysis (FIA) program characterize only the volume, and thus carbon, of a tree's main stem in the case of timber species (i.e., from a one foot stump to a top diameter of four inches or the point where all limbs are smaller than a 4" diameter) or the stem, bark, and large branches in the case of woodland species (Woudenberg et al., 2010). These estimates are not derived from direct volume measurements, but from standard FIA field measurements which are input to the same allometric equations used on live trees to arrive at an aboveground volume estimate (Domke et al., 2011). Due to their focus on the tree's bole, these estimates neglect to characterize the volume of a SDT's entire stem and branches, especially when stem

breakage and branch drop cannot be accurately accounted for. Recent studies have proposed methodologies which incorporate structural loss adjustments (SLAs) and density reduction factors (DRFs) to account for the inherent morphological differences of SDTs vs. their live counterparts (Domke et al., 2011). These adaptations have resulted in more accurate estimates of SDT volume and carbon, yet are still based on allometric equations and qualitative decay class assignments, which may limit their overall accuracy in comparison to quantitative remote sensing-based methodologies. Currently, these SLAs and DRFs have yet to be developed and evaluated for a wide range of species and regions, leaving more generalized estimates as the pragmatic approach in most situations.

Light detection and ranging (lidar) is an active remote sensing system which utilizes laser pulses to precisely measure the distance from the lidar sensor to an object by measuring the elapsed time between the transmission and return, at the sensor's receiver, of a laser pulse which has been reflected off an object (Lefsky et al., 2002). The elapsed time measurement may be multiplied by the speed of light through air to obtain the total distance travelled by the laser pulse and subsequently divided by two to determine the distance from the lidar sensor to the object which reflected the pulse (Shan and Toth, 2008). Lidar sensors are broadly categorized into two groups with respect to how the sensor records returned signals: discrete return systems identify significant amplitude peaks in the returned pulse which correspond to the energy reflected by physical objects and are thus recorded as individual points; while full waveform systems characterize the entire duration of the laser pulse by recording the amplitude of the

received pulse as it varies with time, thus digitizing and recording the entire reflected waveform (Lefsky et al., 2002).

Modern lidar sensors are typically of the "scanning" variety, meaning they utilize rotating or oscillating mirrors, fiber optics, or rotating sensor heads to collect data in the across-track direction and may emit thousands of laser pulses per second, resulting in dense data sets which provide a detailed, three-dimensional characterization of an area (Wehr and Lohr, 1999). Lidar sensors are deployed on an assortment of platforms to meet a variety of research objectives at a broad range of spatial and temporal scales, each with unique acquisition challenges. Common lidar platforms include spaceborne (e.g., satellites), airborne (e.g., manned aircraft, unmanned aerial vehicles), terrestrial (e.g., mounted on a stationary tripod), and mobile platforms (e.g., handheld sensors, ground-based vehicles) (Van Leeuwen and Nieuwenhuis, 2010).

In the context of forestry studies, airborne laser scanning (ALS) has been used to estimate biomass or volume (Anderson et al., 2008; Drake et al., 2002; Hudak et al., 2012; Lefsky et al., 2005; Popescu et al., 2003; Sheridan et al., 2014) as has spaceborne lidar (Guo et al., 2010; Lefsky et al., 2005; Simard et al., 2011), but spaceborne systems are better-suited for regional or global estimates, respectively, and lack the precision required to reliably provide accurate individual tree estimates and change detection capabilities. While ALS can effectively characterize a forest canopy and has been used to observe individual trees (Hyyppä et al., 2001; Popescu, 2007), terrestrial laser scanning (TLS) has the potential to provide significantly more detailed observations at the individual tree level. Collecting data from a terrestrial vantage point, TLS has

several advantages over ALS when considering objectives at the individual tree level: (1) the ability to characterize intermediate, suppressed, and understory trees which would often be subjected to significant occlusion from dominant and codominant trees with ALS; (2) the ability to more-completely capture the complex morphological characteristics of the entire tree (e.g., fine branches, stem sections) which would not be apparent from the aerial perspective of ALS; (3) higher point density and reduced point spacing in comparison to ALS; and (4) collection procedures which are more conducive to repeated observations at desired temporal intervals. The general limitations of TLS in forest systems include: (1) occlusion (i.e., shadowing) caused by nearby vegetation or branches on the tree of interest; (2) fewer dedicated software packages and established methodologies for analyzing TLS data, particularly at the individual tree level; (3) potentially time-consuming data collection procedures; and (4) noise points caused by tree movement due to wind during scanning operations.

TLS has been used to estimate tree volume at both the plot level and individual tree level. Aboveground biomass is commonly estimated as well, which is closely related to carbon content in that 50% of a tree's biomass is commonly attributed to carbon (Penman et al., 2003), as is aboveground volume with the use of species-specific wood density estimates. One approach to estimating tree volume or biomass with TLS consists of scanning trees at the plot or individual tree level, extracting metrics (e.g., height percentiles, point densities, skewness) or measurements (e.g., DBH, tree height, crown area) from the resultant point clouds which serve as a proxy for traditional field measurements, and subsequently using these measurements as inputs to allometric

equations (or regression models based on allometric equations) to estimate volume or biomass (Hopkinson et al., 2004; Ku et al., 2012; Tansey et al., 2009; Yao et al., 2011). While these studies have shown that TLS-derived metrics and tree measurements can work reliably with allometric equations, the reliance on allometric equations for volume estimates, biomass estimates, or accuracy assessments neglects to characterize the variation present in trees with the same morphological parameters (e.g., DBH or height), particularly with respect to SDTs (Hosoi et al., 2013).

TLS-derived volume estimates through 3D reconstruction of individual trees provide a nondestructive methodology which functions without the need for allometric equations, structural loss adjustments, or detailed field measurements. Individual tree 3D reconstructions, with the objective of estimating a tree's total volume, may be broadly categorized into two, sometimes used in tandem, approaches: (1) fitting geometric primitives (e.g., cylinders, cones) to tree components; and (2) converting point clouds to voxels and creating voxel-based tree models. Côté et al. (2009) created approximated individual tree reconstructions of live trees, including foliage, by utilizing geometric primitives derived from tree skeletons and estimated convex hull volume with a mean root mean square error (RMSE) of 14.83%. Delagrange and Rochon (2011) estimated the crown volume of a single hybrid poplar sapling using tree skeletons and fitted cylinders, resulting in a volume estimate deviation of 14.5% from a reference volume estimated by treating each point in their point cloud as a 1 cm^3 voxel and summing their aggregate volumes. The use of the point cloud data, which was used to

generate the tree model, to estimate a reference volume leads to uncertainty with regards to the validity of the accuracy assessment.

Dassot et al. (2012) in a semi-automated procedure, used tree skeletons and fitted cylinders to estimate solid wood (i.e., branches or stems greater than 7 cm in diameter) volume for a variety of tree species, in leaf-off conditions, at the individual-tree level. The authors estimated solid wood volume of main stems within ~10% and total branch volume within ~30% for the majority of trees used in the study. It should be noted that, in contrast to the two aforementioned studies, the authors used destructive sampling (i.e., felled the individual trees and used diameter measurements and taper equations to estimate the volume of stem and branch sections), resulting in a presumably more reliable accuracy assessment. Kaasalainen et al. (2014) used a methodology referred to as quantitative structure modeling (QSM) (Raumonen et al., 2013) which utilizes fitted circular cylinders applied to a point cloud in accordance with the morphological rules of tree structure (e.g., smaller branches attaching to larger branches, which are attached to the stem) to estimate the total volume of a large aspen branch, approximately 2 m in length, with multiple sub-branches. Using the QSM methodology, the authors estimated the branch's volume within approximately 12% of reference volumes which were calculated by weighing branch sections and calculating their density via water displacement.

Hackenberg et al. (2014) utilized a sphere-cutting routine to extract point clouds corresponding to cross sectional areas of stems and branches, which were fitted with cylinders and then refined to produce a final model consisting of many connected

cylinders. This method was assessed to have coverage values (i.e., the percentage of points within 3 cm of a cylinder in the final model) of approximately 99% when applied to two high quality point clouds and 84.45% when applied to 26 lower quality point clouds, all of which were scanned in an agroforestry system. Testing volume estimation accuracy on 14 branches, each consisting of multiple small and fine branches, the method had an RMSE of approximately 0.123 L.

Lefsky and McHale (2008), in one of the earliest studies to quantify wood volume with TLS voxels, utilized cylinders fitted to voxelized TLS data to estimate the volume of the main stem and large branches of individual trees in leaf-on condition. The authors used cubic voxels ranging in size from less than 3.1 cm to 20 cm, based on limitations of available computer memory with respect to the number of points present in the original TLS point clouds. As the authors did not model fine branches or compare their results to reference volume measurements, an accuracy assessment of their methodology is unavailable. Moskal and Zheng (2011) scanned individual trees, in leaf-on condition, from a single location with TLS and used voxels to estimate total aboveground volume by multiplying the total number of points in the original TLS point cloud by the volume of an individual voxel and adding a "volume adjustment" factor, derived from an estimate of the main stem's volume via the tree's DBH and height as measured in the TLS point cloud. The authors found their methodology to account for an average of 18% of an individual tree's volume and attributed the low accuracy to occlusion effects caused by the use of a single scan position during data collection, suggesting that multiple scan positions or alternative processing methods designed to

compensate for point cloud occlusion may be necessary to increase the accuracy of volume estimates in future studies.

Vonderach et al. (2012) used TLS to scan nine deciduous trees in leaf-off conditions and reconstruct the trees with 1 cm voxels to estimate the total volume of each tree. Each tree was scanned from three to five positions and filtering was conducted to remove spatially isolated voxels from the initial model. To fill interior sections of the stem and branches, horizontal layers of one voxel-thickness were processed by traversing each layer in four orthogonal directions, with respect to each voxel in the layer. Voxels which were counted four times during this process were considered to be interior voxels and thus added to the tree's voxel model. This interior filling process sometimes resulted in erroneously filled voxels, appearing between branch segments, which were then removed with a region growing algorithm implemented to segment individual branches from inadvertently filled voxels. The volume of each layer was calculated by averaging the area of the branches with and without the original surface voxels and multiplying this resultant area by the voxel height to determine the volume of that particular layer. The volume of each layer was then summed and a filtering process was carried out to remove sparsely populated voxels (i.e., voxels containing a small number of points) from the final model. The authors felled and weighed the nine trees, taking samples at a range of heights to arrive at a total reference volume; resulting in accuracies ranging from -5.1% to +14.3% for their final volume estimates.

Hosoi et al. (2013) used TLS to scan a Japanese zelkova (*Zelkova serrata*) tree in leaf-off conditions from six positions and performed a complete tree reconstruction using 0.5 cm voxels to estimate the tree's total volume. The authors presented an automated algorithm which converts the point cloud to voxels and processes horizontal layers of one voxel-thickness to create the model. Large branches and stem sections were first distinguished from small branches, under the premise that small branches would not require the contour and filling processing necessitated by the larger branches and stem. In each horizontal layer, an implementation of Moore's neighbor-tracing algorithm was used to segment voxels into discrete branches which were then processed with linear interpolation to form a closed contour model of each branch segment. The segments were then filled (i.e., voxels in the interior of the stem/branch were added to the model) by scanning the segment in the positive X and Y directions, such that voxels which were intersected twice during the scanning were considered to be interior voxels. Once each horizontal layer had been processed, the stem and large branches which had been filled were merged with the small branches, which were not filled, to form a completed reconstruction of the tree. The Hosoi et al. (2013) algorithm estimated small branch (diameter $\leq$ 1 cm) accuracy with a mean average percentage error (MAPE) of 34% and large branch and stem volume with a MAPE of 6.8%, determined by averaging the percentage errors of volume estimates, compared to direct volume measurements taken with clay molds of the target tree, among 0.3 meter height intervals along the main stem and a portion of the tree's large and small branches.

Bienert et al. (2014) scanned 13 young Norway maple (*Acer platanoides*) trees, in leaf-off conditions, from four positions each using TLS to estimate the total wood volume of each tree. The authors used an algorithm similar to that presented in Hosoi et al. (2013), but used axis-parallel bounding boxes, based on point distribution within voxels, to characterize the contour of large branch and stem sections to avoid volume overestimates. The authors felled the thirteen trees and measured their volume by cutting the trees into small segments and weighing the amount of water displaced by each individual tree, which is considered to be the most accurate method of measuring a tree's volume; resulting in an absolute error of 6.8% and an RMSE of 18.5% when comparing the summed reference volume to the estimated volume of the entire dataset of 13 trees. Small and fine branches, when considered separately from the trunk of each tree, were estimated with percentage errors ranging from -80.2% - 70.1%.

As current SDT volume, and thus carbon, estimates are derived primarily from field-based inventory measurements input into allometric equations which only account for a SDT's main stem volume, the development of accurate TLS-based volume estimates, which do not rely on field measurements or allometric equations and characterize the entire SDT, may potentially provide a more accurate and direct means of estimating individual SDT volume and carbon in forest ecosystems. By avoiding the generalizations of allometric equations and regression modelling, the proposed methodology facilitates non-destructive, detailed volume estimations of individual trees as well as the potential to evaluate and refine existing allometric equations or the development of new allometric equations without the constraints of laborious destructive

sampling typically required for field measurements. This study presents a novel voxel-based SDT volume estimation technique which is designed to be robust with respect to mitigating the common error sources encountered in point clouds collected in dense forest systems. The methodologies proposed in this study have the potential to be applied to a variety of tree species and field conditions, making them well-suited to filling current information gaps. Such volume estimation methodologies could serve as useful components to a variety of programs such as the U. S. Environmental Protection Agency (EPA) National Greenhouse Gas Inventory (NGHGI), FIA national inventory, and similar programs around the world when combined with regional sampling of SDTs. Additionally, these methodologies could be useful to a variety of research interests such as regional carbon flux studies, tree morphology, tree structural loss and decay dynamics, nutrient cycling, species composition dynamics, wildlife habitat, and fuel loading with respect to wildland fires.

The overall objective of this study is the development of a methodology to accurately estimate the volume of standing dead trees using terrestrial lidar data. The specific objectives are:

1) The development of an automated, voxel-based volume estimation algorithm to accurately estimate the volume of SDTs when scanned with a TLS in dense forest conditions.
2) The implementation of novel, adaptive processing techniques and user-selectable algorithm parameters designed to mitigate modelling errors caused by imperfect point clouds.

2.2 Methods

2.2.1 Study Area

The study area consisted of three separate sites, each containing one scan location, all located in southeastern Texas (Figure 1). Site 1 was in Lick Creek Park, located in College Station, Texas, and is within a dense, upland post oak woodland environment. Site 2 was in a mixed pine-hardwood forest in the Sam Houston National Forest, located near Huntsville, Texas. Site 3 was located in Research Park, in College Station, Texas and consisted of manicured grasses and mostly-isolated oak trees.

2.2.2 Data

Each site was scanned with a TLS to obtain point clouds of standing dead trees for the purposes of algorithm development and testing. Each scan site was focused on a single standing dead tree, resulting in three SDTs being used for algorithm development; a post oak (*Quercus stellata*) from site 1, loblolly pine (*Pinus taeda*) from site 2, and post oak from site 3. Sites 1 and 2 were scanned with a Leica ScanStation 2 and site 3 was scanned with a FARO Focus^{3D} X 330. The FARO TLS was acquired during the course of the study and, as an example of a newer generation of TLS, enabled scans to be conducted at a higher resolution from additional scanning positions while reducing the total amount of time spent conducting scanning operations.

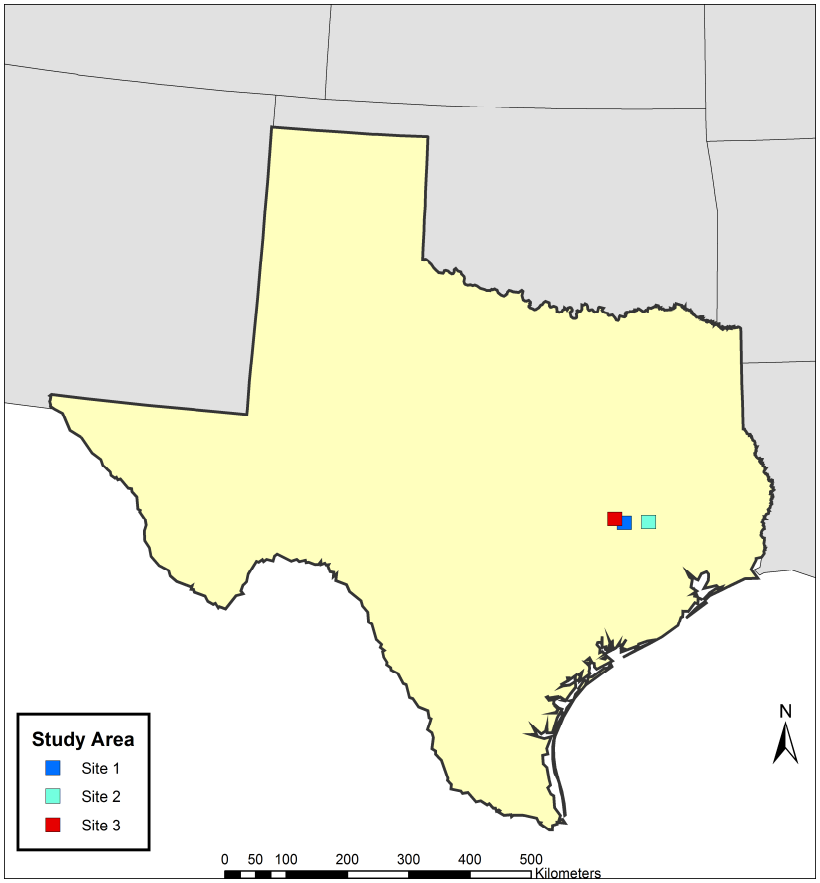

Figure 1: Study sites in southeastern Texas.

2.2.2.1 Leica TLS

The Leica ScanStation 2 is a high density, discrete return, 3D TLS utilizing a green laser, at a wavelength of 532 nm, with a 50 kHz scan rate (Figure 2). The ScanStation 2 has a single scanning mirror and a direct-drive rotating turret, enabling a vertical and horizontal field of view of 270° and 360°, respectively, a laser spot size of approximately 4 mm within a 50 m range, and a mean position and distance accuracy of ±6 mm and ±4mm, respectively (Leica Geosystems, 2006). The scanner was mounted

on an aluminum tripod and precision-levelled with Cyclone 9.0 (Leica Geosystems, 2012), the software package ran in the field on a laptop computer to operate the ScanStation 2, ensuring accurate recorded measurements regardless of the scan location's topography and relative orientation of the TLS.

Figure 2: Leica ScanStation 2 terrestrial laser scanner and flat scanning target at site 1.

The post oak SDT at site 1 (from here on referred to as SDT1) was scanned from four positions, located at approximately 90^{o} intervals with respect to the center of the tree with a vertical and horizontal resolution of 3 cm, at a range of 50 m, and scanned from an average distance of approximately 3 m. The loblolly pine SDT at site 2 (from here on referred to as SDT2) was scanned from two positions, located at approximately 180^{o} intervals with respect to the center of the tree with a horizontal and vertical

resolution of 10 cm, at a range of 50 m, with an average scanner distance of approximately 7 m. Exact scanner placement was determined in an attempt to maximize coverage of the target trees and minimize occlusion due to understory vegetation. Two Leica High Definition Survey targets, with their locations measured using a Trimble GeoExplorer 6000 handheld GNSS unit with a Trimble Zephyr Model 2 antenna (Trimble, 2010), were used to coregister and georeference SDT1 and SDT2 with differentially corrected target positions.

2.2.2.2 FARO TLS

The FARO Focus^{3D} X 330 is a high density, phase-based, 3D TLS utilizing a near-infrared laser, at a wavelength of 1550 nm, with a maximum scan rate of 976 kHz (Figure 3). The Focus^{3D} X 330 has a single scanning mirror and rotating turret, enabling a vertical and horizontal field of view of 300^{o} and 360^{o}, respectively, and a beam diameter, at exit, of 2.25 mm, with a mean distance accuracy of ±2 mm (FARO, 2013). The scanner was mounted on a carbon fiber tripod and levelled using the Focus^{3D} X 330's onboard inclinometer.

The post oak SDT at site 3 (from here on referred to as SDT3) was scanned from four positions, located at approximately 90^{o} intervals with respect to the center of the tree with a scan resolution of 3.068 mm (i.e., ½ resolution as defined by FARO system settings), at a range of 10 m, with an average scanner distance of approximately 3 m and a quality setting of 2X. SDT3 was spatially isolated in an area consisting primarily of manicured grass, resulting in minimal occlusion.

Figure 3: FARO Focus^{3D} X 330 terrestrial laser scanner and spherical scanning targets at site 3.

Five spherical laser scanning targets, with the location of each target being measured with a Trimble GeoExplorer 6000 handheld GNSS unit with a Trimble Zephyr Model 2 antenna, were utilized to coregister and georeference SDT3 with differentially corrected target locations using the FARO SCENE 5.5 software package (FARO, 2015).

2.2.2.3 Terrestrial Lidar Preprocessing

The georeferenced point clouds were processed with Quick Terrain Modeler (Applied Imagery, 2009) to manually extract the three individual SDTs (Figure 4) from each site's point cloud, such that all returns caused by the ground surface or nearby vegetation were removed. Intensity values were normalized as 8 bit integers (i.e.,

ranging from 0 – 255), thus providing a uniform range of intensity values between the two scanners and varying scan conditions.

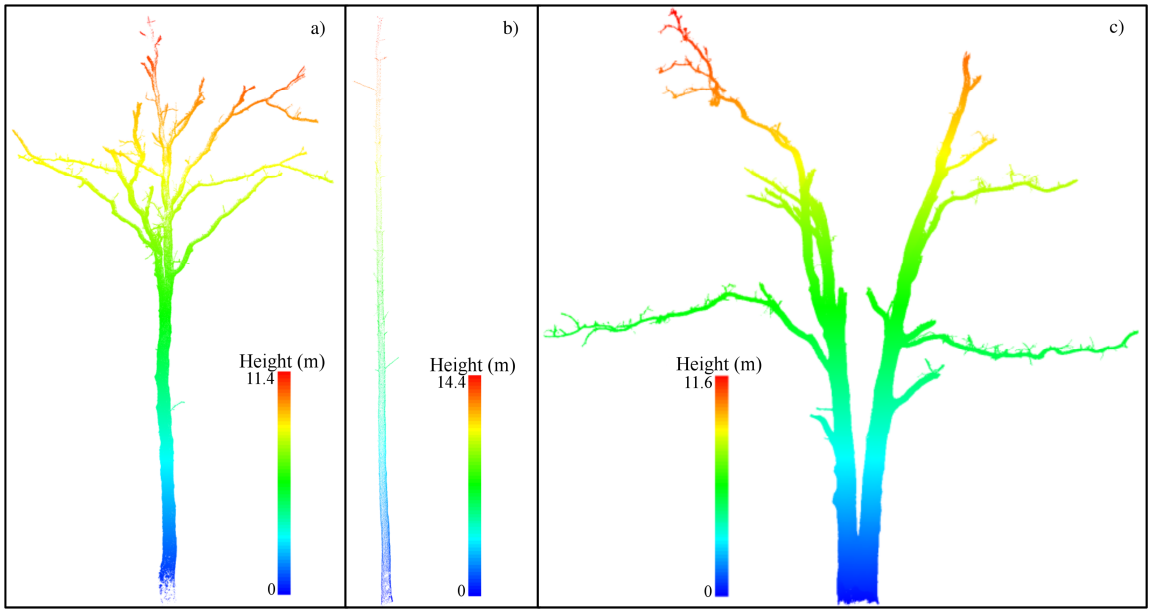

Figure 4: Individual SDT point clouds used for algorithm development and testing. a) SDT1; b) SDT2; c) SDT3.

The three point clouds used for algorithm development varied in their relative quality with respect to reconstructing solid tree models. The relative quality of each point cloud, in terms of point density and the extent of occlusion effects, was characterized by visual assessment as well as the descriptive statistics: total number of points, point density (i.e., the average number of points per square meter), and mean nearest neighbor distance (i.e., the average Euclidean distance to each point's nearest

neighbor in 3D space) (Table 1). While the number of points and point density provide an approximate sense of point cloud quality, they are also strongly influenced by the height and structural complexity of each particular tree, where the mean nearest neighbor distance metric provides a more objective relative quality assessment by only considering the spacing between individual points. SDT3, with the lowest mean nearest neighbor distance and highest point density, was assessed as a high quality point cloud, while SDT1 and SDT2 were considered to be medium and low quality, respectively.

Table 1: Tree measurements, descriptive statistics, and quality assessment of the three point clouds used for algorithm development.

ID	Scanner	Species	Height (m)	DBH (cm)	Number of Points	Point Density[a]	Mean NN Distance[b] (cm)	Relative Quality
SDT1	Leica	*Quercus stellata*	11.4	37.53	975,681	97,437.70	0.2912911	Medium
SDT2	Leica	*Pinus taeda*	14.45	21.9	37,464	71,958.55	0.7558868	Low
SDT3	FARO	*Quercus stellata*	11.59	35.45	8,483,915	501,220.12	0.1542635	High

[a] Number of points per m^2

[b] Average Euclidean distance to nearest neighbor

2.2.2.4 Accuracy Assessment

The algorithm's accuracy was evaluated using two point cloud datasets, one consisting of stem and large branch samples and the other consisting of small and fine branch samples, and comparing the voxel-based volume estimates of each sample to a

reference measurement. The stem and large branch accuracy assessment dataset was collected by scanning a post oak SDT with the FARO Focus^{3D} X 330, felling and extracting 13 cross sectional stem and large branch samples from the felled tree. The volume of each sample was determined with a xylometric approach by measuring the increase in water displacement observed when submerging each sample in a circular water container. The extracted samples ranged in diameter from approximately 11 – 38 cm. Prior to scanning, paint was used to designate samples on the SDT, facilitating accurate extraction of the samples in both the point cloud and from the felled tree. The SDT was scanned from four positions with a resolution setting of ½, a quality setting of 2X and imagery was collected with the scanner's integrated color camera in order to identify and extract the samples from the final voxel models using the colorized point cloud as a guide.

To assess the algorithm's accuracy with regards to small and fine branches, a reference dataset created and made publicly available by Hackenberg (2015) was utilized. This dataset consists of 15 TLS point clouds of leaf-off branches, from the species *Prunus avium*, *Acer pseudoplatanus*, *Quercus robur*, and *Fraxinus excelsior*, which were collected and scanned indoors from four positions each. Each point cloud is considered to be of overall high quality and density, but the effects of occlusion and reduced point density, particularly among fine branches, are still present. The branches range from 2 – 3 m in length and consist of small and fine branches, with diameters ranging from approximately 2 mm to 5 cm. The volume of each branch was estimated by performing two perpendicular caliper measurements at 5 cm intervals along the

branch, averaging the four diameter measurements, using the average diameter for each 5 cm segment to calculate the volume of a cylinder representing the segment, and summing the estimated volume of each segment.

2.2.3 Voxel Concept

A voxel (i.e., "*vol*umetric *el*ement") is analogous to a 3D pixel and represents a particular element of a 3D space that has been divided into a grid of identically-sized and equally-spaced cubes (Figure 5). While a lidar point cloud consists of dimensionless points which are arranged unevenly throughout the 3D space, voxels have the defined, morphometric properties of cubes and form a uniform grid of elements, making the voxel model conducive to systematic modelling and raster-like processing techniques. A voxel model is also capable of characterizing complex objects consisting of overhanging components, large amounts of negative space, and components with a variety of sizes, shapes, and orientations. The voxel models used in this work are stored in the sparse format, such that only voxels containing points are included in the voxel model and arrays of X, Y, and Z centroid coordinates are used as the fundamental distinction between each particular voxel; in contrast to a dense voxel format in which both empty and filled voxels are stored and referenced by their relative positions in each respective equally-sized, horizontal voxel slice. In the sparse voxel format each individual voxel contains at least one point, but may contain many points within its extent.

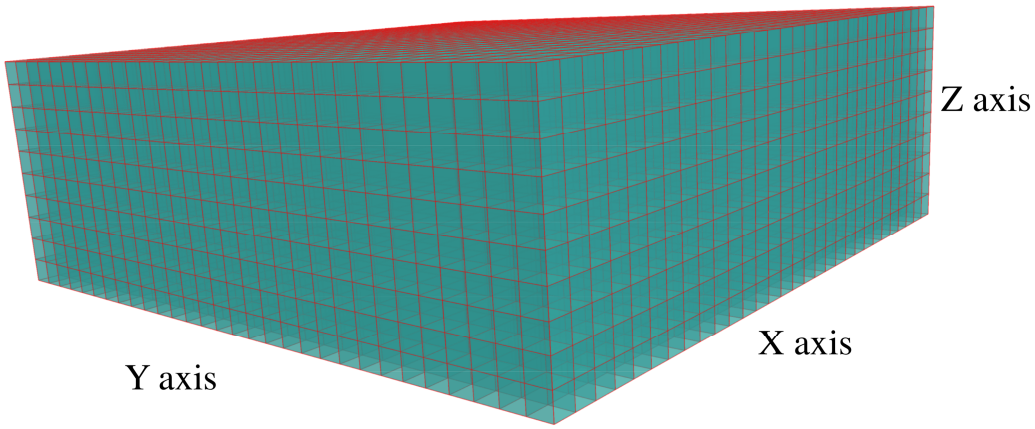

Figure 5: A 3D space represented as uniform cubic voxels.

2.2.4 Volume Estimation Algorithm Overview

An overview of the volume estimation algorithm's major steps is presented in Figure 6; dashed lines indicate optional procedures which may be performed based on the characteristics and quality of a particular SDT point cloud. The volume estimation algorithm is conceptually similar to one presented by Hosoi et al. (2013) and utilizes voxel-based processing to reconstruct a solid voxel model of a SDT, but provides several novel methods (i.e., adaptive contour interpolation, incremental ellipse segmentation, and vertical point cloud resampling) designed to reduce the effects of common point cloud imperfections on modelling accuracy. The algorithm operates on slices (i.e., horizontal cross sections of one-voxel thickness) such that the voxels in a slice are first segmented into distinct stem and branch segments. As lidar can only characterize the exterior surface of an object, interior voxels and exterior voxels absent from the model

due to occlusion and point density limitations must be identified and filled to perform an accurate reconstruction.

An ellipse is fitted to each segment within a slice and the spatial characteristics of the segment are evaluated in comparison to the ellipse to determine if the segment sufficiently portrays the expected true shape of the branch. Segments which have voxels well-distributed around the perimeter of the best-fit ellipse are considered to be accurate representations of the true branch shape and will have their contour defined with linear interpolation, while segments whose voxels only cover a small portion of the ellipse perimeter are considered to be heavily occluded and the best-fit ellipse is then used to define their contour. Each segment in the slice is then filled by inserting the voxels which are inside its defined contour. This process is repeated for each slice in the voxel model and the SDT's final volume is estimated by summing the volume of the reconstructed tree model's (RTM) voxels. The algorithm is written in R (R Core Team, 2016) and utilizes the packages "data.table" (Dowle and Srinivasan, 2017), "spatstat" (Baddeley et al., 2015) and "conicfit" (Gama and Chernov, 2015). The presented algorithm is planned to be released as an R package under the name "TreeVolX" at a later date.

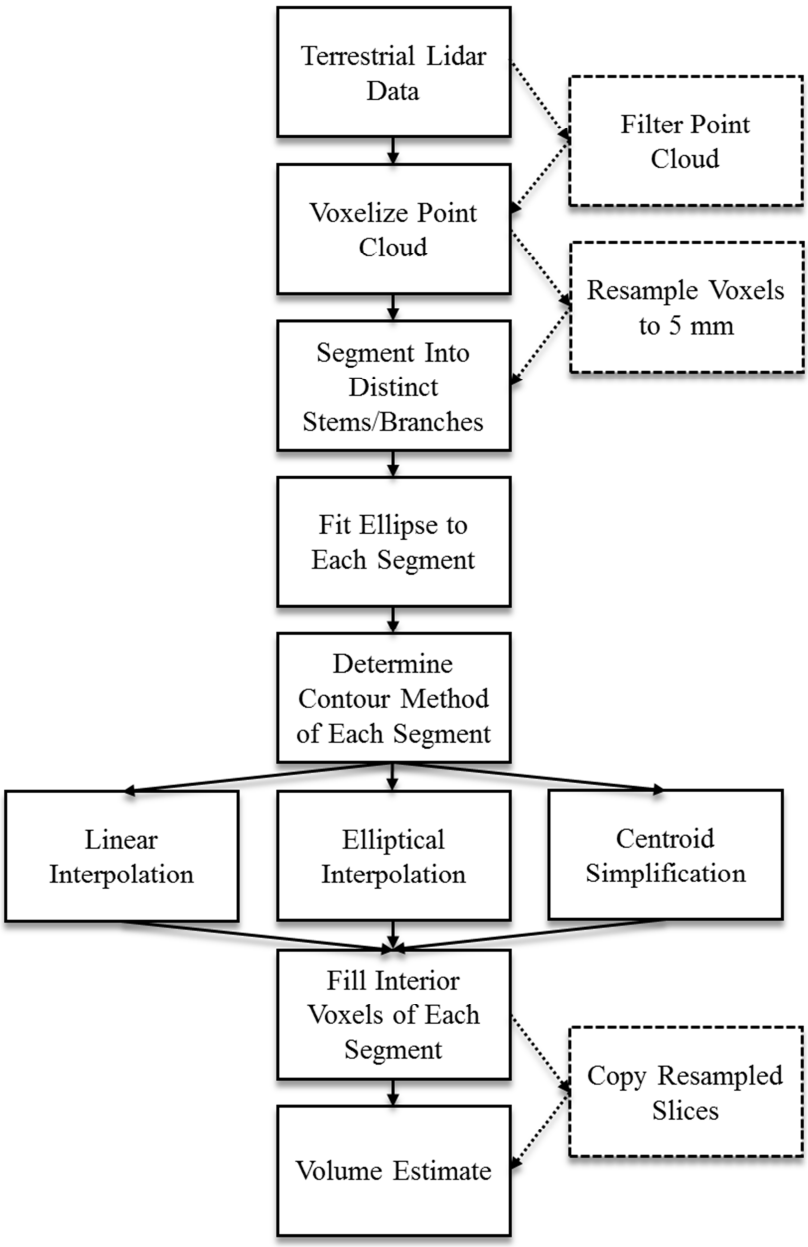

Figure 6: Flowchart of major volume estimation algorithm steps.

2.2.5 Volume Estimation Algorithm Description

2.2.5.1 Point Cloud Filtering

A common challenge when scanning vegetation with a phase-based TLS is the identification and removal of noise points, sometimes referred to as "ghost" points (Aschoff et al., 2004; Cifuentes et al., 2014; Litkey et al., 2008; Pueschel, 2013). Noise points are thought of as erroneous points which do not accurately characterize the target object and are typically caused by the laser being reflected off multiple surfaces around object edges, as the instrument receives more than one return pulse and calculates an ambiguous distance measurement. Thus, noise points were predominantly observed in the vicinity of bifurcated stem and branch sections as well as around fine branches. It should be noted that while modern ALS systems are capable of properly detecting multiple returns, this technology has not yet been implemented in the majority of commercially available phase-based TLSs. Noise points, if left unfiltered in the point cloud, can cause modelling errors and often result in an overestimation of SDT volume as distinct branches are erroneously clustered together due to the presence of noise in areas that are empty space in reality.

SDT3, being scanned with the phase-based FARO Focus^{3D} X 330, contained a significant amount of noise points while SDT1 and SDT2, which were scanned with the discrete-return Leica ScanStation 2, contained few noise points and were not filtered as described below. Noise points in the SDT3 point cloud were empirically observed to have two characteristics which generally distinguished them from valid returns: 1) lower point density and increased spatial isolation; and 2) lower intensity values.

The removal of noise points was achieved using a voxel-based method of identifying spatially isolated points (i.e., areas of relatively low point density) as well as an adaptable intensity filter which utilizes the *k*-means algorithm (MacQueen, 1967) to remove points with low intensity values (Figure 7).

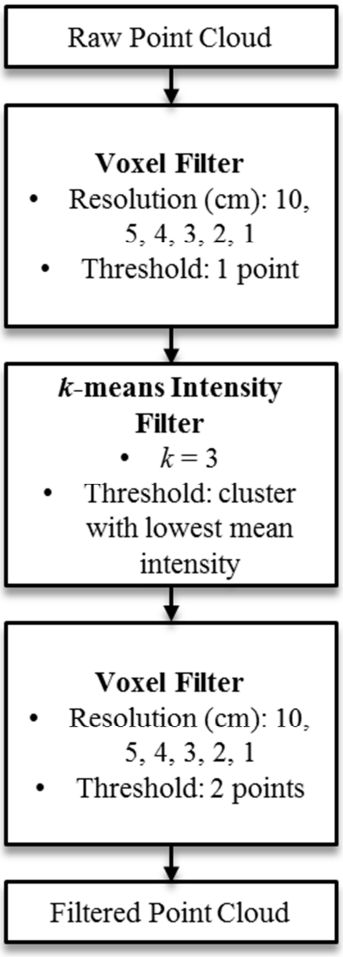

Figure 7: Flowchart of point cloud filtering procedure. Each voxel filter stage is executed iteratively with the filtering-voxel size decreasing in each iteration.

The voxel-based point count filtering iteratively voxelizes the point cloud and removes all of the points within a particular voxel if the total number of points within that voxel is less than a defined threshold value. It should be noted that this methodology operates on the assumption that the point cloud is of very high density such that voxels characterizing valid returns typically contain many more points than those voxels resulting from noise points. This procedure was repeated with an incrementally decreasing voxel size to remove the most likely noise points (i.e., those which are furthest from valid return points) first and progressively remove points which are less likely to be true noise points.

The incremental point count filtering was first conducted with a threshold of one point at voxel resolutions of 10 cm, 5 cm, 4 cm, 3 cm, 2 cm, and 1 cm. Next, the remaining points were clustered into three groups, based on their intensity values, using the *k*-means algorithm. The cluster with the lowest mean intensity value was considered to consist of noise points and the entire cluster was removed from the point cloud. Finally, the voxel-based filtering was again applied to the remaining points with a threshold of two points at the same set of voxel resolutions used initially, resulting in a final filtered point cloud with a significant noise reduction (Figure 8).

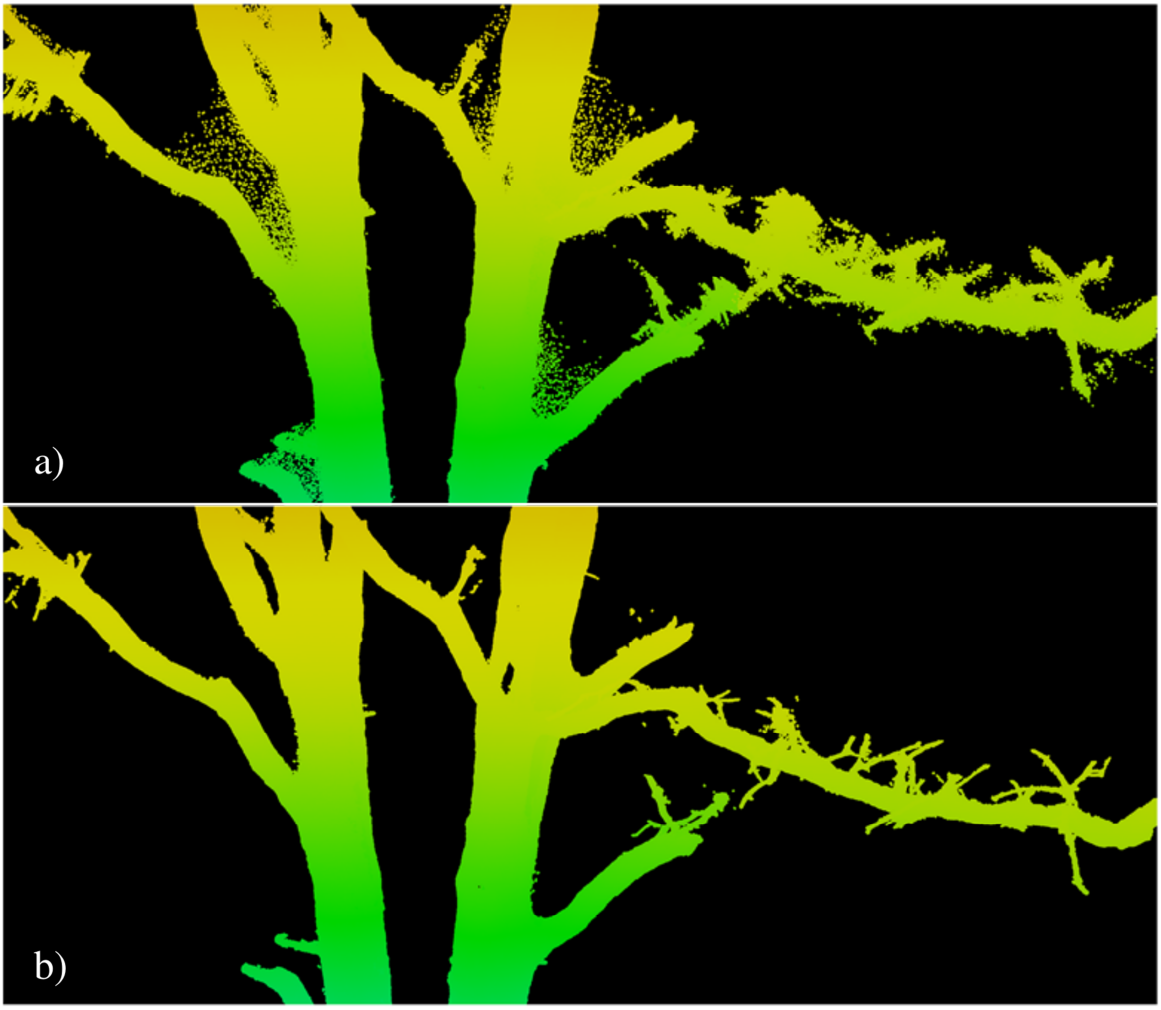

Figure 8: a) Significant noise present around branch junctions and fine branches in SDT3 prior to filtering; b) the majority of noise points were removed by the filtering procedure.

2.2.5.2 Voxelization

The point clouds were each then voxelized into a sparse voxel format with the following equations (Hosoi and Omasa, 2006):

$$X_v = Round\left(\frac{X_p - X_{min}}{10\Delta V}\right) \times 10\Delta V \qquad \text{Equation (1)}$$

$$Y_v = Round\left(\frac{Y_p - Y_{min}}{10\Delta V}\right) \times 10\Delta V \quad \text{Equation (2)}$$

$$Z_v = Round\left(\frac{Z_p - Z_{min}}{10\Delta V}\right) \times 10\Delta V \quad \text{Equation (3)}$$

where (X_v, Y_v, Z_v) are the coordinate arrays of each resultant voxel's centroid, $Round$ is a function rounding the value to one decimal place, (X_p, Y_p, Z_p) are the coordinate arrays of the SDT in point cloud format, $(X_{min}, Y_{min}, Z_{min})$ are the minimum values of (X_p, Y_p, Z_p) for the entire SDT, and ΔV is the length of one side of the resultant voxel in meters. Since cubic voxels were used in this study, a ΔV value of 0.02, for example, would result in cubic voxels of dimensions 2 cm x 2 cm x 2 cm when utilizing a UTM coordinate system.

The voxel size used during modelling is a crucial consideration that will impact the accuracy of the final volume estimation. A voxel size that is too large will result in an overestimation of volume and loss of modelling precision, while a voxel size that is too small will cause many horizontal slices of the voxel model to be so sparsely populated that it becomes difficult to apply any meaningful form of systematic processing. In general, the smallest possible voxel size which results in meaningful slices is the ideal size to use for this methodology.

The appropriate voxel size selection for a SDT is dependent on the point cloud's density and coverage. A voxel size of 5 mm was empirically determined to be appropriate for SDT1 and SDT3, but was too small for the lower relative quality point cloud of SDT2. A stem and branch section of SDT3, as seen in Figure 9, illustrate the importance of selecting an appropriate voxel size when modelling a high quality point

cloud; the 5 mm voxels most-faithfully represent the SDT while the larger voxels increasingly result in a loss of precision and obvious overestimation of volume.

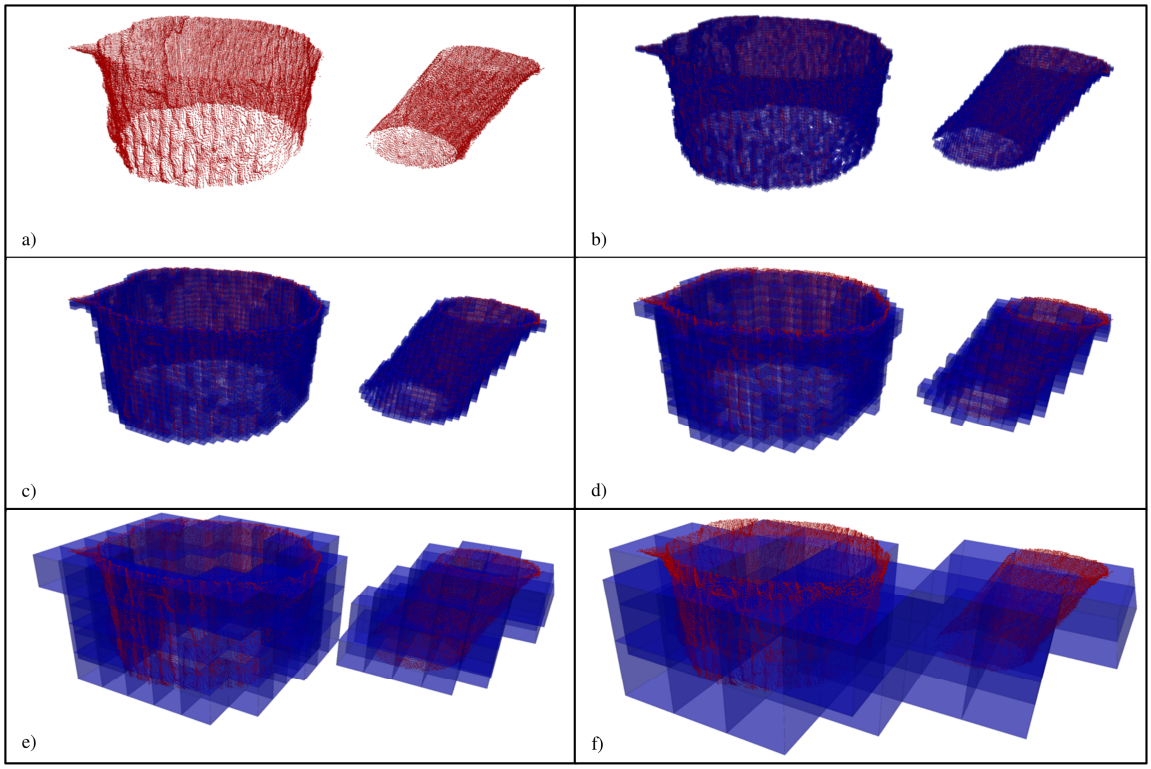

Figure 9: Stem and branch cross section from SDT3 illustrating the effects of voxel size selection on modelling precision and volume estimation when processing a high quality point cloud. a) original point cloud; b) 5 mm voxels; c) 1 cm voxels; d) 2 cm voxels; e) 5 cm voxels; f) 10 cm voxels.

In contrast, Figure 10 depicts the challenge of modelling lower quality point clouds with voxels; the 5 mm, 1 cm, and 2 cm voxels result in horizontal slices which are too sparse to properly process, while the 5 cm and larger voxels provide horizontal

slices which are populated densely enough to be properly processed at the expense of a loss of precision and general overestimation of volume.

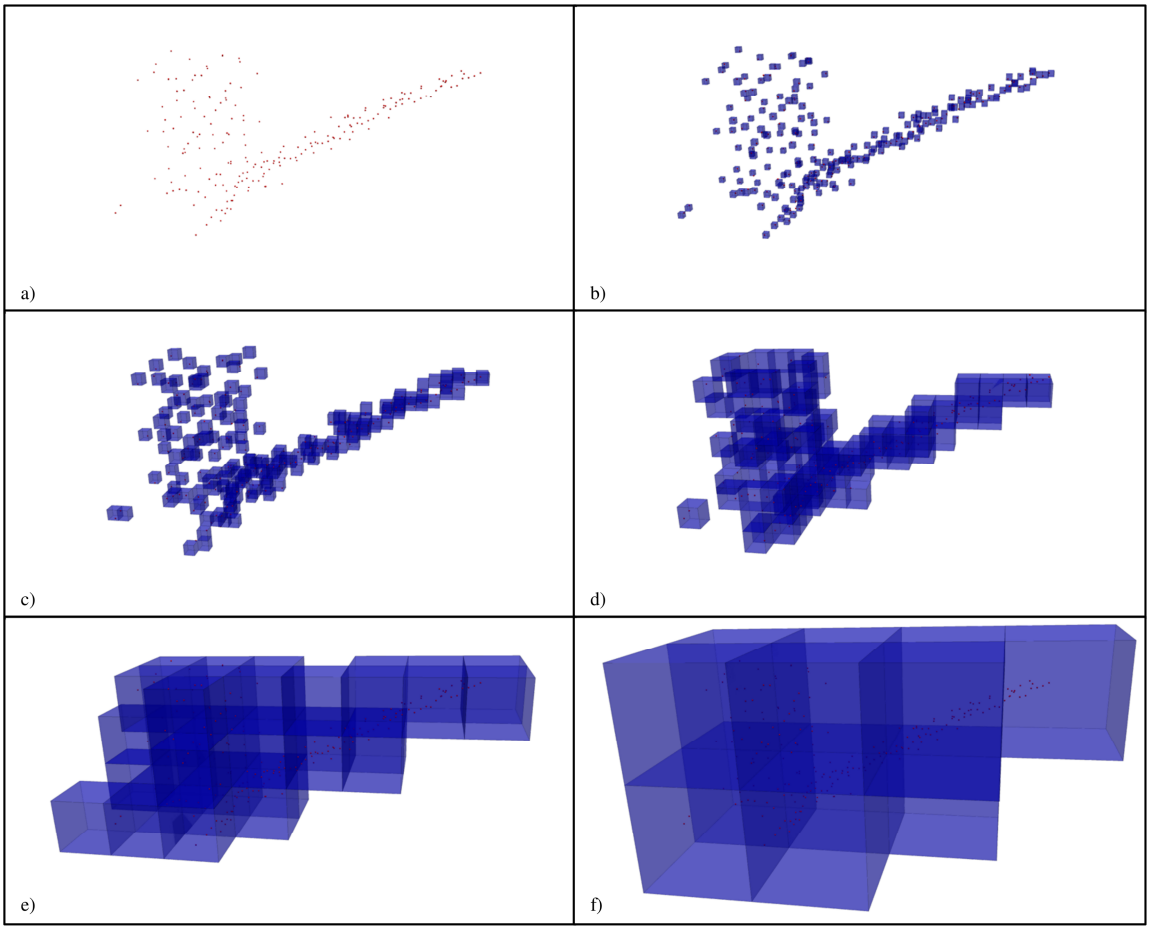

Figure 10: Stem and branch cross section from SDT2 illustrating the effects of voxel size selection on modelling precision and volume estimation when processing a low quality point cloud. The use of larger voxels may effectively allow a low quality point cloud to be processed, but results in an obvious volume overestimation. a) original point cloud; b) 5 mm voxels; c) 1 cm voxels; d) 2 cm voxels; e) 5 cm voxels; f) 10 cm voxels.

Vertical point cloud resampling is described in Section 2.2.5.3 and facilitated the use of a uniform 5 mm voxel size among the various quality point clouds, eliminating the inherent overestimation of volume which would have otherwise been caused by the use of larger voxels in compensation for the lower relative quality of SDT2.

2.2.5.3 Vertical Point Cloud Resampling

The concept of vertical point cloud resampling (VPCR) was developed to address the inherent volume overestimation which would have resulted from the use of larger voxels in compensation for low point cloud quality. A low quality point cloud is first voxelized using large voxels (e.g., 5 cm) and the points contained within each 5 cm horizontal voxel slice are projected onto horizontal planar surfaces (i.e., "flattened") and then voxelized at a resolution of 5 mm (Figure 11). The VPCR process thus provides 5 mm voxel slices with a sufficient number of voxels to facilitate further processing. While VPCR results in a generalization of a SDT's morphology, it allows for greater modelling precision than the use of a larger voxel size. The vertically-resampled 5 mm voxels are then processed in the same manner as 5 mm voxels from a high quality point cloud (i.e., sections 2.2.5.4 – 2.2.5.7) and once processing is complete, each vertically-resampled slice is duplicated to fill the height interval of the larger voxel size (e.g., a 5 mm vertically-resampled slice would be duplicated 10 times at height intervals of 5 mm to fill an original voxel size of 5 cm).

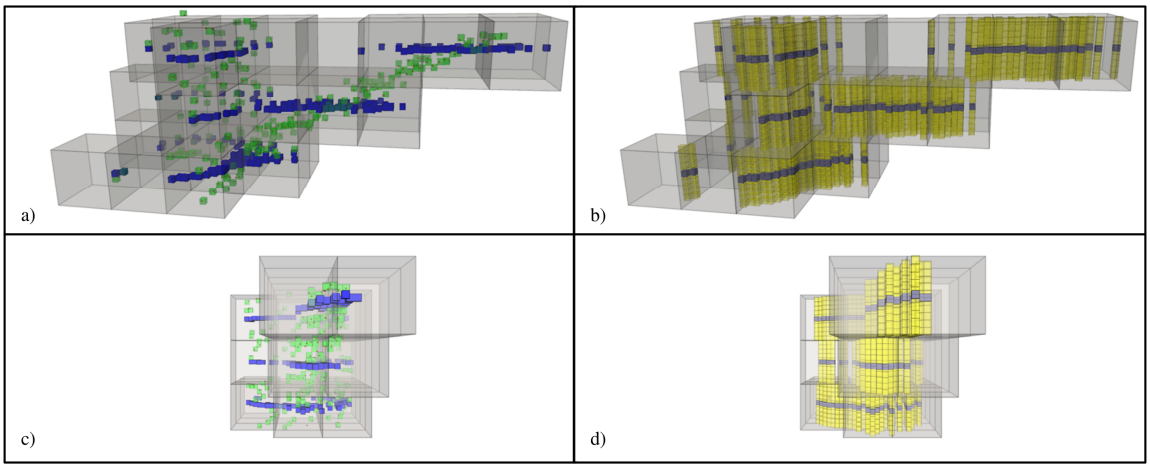

Figure 11: Illustration of the vertical point cloud resampling process as applied to SDT2; green – original 5 mm voxels, blue – resampled 5 mm voxels, yellow – duplicated resampled 5 mm voxels, white – 5 cm resampling voxels. (a) and (c) show the resampled slices (blue) are populated densely enough to be processed further following vertical resampling. (b) and (d) illustrate the theory of duplicating the resampled 5 mm voxel slices (yellow) rather than using larger 5 cm voxels (white) for modelling, avoiding a significant overestimation of volume.

The choice of appropriate large voxel sizes to use for VPCR was determined empirically during the development and testing process with the general goal of selecting the smallest size which would result in adequately dense 5 mm voxel slices. SDT2 was vertically-resampled using 5 cm voxels to generate a 5 mm voxel model, while SDT1 and SDT3 were not processed with VPCR and were able to be processed at an original voxel resolution of 5 mm.

2.2.5.4 Segmentation

Voxel slices were segmented to form distinct objects which represent individual branches or stems, based on the spatial characteristics of the voxels' centroids. Due to variations in voxel density and occlusion, both within a single SDT model and between

different SDT models, an iterative incremental ellipse segmentation approach which utilized proximity-based clustering in combination with least squares ellipse fitting was implemented to provide a general solution for a variety of situations, particularly medium to low relative quality point clouds.

Each voxel slice was first clustered with respect to the Euclidean distance between voxel centroids, such that all pairs of voxels whose centroids were closer than a specified distance threshold are assigned to the same segment. Each segment was then fitted with an ellipse using a direct least squares ellipse fitting algorithm (Fitzgibbon et al., 1999) as available in the R package "conicfit" (Gama and Chernov, 2015) to provide an estimate of the segment's true shape in the case of significant occlusion. Erroneous segment ellipses, defined as any ellipse with a maximum voxel centroid-to-ellipse distance of greater than 6 cm or a semi-major or semi-minor axis that is greater than 3X or 2X, respectively, the largest range (i.e., either the X or Y range) of the segment, were omitted from the slice. Each segment with a valid ellipse had 50 equally-spaced ellipse perimeter points temporarily added to the segment and was re-clustered with the same distance threshold used initially. The temporary ellipse perimeter points were then removed and the ellipse-fitting, erroneous ellipse removal, temporary addition of ellipse perimeter points, and re-clustering steps were repeated one more time on the resultant segmentation from the first iteration.

The above procedures were repeated using increasing clustering distance thresholds of 2 cm, 3 cm, 4 cm, 5 cm, 6 cm, 7 cm, 10 cm, 13 cm, and 16 cm. Once a segment is identical (i.e., consisting of the same voxels) through three consecutive

distance thresholds, it was considered to be accurately segmented and is removed from the slice; this procedure was repeated until all voxels in the slice have been assigned to a final segment. Any voxels which did not form a consistent segment among three consecutive passes were segmented with a simple distance threshold of 4 cm and added to the final segmented slice.

The algorithm also includes an option to perform a Euclidean distance-only segmentation instead, such that each slice is segmented solely on the basis of the Euclidean distance between voxel centroids. The user may elect to use this segmentation method and specify a distance threshold to be used for clustering. A distance-only segmentation, with a small distance threshold (e.g., 1 – 3 cm), may provide a more precise reconstruction when the SDT point cloud is of very high quality and has been scanned from at least four positions to minimize occlusion, but will not reliably segment a lower quality point cloud with more occlusion or reduced point density.

As a lower-quality, vertically-resampled SDT voxel model, SDT2 was densified to further increase its suitability to be reconstructed with a 5 mm voxel size prior to segmentation. Each resampled slice was densified by adding a point at the midpoint of a straight line connecting each voxel to its nearest neighbor voxel, if the voxel pair was separated by a distance of 20 cm or less. The densified points were used for the purposes of segmentation only and were removed from each resampled slice after segmentation had been completed. SDT1 and SDT2, being higher-quality voxel models, were not densified but were segmented using two contiguous slices at a time (i.e., a

particular slice and the slice directly above it) to help mitigate the effects of intermittent low-density areas.

2.2.5.5 Ellipse Fitting

Following the segmentation procedures, each distinct segment of a SDT was fitted with an ellipse using a direct least squares ellipse fitting algorithm (Fitzgibbon et al., 1999). Segments with fewer than five voxels were flagged and set aside as a minimum of five observations are required to fit an ellipse using the Fitzgibbon et al. algorithm. The five geometric parameters of each ellipse (i.e., center X coordinate, center Y coordinate, semi-major axis, semi-minor axis, and angle of rotation) were stored with each respective segment and the resultant ellipses were then used to determine an appropriate contour interpolation and interior fill method.

2.2.5.6 Contour Method Selection

Before the occluded interior voxels of each segment may be filled, an appropriate method of constructing a closed contour form must be selected. The method of contour interpolation, either linear or elliptical, is determined by the continuity and distribution of voxels within each particular voxel segment, hereafter referred to as "segment completeness." Segment completeness is a binary parameter defined by two factors: the total linear distance covered by the segment's voxels relative to the size of the segment's fitted ellipse (i.e., coverage) and the number of voxels present in each of six 60^{o} sectors (i.e., distribution), calculated with respect to the ellipse center. The segment completeness parameter (Equation 4) provides a quantitative method of selecting an appropriate contour generation method for each individual voxel segment.

$$Segment\ Completeness = TRUE\ if \left(\frac{Seg_N \times \Delta V}{(\frac{a+b}{2})} \geq 2.5\ \&\ Distribution\ \geq 2 \right) \qquad \text{Equation (4)}$$

Where Seg_N is the number of voxels in the segment, ΔV is the length of a voxel's edge, a and b are the semi-major and semi-minor axes, respectively, of the segment's ellipse, and $Distribution$ is the number of voxels present in the sector containing the fewest number of voxels.

Linear interpolation provides a more precise reconstruction when a voxel segment is nearly continuous, but fails to accurately characterize a voxel segment when contiguous sections of the branch are missing. When a voxel segment has a minimum of two voxels present in each sector and a coverage value of at least 2.5, the segment completeness parameter is considered to be true and the segment's contour is subsequently designated to be processed with linear interpolation. Direct least squares ellipse fitting provides a more robust contour generation in the case of a significantly occluded segment, as this method avoids the significant volume underestimation which would occur using linear interpolation under the same circumstances. Fine branches, considered to be segments whose ellipse has a semi-major axis of less than 6 mm, a semi-minor axis less than 5 mm, or contain fewer than five voxels, were identified and designated to be processed by centroid simplification. Segments which have a semi-major axis greater than 2 m, or a semi-major axis which is greater than ten times the length of the semi-minor axis are considered to be the result of an erroneous segmentation and are omitted from the interior filling process, but their original voxels

remain in the final RTM. All other segments were flagged as linear interpolation or ellipse interpolation and processed accordingly during the interior fill function.

2.2.5.7 Interior Fill

Interior voxels of branches and stems are inherently missing from TLS data sets, as the scanner can only obtain a return from the exterior surface of a SDT; as such, these interior voxels must be accounted for in order to provide an accurate volume estimate. Once every stem and branch segment of a SDT had been assigned a contour interpolation method, a closed contour form of each segment was interpolated then occluded interior voxels were filled to create a solid model characterizing the true segment structure.

A grid representing the centroids of potential interior voxels was first created for each segment such that the grid extended beyond the minimum and maximum X and Y extent of the original segment by 10 voxels in the case of a linear-method segment and 45 voxels for an ellipse-method segment. Linear-method segments were filled by creating a polygon whose vertices consisted of the segment's voxels, dilating then eroding the polygon using a disk with a radius equal to one half the voxel resolution (i.e., 2.5 mm) to remove artifacts caused by segments whose perimeter exceeds one voxel thickness, and selecting grid points which lie on or within the polygon boundary to be filled as interior voxels. Ellipse-method segments are filled in the same manner as linear-method segments, using 50 equally-spaced ellipse perimeter points to define the vertices of a polygon, but were not dilated and eroded. Fine branches, flagged to be processed by centroid simplification, are reduced to a single voxel placed at the

segment's centroid; thus reducing the tendency to overestimate the volume of fine branches when using voxels.

The closed contour, filled segments represent the final reconstructed tree model whose total volume is calculated by summing the volume of the RTM's voxels (Equation 5).

$$V_{RTM} = N_v \times \Delta V^3 \qquad \text{Equation (5)}$$

Where V_{RTM} is the RTM's total volume in cubic meters, N_v is the number of voxels comprising the RTM, and ΔV is the length of one side of a voxel in meters. If the voxel model was vertically-resampled, as described in section 2.2.5.3, each closed contour, filled slice is duplicated at 5 mm height intervals to fill the height range of its original large voxel slice.

2.2.6 Accuracy Assessment

For the stem and large branch accuracy assessment, the algorithm procedures were performed on the coregistered set of all four scans, as well as three sets of manually occluded samples to assess the importance of point cloud quality in terms of volume estimation accuracy. The colorized point cloud was used as a guide to extract the 13 samples from the final RTMs, in the case of the coregistered scans, and from the point cloud in the case of the manually occluded samples (Figure 12). Manually occluded samples were created by first extracting each sample from the point cloud, calculating the centroid of each segment and removing all points that had a coordinate value greater than the centroid in the X or Y plane, respectively, thus removing approximately half of each segment and simulating a severely occluded large branch. Several model runs were

conducted to assess the impact of voxel size selection, segmentation method (i.e., distance-only vs. incremental ellipse), and the ability of adaptive contour interpolation to minimize errors caused by point cloud occlusion.

Each small/fine branch point cloud was processed separately using 5 mm voxels and two trials were conducted, testing both the distance-only, with a distance threshold of 2 cm, and incremental ellipse fitting segmentation methods.

Figure 12: *Q. stellata* SDT (a) and colorized point cloud (b) with painted stem and branch sections used to identify and extract the accuracy assessment samples in the processed voxel model after the tree was felled and sectioned.

2.3 Results and Discussion

2.3.1 Volume Estimation Accuracy

The algorithm's accuracy, when processing point clouds collected under ideal scanning conditions, was evaluated with respect to both large and small branches. Table 2 shows the results of the large branch accuracy assessment, of 13 samples, when using 5 mm voxels with each segmentation method. The distance-only segmentations were conducted with a distance threshold of four times the voxel size for each voxel size tested. Processed voxel samples were extracted by using the colored point cloud as a guide such that each separate RTM was clipped at precisely the same locations for each respective sample. While this approach was considered to be the most consistent option, it may also result in minor artifacts, particularly when evaluating the accuracy of larger voxel sizes, as the clipping planes may happen to include or exclude an additional slice of voxel centroids at the uppermost or lowermost extent of the sample. The distance-only segmentation method was slightly more accurate than the incremental ellipse method due to several areas of minor over-clustering where a sample was in close proximity to another branch.

Table 2: Large branch accuracy assessment results with each segmentation method, both using 5 mm voxels.

	Segmentation Method	
Error	**Distance-Only**	**Incremental Ellipse**
RMSE (L)	0.4941	0.5042
RMSE (%)	7.27	8.45

The distance-only and incremental ellipse segmentation methods accounted for 99.6% and 99.5%, respectively, of the variance when regressed on the xylometric volume measurements of each sample (Figure 13). The accuracy assessment point cloud was processed with 1 cm voxels, 2 cm voxels, and vertically-resampled 5 cm voxels to assess the sensitivity of volume estimation to these algorithm parameters. Processing the SDT with 2 cm voxels, using the distance-only segmentation, resulted in a general overestimation of sample volume and an RMSE of 25.38%, as the larger voxel size resulted in a reduced ability to characterize the details of the large branch samples as well as an increased tendency to over-cluster with neighboring branches (Figure 14).

A voxel size of 1 cm resulted in an RMSE of 6.81%, contrary to the expectation that larger voxel sizes generally provide less accurate volume estimations. It is possible that artifacts caused by the described sample clipping procedure contributed errors to the process and erroneously resulted in an RMSE which was lower than the 5 mm voxel size. The vertically-resampled 5 cm voxels, with a final size once resampled of 5 mm, had an RMSE of 13.54% and were more accurate than the 2 cm voxel size, suggesting that the VPCR procedure provided in the algorithm provides a desirable alternative to using large voxel sizes in compensation for lower quality point clouds.

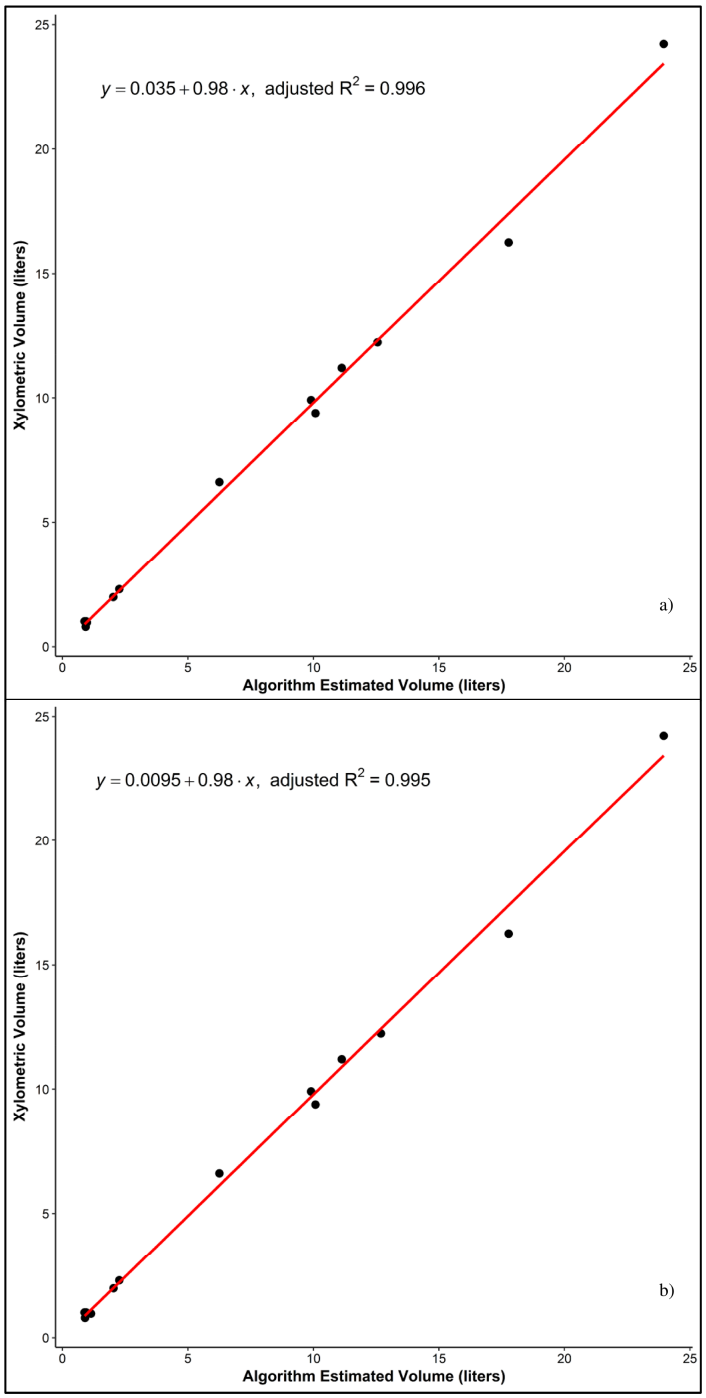

Figure 13: Scatter plots and best-fit regression line of estimated large branch volume vs. measured xylometric volume. a) distance-only segmentation; b) incremental ellipse segmentation.

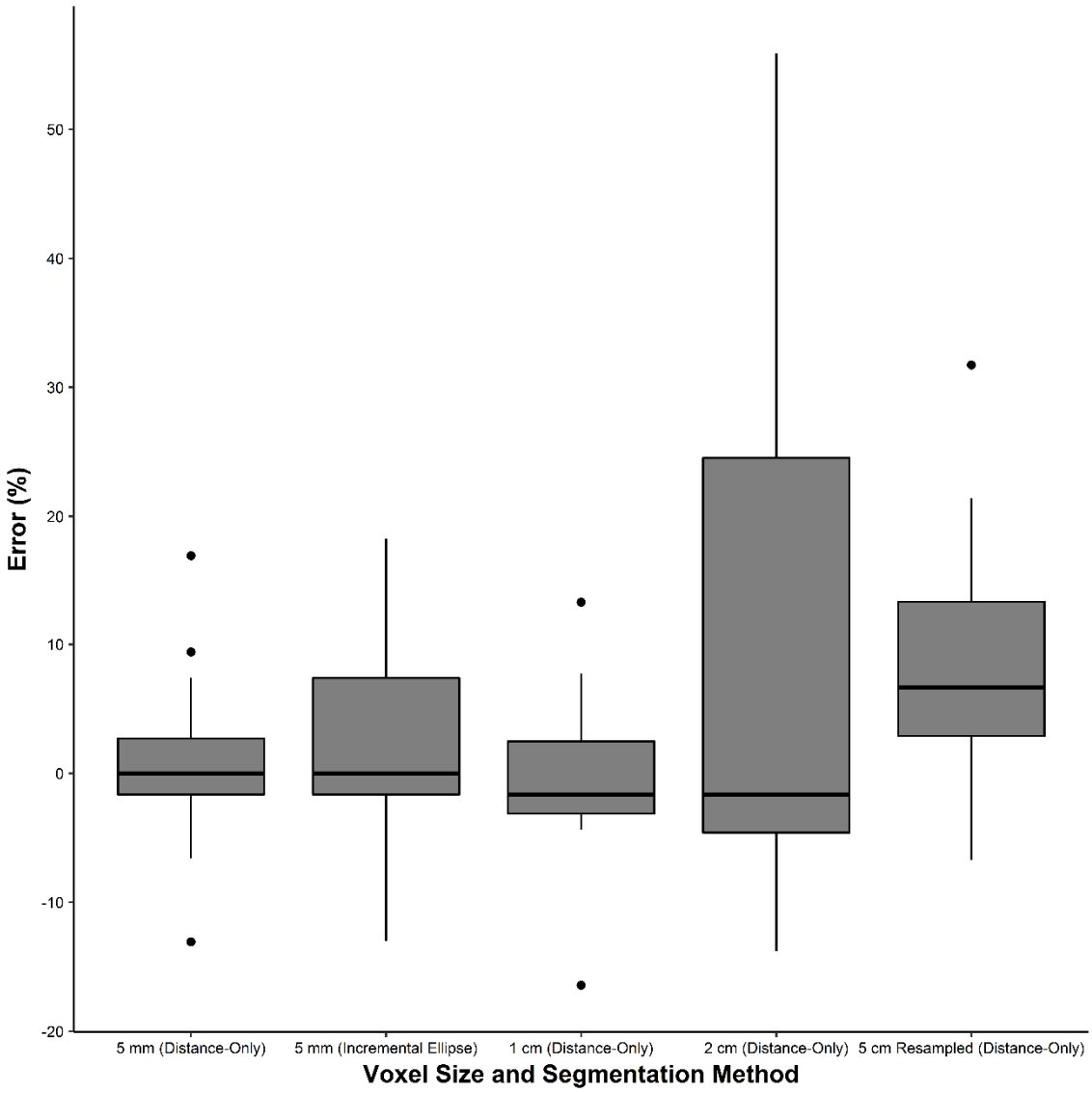

Figure 14: Boxplot of large branch volume estimation percent error.

The algorithm's ability to estimate volume in instances of severe occlusion was assessed with the two large branch sample point cloud sets that were manually occluded in the X or Y plane to remove approximately 50% of each sample along an 180^{o} sector with respect to each sample's centroid. The occluded samples were then processed with

5 mm voxels using a linear-only contour interpolation method or the adaptive contour method (described in section 2.2.5.6) which utilizes a best-fit ellipse to define a branch's contour when occlusion is detected or linear interpolation otherwise. The linear-only contour method consistently underestimated the volume of each severely occluded large branch sample, while the adaptive contour method generally underestimated and occasionally overestimated sample volume. Although both methods resulted in volume underestimations, the adaptive contour method was more accurate for both the X plane and Y plane sample sets, with RMSEs ranging from 27.01% - 37.75%, while the linear contour interpolation method resulted in RMSEs ranging from 52.99% - 66.57% (Figure 15).

Another test was performed by merging each respective sample that was occluded in the X and Y plane, such that each merged sample contained approximately 75% of its original points along a 270^{o} sector with respect to each sample's centroid, and processing each occluded sample with 5 mm voxels using linear-only and adaptive contour interpolation methods. The linear-only contour interpolation method shows a general tendency to underestimate volume, with RMSEs of 13.55% and 37.65% when using the incremental ellipse and distance-only segmentation methods, respectively.

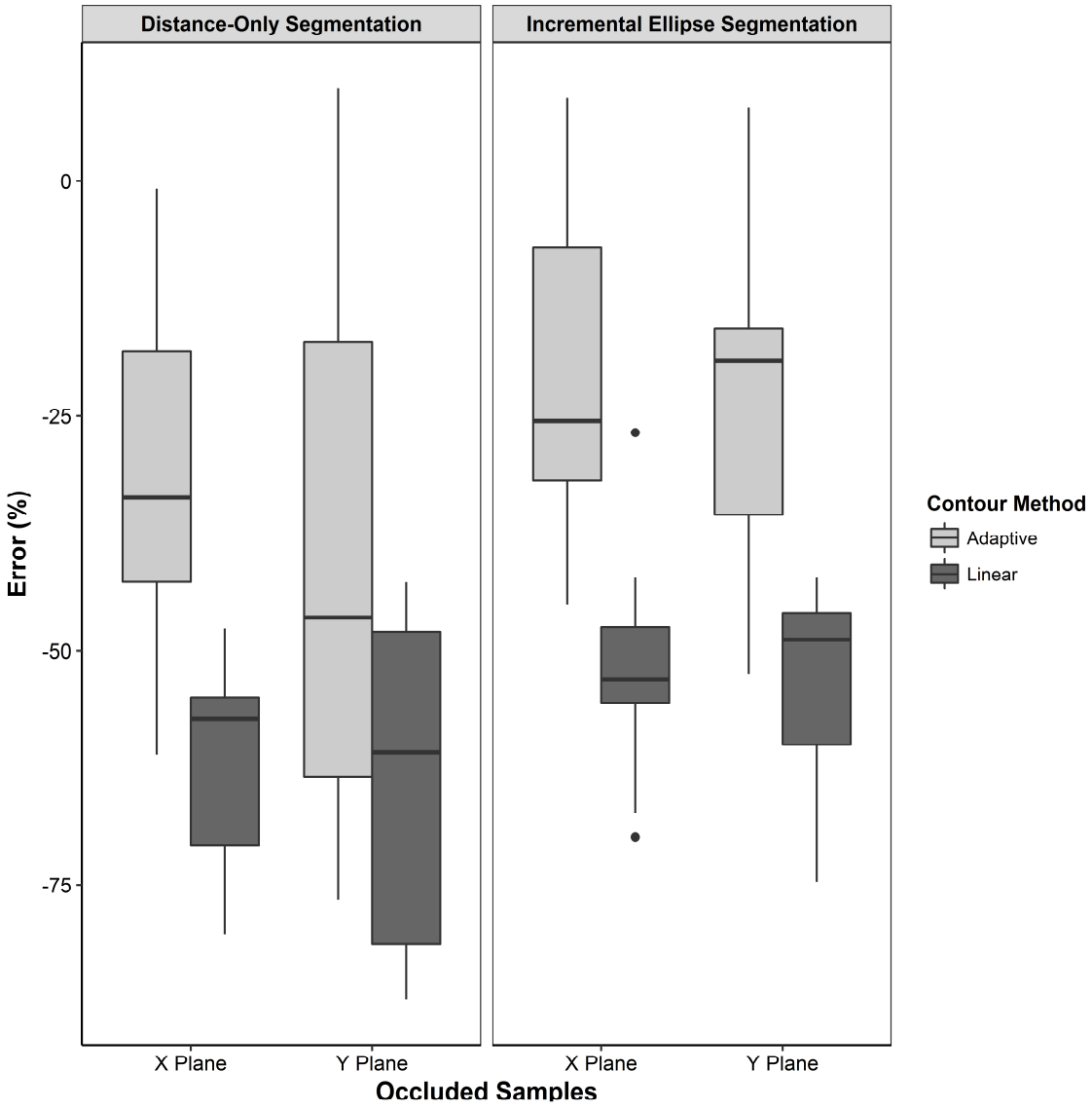

Figure 15: Boxplot of severely occluded (~50% of each sample removed) large branch volume estimation percent error using 5 mm voxels with each segmentation method; comparing adaptive and linear-only contour interpolation methods.

The adaptive contour interpolation method had a slight tendency to underestimate volume when using the distance-only segmentation, with an RMSE of 18.29%, while the incremental ellipse segmentation method was approximately balanced

with regards to underestimating or overestimating volume, with an RMSE of 13.24% (Figure 16).

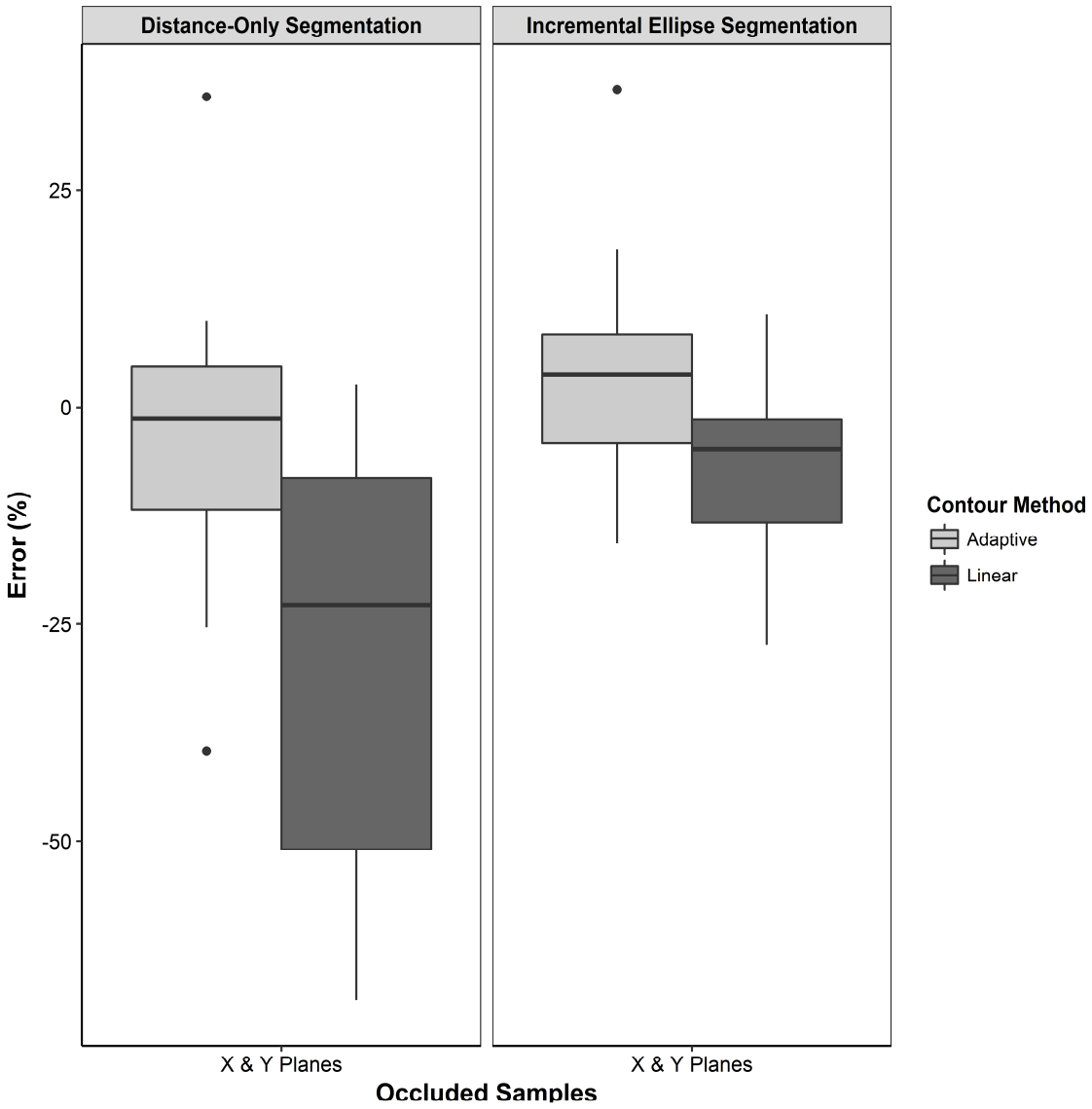

Figure 16: Boxplot of moderately occluded (~25% of each sample removed) large branch volume estimation percent error using 5 mm voxels with each segmentation method; comparing adaptive and linear-only contour interpolation methods.

While ideal terrestrial lidar data collection procedures (e.g., scanning a tree from four or more positions and clearing obstructions such as understory vegetation) may reduce the occurrence of point cloud occlusion, it is difficult to completely eliminate this source of error when scanning in forest environments. The number of scanning positions utilized in the field may be limited by the presence of neighboring trees or dense understory vegetation, equipment limitations, time constraints, or weather conditions (e.g., high winds), making point cloud occlusion a common challenge in terms of reconstructing accurate three dimensional tree models. The complex branching structure of some trees can also be a source of point cloud occlusion, even when scanned from multiple positions, as the presence of many large branches can often prevent the laser from reaching all parts of the tree's crown. In all three manually occluded sample sets, the adaptive contour interpolation method outperformed the linear contour interpolation with respect to both RMSE and the extent to which each sample was generally underestimated. By providing an adaptive contour interpolation method, the algorithm is able to consistently reduce errors associated with occluded branch and stem segments through the usage of elliptical contours, while still utilizing a more precise linear contour interpolation to characterize the fine details of irregularly-shaped branches when a sufficient point distribution is present.

The volume of small and fine branches were estimated with an RMSE of 13.84% and 75.92% when using the distance-only and incremental ellipse segmentation methods, respectively, and a 5 mm voxel size (Table 3).

Table 3: Small branch accuracy assessment results with each segmentation method, both using 5 mm voxels.

	Segmentation Method	
Error	**Distance-Only**	**Incremental Ellipse**
RMSE (L)	0.02042	1.1797
RMSE (%)	13.84	75.92

The distance-only and incremental ellipse segmentation methods accounted for 88.6% and 38.1%, respectively, of the variance when regressed on the reference circular cylinder volume measurements of each sample (Figure 17).

The incremental ellipse segmentation resulted in significant segmentation errors, where distinct small branches were erroneously considered to be to a single branch, and thus what was negative space in reality was filled with voxels in the resultant model. When several small branches are in close proximity to each other in a voxel slice, they may often be situated such that the perimeter of a best-fit ellipse includes multiple distinct branches. In combination with the increasing distance threshold used for each stage of segmentation in the incremental ellipse method, it was expected that small branches in close proximity would be estimated with reduced accuracy in comparison to the distance-only segmentation. These segmentation errors caused the incremental ellipse method to consistently overestimate the volume of the 15 small and fine branch samples. The distance-only segmentation method provided a significantly more accurate volume estimation as it is less prone to over-clustering distinct branches, allowing them to be reconstructed more faithfully to their true size and shape.

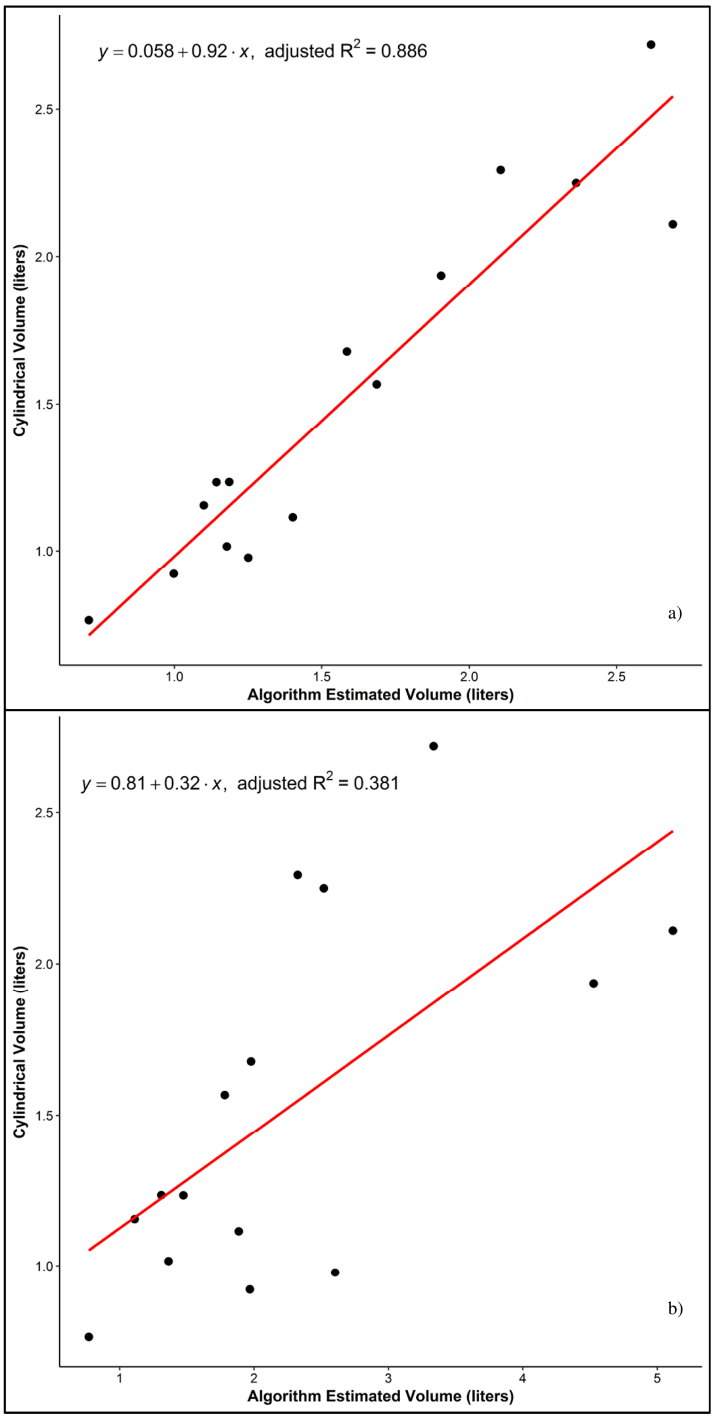

Figure 17: Scatter plots and best-fit regression line of estimated small branch volume vs. reference caliper volume. a) distance-only segmentation; b) incremental ellipse segmentation.

2.3.2 Analysis of RTMs

All three SDTs were successfully processed with the TreeVolX algorithm, having an average runtime of 9.3 minutes per tree, producing three reconstructed tree models. Each RTM consisted of consecutively filled interior voxels (Figure 18), providing a solid model and means of estimating the entire aboveground volume of each tree (Table 4). Due to variation in the quality of the original point clouds, each SDT was processed with algorithm parameters intended to provide the most accurate result possible at each relative quality level and assess the algorithm's ability to accurately model trees which were scanned in challenging environments. Every model run utilized the adaptive contour interpolation method while the segmentation method and VPCR technique were selectively applied in accordance with point cloud quality. SDT2, being considered a relatively low quality point cloud, due to lower point density and intermittent occlusion, was processed using the VPCR technique, such that 5 cm voxels were used to vertically-resample the point cloud to facilitate a final voxel size of 5 mm, and was segmented with the incremental ellipse segmentation approach.

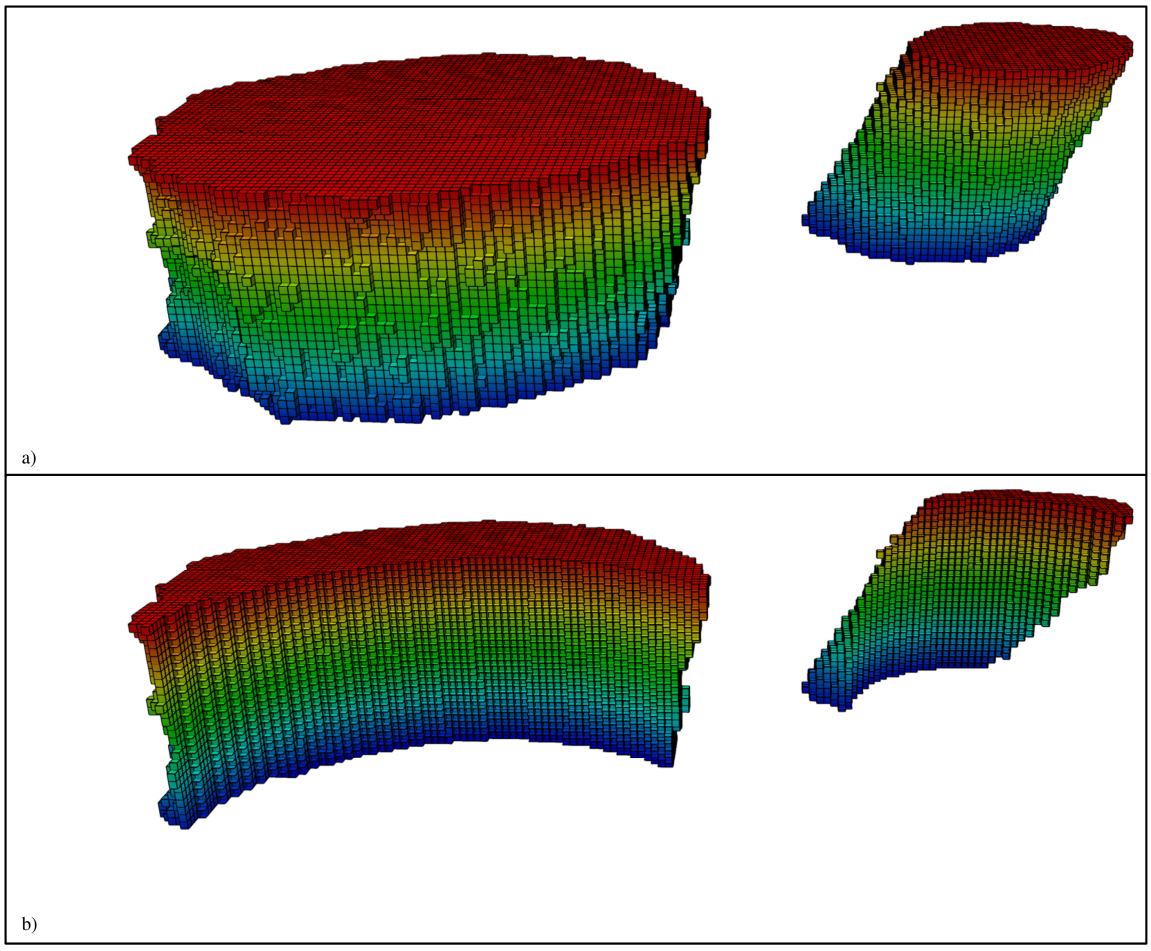

Figure 18: a) Stem and branch RTM output and b) cutaway view of SDT3 illustrating solid interior filled with adjacent 5 mm voxels.

Table 4: Volume estimation results.

ID	Scanner	Species	$Height_{TLS}$ (m)	DBH_{TLS} (cm)	Estimated Volume (L)
SDT1	Leica	*Quercus stellata*	11.4	37.53	456.24
SDT2	Leica	*Pinus taeda*	14.45	21.9	257.98
SDT3	FARO	*Quercus stellata*	11.59	35.45	1844.26

$_{TLS}$ measurement estimated from point cloud

The effects of VPCR can be seen in Figure 19, where a stem section from SDT2 is shown in the form of a vertically-resampled and non-resampled RTM, both with a final voxel size of 5 mm. Due to the low point density of the source point cloud, the non-resampled RTM shows an obvious and significant underestimation of volume, as each voxel slice does not contain enough voxels to be processed correctly.

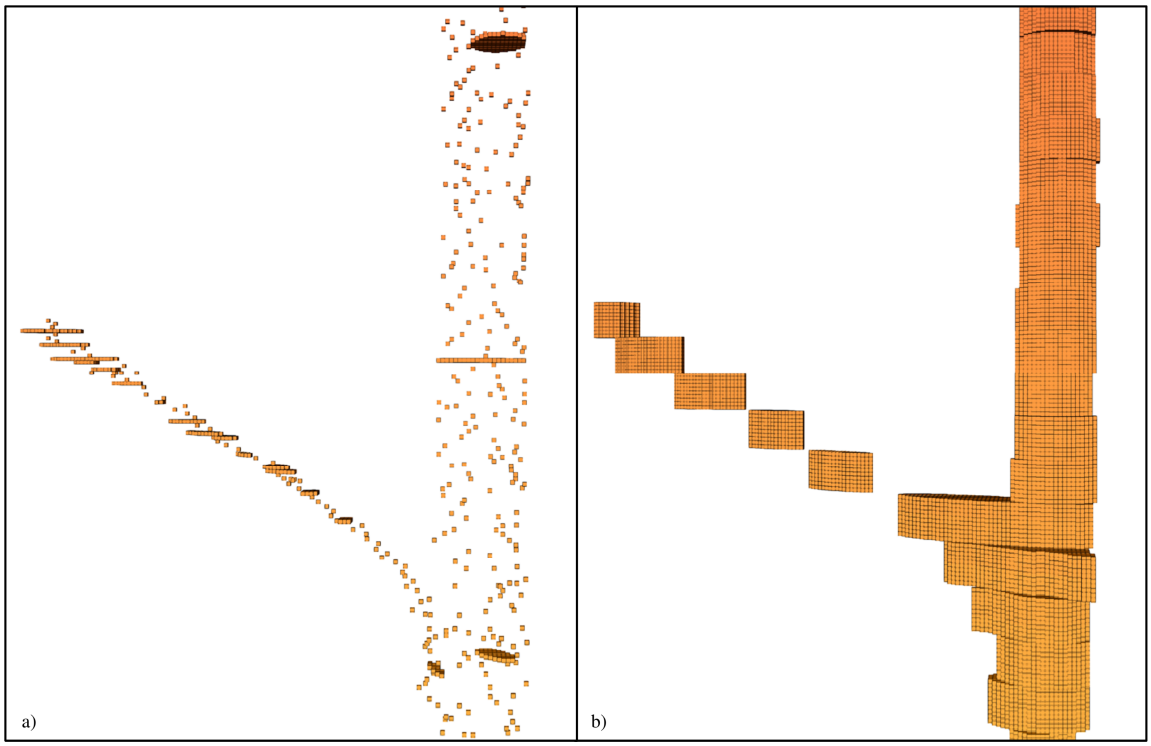

Figure 19: SDT2 RTM stem and branch detail using a) non-resampled 5 mm voxels and b) vertically-resampled 5 cm voxels with a final size of 5 mm.

The VPCR process was able to successfully model the areas of low point density without having to resort to using a larger voxel size, which would generally overestimate

volume throughout the tree. Although VPCR results in a level of generalization and may induce some modelling errors (e.g., over-clustering near branch junctions and overestimating the volume of small branches) it provides a reasonable solution to handling lower quality point clouds and was considered to provide a more accurate RTM than the non-resampled processing technique for SDT2 (Figure 20).

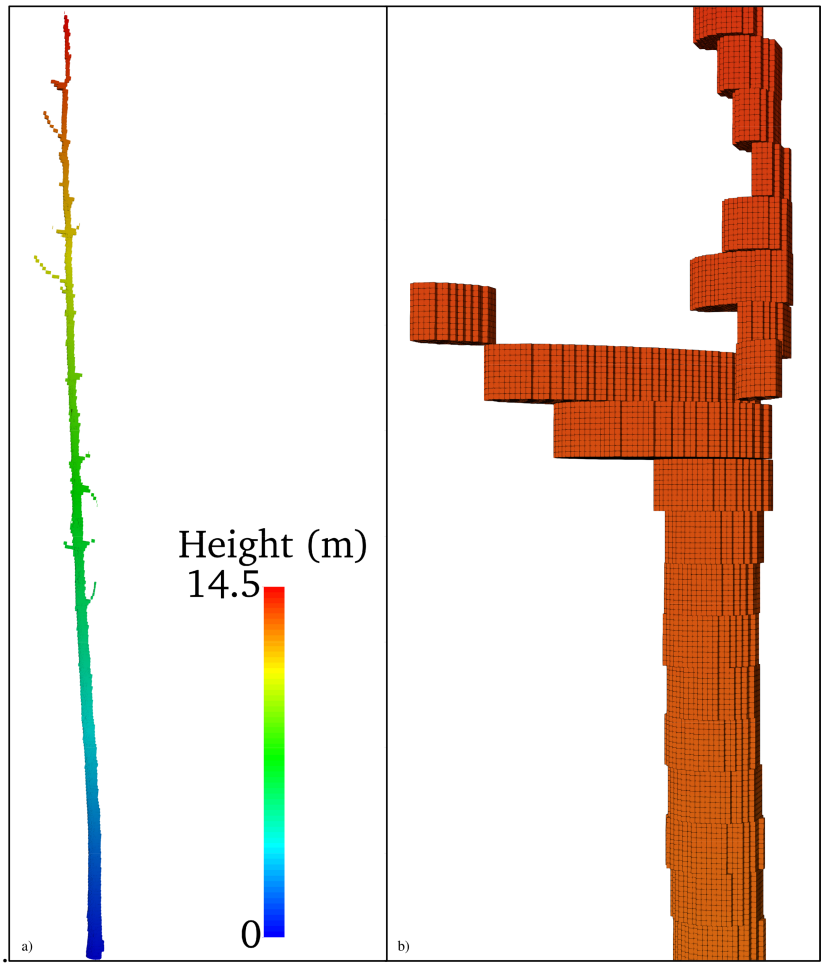

Figure 20: a) SDT2 5mm voxel RTM output; b) detail of over-clustering near branch junction.

As a medium quality point cloud, SDT1 was processed using non-resampled 5 mm voxels and the incremental ellipse segmentation method. The resultant RTM was considered to provide an accurate reconstruction of the original point cloud (Figure 21).

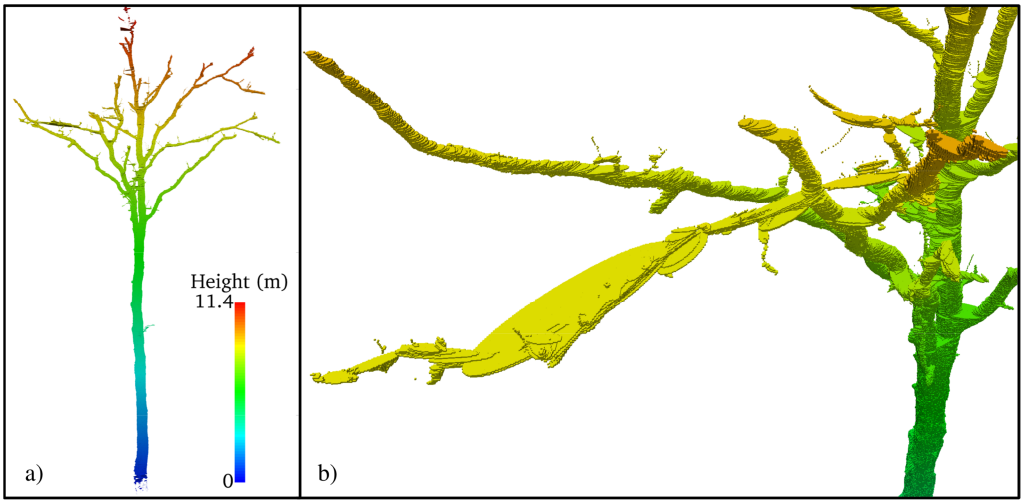

Figure 21: a) SDT1 5 mm voxel RTM output; b) detail of erroneous ellipse fitting along a horizontal branch.

A visual analysis of the RTM revealed several errors in the form of over-clustering, and subsequent overestimation of volume, of small branches and large branch junctions, the fitting of excessively wide ellipses to long, horizontal branches, and several small void spaces caused by occlusion or low point density.

The SDT3 RTM, processed using 5 mm voxels and the distance-only segmentation with a threshold of 2 cm, was the most accurate model due to the quality of its source point cloud and thus its ability to utilize the most precise modelling techniques

available in the presented algorithm. Minor errors were observed mainly in the form of excessively large ellipses being fit in areas of reduced point density, occlusion, or noise points. These errors were likely due to under-clustering during the segmentation process such that an ellipse was being fit to a small number of voxels which did not correspond to an entire branch section (Figure 22).

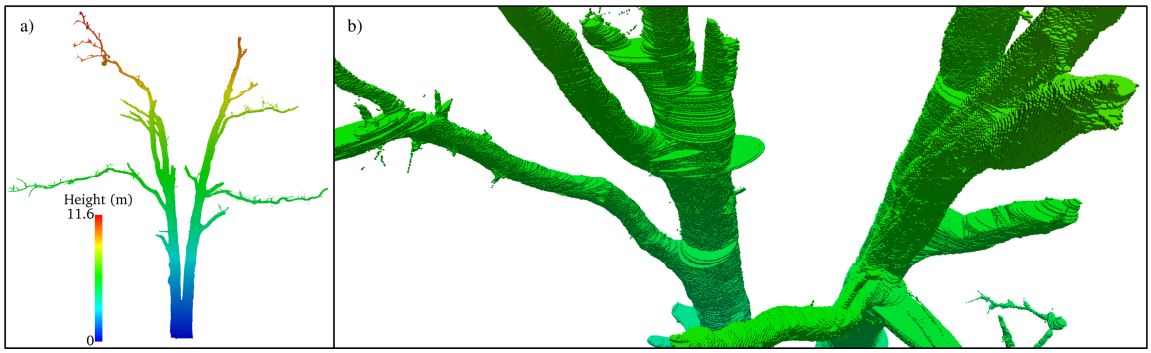

Figure 22: a) SDT3 5 mm RTM output; b) detail of excessively large ellipse fit to stem as a result of segmentation error.

Based on the modelling results, accuracy assessment, and empirical observations during algorithm development, the accuracy of an RTM can be maximized by scanning a tree from a minimum of four positions at a high resolution setting, using a voxel size of 5 mm, and utilizing the distance-only segmentation and adaptive contour interpolations methods. As noted by Hosoi et al. (2013) and Bienert et al. (2014), the selection of a small voxel size and linear contour interpolation method can accurately characterize irregularly-shaped branches without resorting to the generalizations associated with

fitting geometric primitives or the use of larger voxel sizes, when modelling a high quality point cloud. Since lower quality point clouds can be a reality of terrestrial laser scanning in dense forest environments, the proposed algorithm offers several processing options (i.e., adaptive contour interpolation, incremental ellipse segmentation, and vertical point cloud resampling) designed to compensate for reduced point cloud quality while attempting to minimize errors commonly caused by generalization.

2.4 Conclusions

This study presents an automated voxel-based technique for accurately estimating the volume of standing dead trees with terrestrial lidar data. Using an adaptive contour interpolation approach, the method is capable of precisely modelling complex shapes with linear interpolation when a branch slice contains sufficiently dense point coverage as well as compensating for areas of occlusion or reduced point density by applying an elliptical contour generation. The incremental ellipse segmentation method offers an ability to more-accurately segment point clouds characterized by moderate, intermittent occlusion and the presented VPCR technique is capable of modelling point clouds with significant occlusion effects or consistently low point density. These features offer a robust solution to estimating the volume of standing dead trees as dense forest systems present a challenging scanning environment with respect to the objective of collecting very high quality point clouds.

Although this study focused on modelling standing dead trees, the method is expected to provide similar results when applied to live trees scanned in leaf-off conditions. With the addition of a foliage filtering step, it could also presumably be

applicable to live trees in leaf-on condition, although the presence of leaves may cause significant levels of occlusion with regards to laser returns from the tree's woody structure, leaving some branches difficult or impossible to model accurately and increasing the overall error of volume estimation. With the inclusion of density measurements or species-specific parameter estimates, accurate volume estimations could be used to estimate biomass, carbon content, or other biogeochemical parameters of interest. The voxel-based modelling technique also facilitates accurate volume estimations of individual tree components, as branches or other areas of interest may be manually extracted from the reconstructed tree models and estimated by simply multiplying the number of voxels present by the volume of an individual voxel. Other potential applications of this modelling technique include evaluating or refining allometric equations, particularly with respect to standing dead trees in various states of decay, conducting change detection analysis to precisely monitor the decay or growth of individual trees over time, using TLS to validate or calibrate regional biomass estimations, and the automated estimation of morphological tree parameters.

Future studies could focus on developing techniques to reduce the overall error of volume estimation, further refining methods intended to minimize errors caused by imperfect point clouds, testing the presented method on additional tree species, and investigating the potential to model individual tree point clouds derived from unmanned aerial systems lidar sensors or structure from motion techniques.

3. DETECTING AND QUANTIFYING STANDING DEAD TREE STRUCTURAL LOSS WITH RECONSTRUCTED TREE MODELS

3.1 Introduction

Standing dead trees (SDTs) influence a variety of processes studied by researchers and forest managers, such as carbon storage and cycling dynamics in forests, nutrient cycling, species composition dynamics, wildland fire, wildlife habitat, and structural diversity of forest stands (Russell et al., 2015). In 2011 and 2012 a severe and extensive drought covered Texas, with precipitation values 50-75% below the long-term average (Hoerling et al., 2013). The drought increased tree mortality approximately 9-times above normal and translated to the estimated death of ~301 million trees statewide and the transformation of approximately 30 Tg of live tree C to a dead pool of C in one year (Moore et al., 2016). The regional C cycling effect of this tree mortality was the equivalent of nearly 50% of the average C annually emitted from forest fires in the continental United States (McKinley et al., 2011). Globally, the pool of SDTs and coarse woody debris (CWD) is estimated to be 36 – 72 Pg C, with the wide range in estimates reflecting that this C pool's dynamics are poorly constrained in terrestrial C cycling models (Cornwell et al., 2009). The performance of these models would be greatly improved if changes in tree structure could be linked to wood decay (Domke et al., 2011).

Nondestructive volume estimates for SDTs are typically calculated using various forms of allometric models, where parameters measured in the field (e.g., diameter at breast height (DBH) and tree height) serve as independent variables to species-specific

equations designed to estimate volume based on empirically observed relationships (Brown et al., 1989). The United States Forest Service (USFS) Forest Inventory and Analysis (FIA) program currently estimates the volume of SDTs using the same allometric relationships designed for living trees, which only account for the volume of a tree's main stem, in the case of timber species, or the stem, large branches, and bark in the case of woodland species (Woudenberg et al., 2010). Since this approach does not distinguish between live or dead trees and focuses primarily on a tree's bole, these estimates fail to account for the structural losses and wood decay which occur in SDTs, as well as the woody material contained in branches and sections of the stem which are not accounted for in allometric equations.

Recent research has recommended the application of structural loss adjustments (SLAs) and density reduction factors (DRFs) to allometric volume estimations to better characterize the structural differences between SDTs and live trees (Domke et al., 2011). The incorporation of SLAs and DRFs provide an opportunity to differentiate between live and dead standing trees, but such estimates based on allometric relationships and qualitative decay class systems and would need to be developed and evaluated for a wide range of species and regions, possibly limiting their utility and accuracy when compared to the potential of emerging remote sensing methodologies.

As observed density reductions fail to completely account for the total amount of biomass lost during the decay process (Fraver et al., 2013; Harmon et al., 1987; Næsset, 1999; Zell et al., 2009), it is important for studies to quantify and incorporate structural losses when modelling the decay rates of SDTs. Laiho and Prescott (2004) reviewed 34

wood decomposition studies and found that only five had considered mass loss as a component of decay, while the remaining studies were based on observed density reductions.

The extent to which decay rates, estimated by reductions in wood density over time, affect the structural loss rates of SDTs is not clearly defined. A number of studies have observed the longevity of standing dead trees or modelled their transition through qualitative decay classes in different regions (Aakala et al., 2008; Cain, 1996; Cline et al., 1980; Conner and Saenz, 2005; Corace et al., 2010; Garber et al., 2005; Landram et al., 2002; Vanderwel et al., 2006), but these approaches often are focused on stand-level observations and not able to quantify the different ways in which SDTs lose volume and mass over time (i.e., fragmentation or structural loss vs. collapse), which could provide valuable contributions towards understanding the flux of woody debris from standing pools to downed pools among various species and regions. In a review of research concerning the decomposition and carbon storage of dead wood in various forms, Russell et al. (2015) conducted a sensitivity analysis and found that structural reductions had the greatest relative influence on the C content of standing dead trees, 59.1%, while wood density had a relative influence of 19.8%. This finding emphasizes the need for accurate volume estimations of SDTs, the increased development of SLAs for additional species and regions, and the development of methodologies which can precisely quantify structural losses of SDTs over time.

Light detection and ranging (lidar) is an active remote sensing technology which, by measuring the elapsed time between a laser pulse and its return after being reflected

by an object, is capable of precisely recording the distance of objects from the lidar sensor and thus facilitating the capture of detailed 3D point clouds (Lefsky et al., 2002). Lidar sensors have been integrated into a wide variety of platforms and systems, such as: spaceborne (e.g., satellites), airborne (e.g., manned and unmanned aircraft), terrestrial (e.g., sensor fixed to a tripod), and mobile platforms (e.g., automobiles, all-terrain vehicles, handheld scanners) (Van Leeuwen and Nieuwenhuis, 2010).

Terrestrial laser scanners (TLS) in particular are capable of producing very dense point clouds of individual trees and have the advantage of being able to scan a tree from multiple vantage points, thus characterizing the fine details of an entire tree in terms of the structure, size, and orientation of its stem and branches, which are difficult to measure using other lidar platforms or traditional measurement approaches. TLS has been used in a wide variety of forestry applications (Dassot et al., 2011; Van Leeuwen and Nieuwenhuis, 2010) and recently has been utilized with the objective of reconstructing solid 3D models of trees derived from TLS point clouds, enabling accurate, nondestructive estimates of volume or biomass. Although this is a relatively new application of TLS, algorithms presented in the literature may be broadly grouped into two common approaches: (1) the fitting of geometric primitives, such as circular cylinders, to tree components (Côté et al., 2009; Dassot et al., 2012; Hackenberg et al., 2014; Raumonen et al., 2013); and (2) converting point clouds to a voxel-based representation and subsequently processing the voxels to derive a solid model (Bienert et al., 2014; Hosoi et al., 2013; Lefsky and McHale, 2008; Vonderach et al., 2012).

Despite the increasing interest in, and successful examples of, reconstructive tree modelling, the use of TLS to perform change detection analysis on individual trees, and structural loss in particular, has not been thoroughly tested in the literature. Kaasalainen et al. (2010) used TLS to quantify the defoliation of Scots pine (*Pinus sylvestris*) and Norway spruce (*Picea abies*) trees scanned in a laboratory environment. Three point cloud parameters were derived, for each tree, to estimate measured biomass changes after needles had been manually removed from the trees: (1) the total number of point cloud returns; (2) the ratio of tree returns to total returns; and (3) the number of ground returns. These parameters were used as predictors for biomass loss in linear regression models, resulting in Pearson correlation coefficients ranging from 0.929 to 0.977. A similar methodology was carried out in a field setting, but visual assessments were used as reference data and quantified linear relationships were not reported. While this study shows the potential of TLS to quantify biomass changes, it is unclear how well this particular methodology would work under a variety of field conditions with varying tree species and significant reductions in tree biomass, such as branch drops or stem breakage.

Srinivasan et al. (2014) used single-position scans with a TLS to estimate the biomass change of 29 loblolly pine (*Pinus taeda*) trees in a forested environment. The authors used linear regression techniques to model biomass change at the individual tree level in comparison to reference biomass changes estimated with allometric equations over a three year period. Out of several different approaches, the most accurate estimate of biomass change was based on the direct changes in two point cloud parameters

between observations, volume beneath top of canopy and 90th percentile height, resulting in an R-squared of 0.50 and an RMSE of 10.09 kg. Kaasalainen et al. (2014) applied the quantitative structure modelling (QSM) methodology to detecting biomass changes in laboratory and field environments, with an accuracy of 12% in estimating the volume of a small branch following the manual removal of branch sections and an unknown accuracy in the field with regards to a estimating the volume of a single live tree over time, which was estimated to be approximately +/- 10%. These estimates were the mean results of 10 modelling runs, which typically exhibited a standard deviation of 5 – 15 % for estimated branch volume due to the stochastic nature of the algorithm. The accuracy of this study suggests that reconstructive tree modeling has the potential to reliably quantify biomass or volume loss in forest environments.

The methodology described in this study presents a novel, voxel-based approach to addressing the current knowledge gaps concerning the structural loss of standing dead trees by developing automated methods to detect, quantify, and characterize volumetric losses over time using solid, voxel-based reconstructed tree models. To the best of the author's knowledge, this study represents the first attempt to characterize the fragmentation of SDTs in a forest environment with the use of multitemporal TLS observations at the individual-tree level. The presented approach may be applied to future studies and has the potential to be applied to a variety of tree species in different forest systems. In the future, this technique, or similar approaches, may be used to provide quantitative structural loss data which could facilitate the development of SLAs

for a variety of species in various regions to increase the accuracy of regional volume and carbon accounting with respect to SDTs.

The overall objective of this study is the development of a methodology capable of detecting, quantifying, and characterizing the structural loss of standing dead trees using multitemporal terrestrial lidar observations. The specific study objectives are:

1) Estimating the volume of 29 standing dead trees using the voxel-based TreeVolX algorithm with terrestrial lidar data.
2) The development and evaluation of novel, voxel-based change detection methodologies to accurately detect and quantify SDT structural loss between subsequent TLS observations.
3) The characterization of SDT annual structural loss rates, for the *Pinus* and *Quercus* genera in southeastern Texas, in percentile height bins.

3.2 Methods

3.2.1 Study Area

The study area consisted of four separate sites located in southeastern Texas (Figure 23). Site 1 was in Lick Creek Park, located in College Station, Texas, covering an area of approximately 209 hectares. The topography of Lick Creek Park is nearly level, with slight, rolling elevation changes and an average elevation of approximately 74 meters above mean sea level. The scan location was within a dense, upland post oak woodland, consisting primarily of post oak (*Quercus stellata*) and winged elm (*Ulmus alata*), with a dense understory of yaupon holly (*Ilex vomitoria*) and American beautyberry (*Callicarpa americana*).

Figure 23: Locations of study sites in southeastern Texas.

Site 2 was in the Sam Houston National Forest, located near Huntsville, Texas, which covers an area of approximately 65,978 hectares. The plots were characterized by nearly flat, gently rolling topography with a mean elevation above mean sea level of approximately 117 meters. Located in mixed pine-hardwood stands, site 2 was composed predominantly of loblolly pine (*Pinus taeda*), with intermixed shortleaf pine (*Pinus echinata*), post oak (*Q. stellata*), sweet gum (*Liquidambar styraciflua*) and an

understory of yaupon holly (*I. vomitoria*), American beautyberry (*C. americana*), and dwarf palmetto (*Sabal minor*).

Site 3 was located in Research Park, in College Station, Texas. This site covers approximately 65 hectares and is nearly flat with a mean elevation above sea level of approximately 96 meters. Site 3 consists primarily of manicured grasses and mostly-isolated post oak (*Q. stellata*) and live oak (*Q. virginiana*) trees in clearings.

Site 4 was located in the Texas A&M University Ecology and Natural Resources Teaching Area in College Station, Texas and covers approximately 73 hectares. Site 4 was located in a post oak savannah consisting of post oak (*Q. stellata*), winged elm (*U. alata*), blackjack oak (*Quercus marilandica*), ashe juniper (*Juniperus ashei*), and a dense understory of yaupon holly (*I. vomitoria*) and American beautyberry (*C. americana*).

3.2.2 Data

Each site was scanned twice with a TLS to obtain multitemporal point clouds of standing dead trees to quantify their volume loss over the observation period. The sites consisted of multiple *Q. stellata* or *P. taeda* SDTs and were scanned with a Leica ScanStation 2 or FARO Focus^{3D} X 330, for a total of 13 post oak and 16 loblolly pine SDTs (Table 5). The FARO TLS was purchased during the duration of the study and replaced the Leica TLS in data collection. The phase-based FARO TLS allowed scans to be conducted from additional positions at high resolution due to its faster setup procedures and scanning times. The trees observed in this study were presumed to have been killed following extreme drought conditions in Texas during 2011 – 2012 (Hoerling et al., 2013), although the exact time of death is not known.

Table 5: Scanning campaign summary and point cloud quality assessment.

Site	Plot	Species Count		$Scanner_I$	$Scanner_F$	$Date_I$	$Date_F$	ΔT (days)	Mean NN $Dist_{I(F)}$ (cm)	Relative $Quality_{I(F)}$
		Q. stellata	*P. taeda*							
1	1	5	0	Leica	FARO	May 2015	Dec 2016	753	0.9898 (0.0877)	Low (Medium)
2	1	0	8	Leica	FARO	June 2015	Dec 2016	588	0.9399 (0.1)	Low (Medium)
2	2	2	3	Leica	FARO	July 2015	Dec 2016	554	1.9313 (0.1568)	Low (Medium)
2	3	0	5	Leica	FARO	Mar 2015	Apr 2017	516	1.93 (0.0951)	Low (Medium)
3	1	2	0	FARO	FARO	July 2016	Jan 2017	171	0.1623 (0.1607)	High (High)
4	1	4	0	FARO	FARO	Jan 2017	Mar 2017	71	0.1144 (0.0831)	Medium (Medium)

$_I$ initial scan

$_F$ final scan

3.2.2.1 Leica TLS

The Leica ScanStation 2 (Table 6) (Leica Geosystems, 2006) was mounted on an aluminum tripod and precision-levelled with Cyclone 9.0 (Leica Geosystems, 2012). The plots in sites 1 and 2 were each initially scanned with the Leica TLS from two positions, located at an approximately 180^o offset with respect to the center of the plot with a horizontal and vertical resolution of 10 cm, at a range of 50 m. Intermittent technical malfunctions with the scanner prevented the collection of multiple scans per tree, necessitating the use of plot-level scanner placements. Exact scanner placement

was determined in an attempt to maximize coverage of the target trees and minimize occlusion due to understory vegetation and other trees; the average distance between the scanner and each tree was approximately 7 m.

Table 6: Technical specifications of terrestrial laser scanners.

	Leica ScanStation 2	**FARO Focus^{3D} X 330**
Type	Time-of-Flight	Phase-Shift
Wavelength (nm)	532	1550
Maximum Scan Rate (kHz)	50	976
Maximum Range at 90% Albedo (m)	300	330
Beam Divergence (mrad)	0.15	0.19
Beam Diameter (1/e) (mm)	3.2 @ 20 m	2.25 @ exit
Vertical Field of View (^{o})	270	300
Horizontal Field of View (^{o})	360	360
Vertical Resolution (^{o})	~ 0.003	0.009
Horizontal Resolution (^{o})	~ 0.003	0.009
Position Error (mm)	6	unknown
Ranging Error (mm)	4	2

Two stationary Leica High Definition Survey (HDS) flat targets were used in the field to coregister (i.e., accurately combine data from multiple scanner positions into one unified dataset) the scans from each plot. Each HDS target was measured with a tape measure to record its height above ground level and the locations of the targets were measured using a Trimble GeoExplorer 6000 handheld GNSS unit with a Trimble Zephyr Model 2 antenna, capable of centimeter-level accuracy following differential correction in post-processing (Trimble, 2010). These procedures allow the TLS data to

be georeferenced (i.e., assign a real-world location to each laser return), facilitating the use of a projected coordinate system to support the creation of voxel models. Each plot's point cloud was georeferenced with differentially corrected target positions using Cyclone 9.0 after being coregistered.

3.2.2.2 FARO TLS

The FARO Focus^{3D} X 330 (Table 6) (FARO, 2013) was mounted on a carbon fiber tripod and levelled using the Focus^{3D} X 330's onboard inclinometer. The final scans at sites 1 and 2 and both initial and final scans at sites 3 and 4 were conducted with the FARO TLS. Each SDT at site 3 was scanned from four positions, located at approximately 90^{o} intervals with respect to the center of the tree with a scan resolution of 3.068 mm (i.e., ½ resolution as defined by FARO system settings), at a range of 10 m, with an average scanner distance of approximately 3 m and a quality setting of 2X. The two SDTs at site 3 were spatially isolated in an area consisting primarily of manicured grass, resulting in minimal occlusion and were subsequently the highest quality point clouds collected in the study. Each SDT for the final scans at sites 1 and 2, as well as both scans at site 4, was scanned from two positions, offset at approximately 180^{o} from the center of each tree. Exact scanner placement for each SDT was selected to minimize occlusion from nearby vegetation, ensure a clear view of the targets, and collect points on other SDTs in the plot.

Five spherical laser scanning targets, with a diameter of 139 mm, were used to coregister the each plot's scans into a unified point cloud using the FARO SCENE 5.5 software package (FARO, 2015). The location of each target was measured with a

Trimble GeoExplorer 6000 handheld GNSS unit with a Trimble Zephyr Model 2 antenna and the coregistered point clouds were georeferenced with differentially corrected target positions using FARO SCENE.

3.2.2.3 Terrestrial Lidar Preprocessing

Following scanning procedures, coregistration, and georeferencing, the point cloud for each site consisted of an easting, northing, height, and intensity measurement (i.e., the amount of backscattered energy measured at the scanner) for each individual emitted laser pulse which resulted in a return of sufficient amplitude to be detected by the scanner. The georeferenced, plot-level point clouds were analyzed in Quick Terrain Modeler (Applied Imagery, 2009) to manually delineate and extract the individual SDTs and scale the intensity values to a uniform range of 0 – 255.

Due to the use of two different generations of terrestrial laser scanners and varying site conditions, the SDT point clouds varied in their overall quality with respect to creating solid voxel models. A high quality point cloud is one that has a very high point density and little to no occlusion, while a low quality point cloud exhibits the opposite characteristics. A visual assessment and mean nearest neighbor distance calculation (i.e., the average Euclidean distance to each point's nearest neighbor in 3D space) were used to assign a qualitative ranking of relative point cloud quality to each dataset (Table 6). The SDTs in site 3, being scanned from four positions each with the FARO TLS and having a low mean nearest neighbor distance, were assessed as high quality point clouds while the SDTs in sites 1, 2, and 4 which were each scanned from two positions each with the FARO TLS, were considered to be of medium quality.

SDTs in sites 1 and 2 which were scanned with two plot-level scans using the Leica TLS were considered to be of low quality with respect to the other point clouds due to the reduced number of scanning positions and relatively high mean nearest neighbor distance.

To increase the modelling suitability of the lower quality point clouds collected during initial observations at sites 1 and 2, they were merged with the point clouds of improved quality from the final observations to increase point density and reduce occlusion effects, in the case of SDTs which were not downed upon the final scan. The merging operations were conducted using the CloudCompare (Girardeau-Montaut, 2016) software package by first manually translating the final point cloud to align with the initial point cloud, achieving an approximate initial alignment, followed by a precise iterative closest point (ICP) alignment (Besl and McKay, 1992). In the case of stem or branch sections which were imperfectly aligned as a result of tree decay or other discrepancies between the two point clouds, care was taken to select the highest quality section available which retained a faithful representation of the SDT's initial condition and avoid errors that would be introduced by retaining duplicated, but non-spatially coincident, stem or branch sections.

3.2.2.4 Reconstructed Tree Modelling

3.2.2.4.1 Volume Estimation Algorithm Overview

The TreeVolX volume estimation algorithm, described in detail in section 2.2.5, was used to estimate the initial and final volume of each SDT with reconstructed, solid voxel models (Figure 24). The algorithm voxelizes a point cloud into a sparse voxel

model and processes individual horizontal slices of one-voxel thickness, beginning by segmenting each slice into distinct segments which represent individual branches or stem sections. Two segmentation methods are available to be selected depending on the quality and density of a point cloud. A proximity-based clustering segmentation may be selected when a point cloud is of sufficiently high quality and density and an incremental ellipse fitting segmentation may be used for point clouds which exhibit lower point density and increased occlusion effects. Each segment is then fitted with a direct least squares ellipse (Fitzgibbon et al., 1999) which is used to estimate the amount of negative voxel space along the segment's perimeter with respect to the contour of the fitted ellipse. Segments which have an adequate number of perimeter voxels to define their contour are processed with linear interpolation between each voxel to generate a closed contour form of the segment, while segments exhibiting moderate to severe occlusion are generalized to a voxelized representation of their best-fit ellipse, forming a closed contour. Each closed contour segment is then filled with interior voxels lying within its perimeter and the steps are repeated for the next horizontal voxel slice until the entire tree has been processed. The result of the algorithm is a solid voxel model reconstruction, referred to as a reconstructed tree model (RTM), of the original point cloud, whose volume is estimated by multiplying the number of voxels in the model by the volume of an individual voxel.

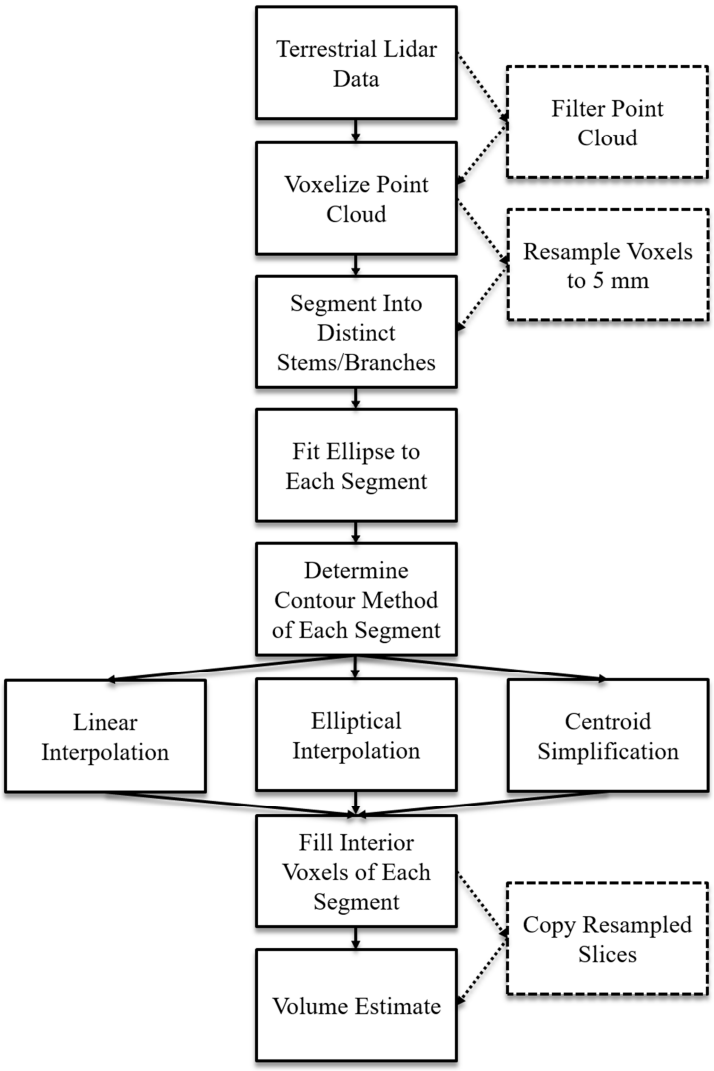

Figure 24: Flowchart of major volume estimation algorithm steps.

3.2.2.4.2 Algorithm Parameters and Modelling Description

The point cloud of each SDT was first filtered to remove noise points prior to processing with the TreeVolX algorithm. Point clouds collected with the Leica ScanStation 2 contained minimal amounts of noise and were thus filtered by manually removing erroneous points. The point clouds obtained with the phase-based FARO

Focus^{3D} X 330 were contained moderate to significant amounts of noise and were cleaned using a voxelized point density and *k*-means intensity clustering filter, described in detail in section 2.2.5.1, followed by a manual removal of remaining noise points, if necessary.

Due to the differences in point density and overall quality among the point cloud data, several options available in the TreeVolX algorithm which were designed to compensate for reduced quality point clouds were utilized. The initial scans in sites 1 and 2 were modelled using the vertical point cloud resampling (VPCR) technique, described in section 2.2.5.3, to compensate for the low point density and occlusion effects present as a result of lower scanner resolution and fewer scanner positions used for data collection. These SDT point clouds were vertically-resampled using 5 cm voxels to construct a denser point cloud which was then modelled using 5 mm voxels. Point clouds from the final scans of sites 1 and 2 and both the initial and final scans from sites 3 and 4 were not resampled and were modelled using 5 mm voxels. The final scan point clouds from sites 1 and 2, as well as all point clouds from sites 3 and 4, were modelled using 5 mm voxels and were not resampled. All point clouds, both the initial and final scans, from sites 1, 2, and 4 were segmented using the incremental ellipse segmentation method, which is well-suited for trees which were scanned from fewer than four positions and thus contain areas of intermittent occlusion or reduced point density. The initial and final scans from site 3, which were collected using four scans per tree, were segmented using the proximity-based clustering method which is appropriate for high quality point clouds (i.e., trees which have been scanned from at

least four positions at a high scanner resolution setting). Six trees were downed between the initial and final scans and were therefore unable to be scanned for a final observation. As such, two observations were possible for 23 trees while only a single observation was possible for six trees, resulting in a total of 52 RTMs, all at a 5 mm voxel size, characterizing the multitemporal observations of 29 SDTs.

3.2.3 Change Detection

Several automated change detection methodologies were implemented to detect, quantify, and characterize the structural loss of each individual SDT. These methods evaluate the multitemporal differences between each pair of initial and final RTMs and are categorized as either simple (i.e., a direct comparison of the two RTMs) or voxel-based (i.e., volumetric changes are analyzed at the voxel-level to determine whether they are truly indicative of structural loss or are a result of various potential error sources).

3.2.3.1 RTM Alignment

Due to the coordinate normalization that occurs during the voxelization process, resultant RTM pairs were often misaligned as structural losses resulted in different X and Y extents between the multitemporal scans. Each pair of RTMs corresponding to a single SDT were aligned using the CloudCompare (Girardeau-Montaut, 2016) software package. Using the RTM derived from the initial scan as the reference model, the final scan's RTM was first manually translated to achieve a rough initial alignment. CloudCompare's implementation of the ICP registration algorithm (Besl and McKay, 1992) was then used to establish the final alignment between corresponding RTM pairs with a rigid, least squares transformation.

3.2.3.2 Simple Net Structural Loss

The simple net structural loss of each SDT was estimated by calculating the difference in total volume between the initial and final RTM of each SDT. In this method, each RTM is presumed to provide an accurate and consistent reconstruction of the SDT and no additional steps were taken to detect or account for modelling errors with respect to one another.

3.2.3.3 Simple Percentile Height Bins

Percentile height bins were used to describe the locations of simple structural loss within each pair of RTMs by comparing the number of voxels present in height bins along the entire SDT. For each RTM pair, percentile height bins were calculated at 5% height increments based on the height of the initial RTM, such that each pair of RTMs was divided into 20 identical, equally sized height bins oriented along the Z axis. The volumetric change in each height bin was calculated by multiplying the difference in voxel count by the volume of an individual voxel; downed trees were treated as having zero voxels in each bin. The simple height bins illustrate where potential structural losses have occurred, as well as providing indications of potential modelling errors or other error sources (e.g., erroneous structural losses or volumetric growth detected along a SDT's main stem due to modelling errors caused by occlusion which cause minor differences in main stem size and shape).

3.2.3.4 Voxel-based Net Structural Loss

The voxel-based structural loss method consists of two primary steps: (1) a preliminary identification of potentially lost voxels from the initial RTM; and (2) an

evaluation of the potentially lost voxels to determine whether they depict actual structural loss. The aligned initial and final RTMs were first downsampled from 5 mm voxels to 5 cm voxels, providing a more generalized set of models, reducing sensitivity to minor discrepancies between the two RTMs, and reducing the number of voxel-to-voxel comparisons which were made for the sake of computational efficiency. For each voxel in the initial RTM, the 3D Euclidean distance to its nearest neighbor in the final RTM was calculated and initial RTM voxels whose nearest neighbor distance was greater than 12 cm were classified as potentially lost voxels.

Due to various potential sources of error (e.g., trees and branches shifting over time, modelling error, noise points, scanner error, and alignment error) some voxels which were classified as potentially lost may in fact still be present in the final RTM and must be identified to prevent an overestimation of volume loss. Potentially lost voxels were first clustered by applying a single-linkage hierarchical clustering procedure to the Euclidean distance matrix of the potentially lost voxels and cutting the resultant hierarchical tree at heights of 30 cm. For each cluster, the number of unique first, second, and third nearest neighbor voxels from the final RTM were calculated and averaged to roughly characterize the relationship between each potentially lost cluster and the final RTM, as clusters with many unique nearest neighbors are potentially indicative of a branch which has shifted positions between scanning observations. Clusters which had an average unique nearest neighbor count of nine voxels or fewer were considered to be truly lost, while those with an average of 10 or more unique

nearest neighbor voxels were considered to be potentially lost and subjected to further analysis.

The remaining potentially lost clusters were then assessed, with respect to the initial and final RTMs, using a combination of ICP alignments and metrics to identify actual structural losses. Clusters whose voxel count was greater than or equal to 20% of the number of voxels in the initial RTM were considered to represent structural losses of significant stem sections, as opposed to potentially shifted branches, and were omitted from the ICP alignment while being flagged as truly lost. An ICP implementation with a rigid transformation, available in the R package "Morpho" (Schlager, 2017) was then used to align each remaining distinct, potentially lost cluster with the final RTM to classify the voxels of that cluster as being truly lost or the result of a shifted branch position. To prevent the clusters from being erroneously aligned with distant branches or stems in the final RTM, three ICP alignments, each operating on the aligned cluster from the previous ICP alignment, were conducted with decreasing maximum distance thresholds (i.e., the maximum allowable distance, from a potentially lost voxel to its nearest voxel in the final RTM, to be considered a valid closest point) and an increasing number of iterations.

The first, second, and third ICP registrations were constrained with maximum distance thresholds of 30 cm, 10 cm, and 5 cm and were conducted with 1, 2, and 10 iterations, respectively. Any cluster which was unable to be aligned, due to a lack of sufficiently close voxels in the final RTM, was considered to be truly lost. Two final checks were performed to detect erroneous alignments for each cluster, such that: (1)

any aligned cluster whose mean nearest neighbor distance, with respect to its original cluster position, exceeded 75 cm was considered to be erroneously aligned and thus representing a true structural loss; and (2) any aligned cluster which had more than 2.8 times its own voxel count within a distance of 12 cm in the final RTM was considered to be erroneously aligned with a larger branch or stem and representative of a true structural loss. Any remaining aligned clusters were presumed to be properly registered with a shifted branch in the final RTM and voxels from the aligned cluster which were greater than 12 cm away from the final RTM were considered to be lost voxels. Finally, all of the 5 mm voxels from the initial RTM which corresponded to each downsampled 5 cm voxel determined to represent real structural losses were identified and summed to reach a final volume loss estimation.

3.2.3.5 Voxel-based Percentile Height Bins

Percentile height bins were also used to characterize the structural loss estimates obtained using the voxel-based methodology and provides a precise quantitative description of where, with respect to the vertical structure of a SDT, volumetric loss occurred. Each respective RTM pair was divided into the same 5% height bin intervals as defined during the simple percentile height bin approach. The 5 mm voxels from the initial RTM, which were determined to be lost by the voxel-based structural loss method, were thus used to quantify the amount of volumetric loss occurring in each 5% height bin. In the case of downed trees, for which a final RTM was not possible, the entire initial RTM was considered to represent voxel-based structural losses.

3.2.3.6 Structural Loss Rate Characterization

Structural loss rates were calculated based on the volumetric losses observed over the elapsed time between the initial and final scan of each SDT. The rate of each SDT's structural loss was determined both with respect to the net volumetric loss of the entire tree as well as within each 5% height bin. By calculating the volumetric loss rate in each height bin, variable structural loss rates, with respect to relative height within a SDT, could be calculated for the *Pinus* and *Quercus* genera.

The structural loss rate of each height bin was defined in two ways: (1) with volume loss in each height bin being calculated as a percentage of the total initial volume of the entire SDT, and (2) with volume loss in each height bin being calculated as a percentage of the initial SDT's volume in that same height bin. Each structural loss rate method was applied to the 5% height bin losses calculated with both the simple and voxel-based approaches.

3.3 Results and Discussion

Volume and structural loss estimates for each of the 29 SDTs are presented in Table 7. Height and DBH were estimated from the TLS point clouds and decay class assignments use the USFS FIA five class system (Woudenberg et al., 2010), with a class of "D" signifying a tree that was downed upon the final site visit. The average runtime per tree, to create the reconstructed tree model, was approximately 5.1 minutes, with the larger, more complex trees being slower to process than smaller, simpler trees. By visually comparing the SDT point clouds to their respective RTMs, the TreeVolX algorithm was considered to provide generally accurate volume estimations, with higher model quality being closely related to point cloud quality.

Table 7: Volume estimation and structural loss results.

SDT ID	Genus[a]	Elapsed Time (Days)	Height[I(F)] (m)	DBH[I] (cm)	Decay Class[I(F)]	Volume[I(F)] (L)	Net Volume Loss[SMP] (L)	Net Volume Loss[VB] (L)	Vol. Loss Method Diff.[b] (%)	Relative PC Quality[I(F)]
1	O	554	14.4 (0)	26.22	2 (D)	460 (0)	460	460	-	L
2	O	554	6.15 (0)	20.06	2 (D)	155 (0)	155	155	-	L
3	O	171	11.59 (10.42)	37.32	2 (2)	1844 (1828)	16	53	2	H (H)
4	O	171	14.3 (14.3)	56.49	2 (2)	2433 (2424)	9	7	0.07	H (H)
5	O	71	6.47 (2.1)	17.76	3 (4)	139 (50)	90	85	3.12	M (M)
6*	O	71	8.6 (8.59)	39.54	2 (2)	617 (619)	-2	0	0.29	M (M)
7	O	71	10.11 (10.11)	32.13	2 (2)	837 (822)	15	2	1.54	M (M)
8	O	71	9.4 (9.4)	33.44	3 (3)	600 (597)	3	9	0.99	M (M)
9	O	753	11.12 (0.82)	20.59	2 (4)	336 (34)	302	311	2.55	L (M)
10	O	753	11.75 (6.5)	22.03	2 (3)	303 (235)	69	92	7.83	L (M)
11	O	753	11.13 (9.86)	32	2 (2)	802 (795)	7	24	2.05	L (M)
12	O	753	9.93 (8.97)	31.34	2 (3)	540 (472)	67	19	8.94	L (M)
13*	O	753	7.43 (7.43)	17.86	3 (3)	156 (167)	-11	0	7.37	L (M)
14	P	588	14.45 (0)	19.82	3 (D)	258 (0)	258	258	-	L
15	P	588	7.97 (0)	19.24	3 (D)	172 (0)	172	172	-	L
16	P	588	21.58 (8.12)	26.76	1 (3)	1233 (402)	831	840	0.68	L (M)
17	P	588	21.26 (17.35)	34.92	1 (2)	1332 (1089)	244	159	6.37	L (M)
18	P	588	21.32 (21.13)	34.11	1 (2)	1814 (1103)	711	497	11.75	L (M)
19	P	588	19.52 (1.64)	27.55	2 (4)	519 (104)	415	408	1.43	L (M)
20	P	588	21.22 (18.58)	24.37	2 (3)	540 (475)	65	25	7.47	L (M)
21	P	588	22.09 (20.05)	30.4	2 (3)	867 (791)	76	14	7.18	L (M)
22	P	554	32.23 (18.99)	67.75	1 (3)	4804 (4126)	679	506	3.59	L (M)
23	P	554	32.51 (2.86)	58.55	1 (4)	3630 (453)	3177	3236	1.63	L (M)
24	P	554	22.19 (0)	45.48	2 (D)	1933 (0)	1933	1933	-	L
25	P	516	25.94 (0)	47.3	1 (D)	2396 (0)	2396	2396	-	L
26	P	516	24 (24)	45.75	2 (2)	2772 (2430)	342	45	10.72	L (M)
27	P	516	27.15 (14.76)	45.73	1 (3)	2472 (1853)	620	600	0.8	L (M)
28	P	516	28.09 (3.49)	65.36	1 (4)	3713 (118)	3595	3221	10.07	L (M)
29	P	516	26.56 (23.5)	58.15	2 (3)	3275 (2730)	546	31	15.73	L (M)

[a] O = oak, P = pine

[I] initial scan

[F] final scan

[SMP] simple structural loss method

[VB] voxel-based volume loss method

[b] volume loss method difference calculated as % of initial volume

* no structural loss

The most common modelling errors observed were incorrect segmentations due to occlusion effects in some point clouds, resulting in either void spaces where the model should have been filled or the erroneous filling of true negative spaces when tree components were in close proximity. The volume of SDT28 was initially significantly underestimated along a 12.5 m long stem section, due to severe occlusion caused by surrounding trees and understory vegetation. This RTM was manually corrected by filling the upper and lower half of the void stem area with 10 cm thick replications of the nearest correctly-modelled stem section above or below the problem area, respectively. A visual analysis of the structural losses detected using the voxel-based approach found that this technique provided more accurate volumetric loss estimations than simply calculating the difference between initial and final volume estimates for each SDT. Assessing the impact of relative point cloud quality and the associated modelling parameters designed to reduce volume estimation error in low and medium quality data, the absolute difference between each structural loss method was calculated and presented as a percentage of each SDT's initial volume.

The mean method difference values were 1.03%, 1.48%, and 5.06% for relative quality class combinations of high/high, medium/medium, and low/medium, respectively. These distinctions can be explained by both the various combinations of point cloud quality as well as the differing algorithm parameters utilized with respect to each relative quality class. Examining the high/high quality combination SDT3, the volumetric loss method difference of 2% was primarily caused by an underestimation of stem volume in the initial RTM along two sections approximately 70 cm and 50 cm in

length, respectively. This error was due to occlusion effects of nearby stems which resulted in an erroneous segmentation and subsequently left void interior spaces which should have been filled with voxels. The remaining error was mostly due to variations at the base of the stem, in the vicinity of the ground, where the final RTM contained significantly more voxels than the initial RTM. This area may be problematic in general for multitemporal comparisons as the process of extracting an individual tree from a larger point cloud on two occasions is likely to result in slightly different levels of data loss, when attempting to precisely remove ground points while retaining all of the laser returns from the target tree. Since the base of a tree stem can often take a complex shape and represent a significant amount of woody volume, small modelling errors in this region can result in significant volumetric differences when using the simple structural loss methodology.

In SDT5, an example of the medium/medium quality combination with a 3.12% volume loss method difference, the majority of the volume loss method difference was caused by the 12 cm distance threshold step in the voxel-based approach. The stem of SDT5 had snapped approximately 1.9 m above ground level, leaving a section of true structural loss along the stem unaccounted for by the voxel-based method since the voxels in the initial RTM which were within 12 cm of the remaining stem section in the final RTM were not classified as being potentially lost during the initial distance threshold step (Figure 25).

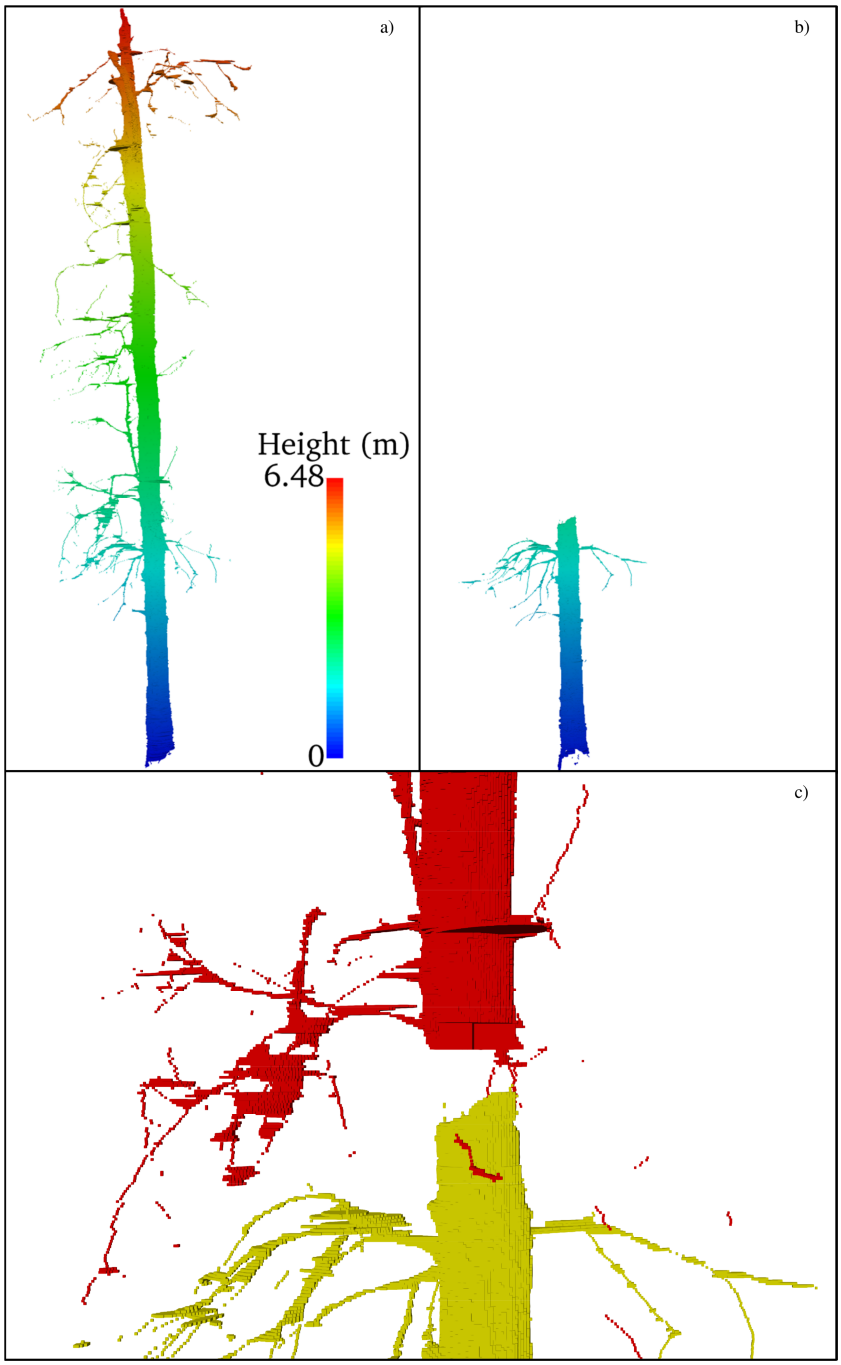

Figure 25: a) SDT5 initial RTM; b) SDT5 final RTM after stem was snapped near ground level; c) Void area between lost voxels and final RTM due to distance threshold used during change detection procedure; red – 5 mm voxels identified as structural losses using voxel-based method, yellow – SDT5 final RTM.

In the case of SDT7, another medium/medium quality combination with a method difference of 1.54%, this difference was accounted for by minor differences in occlusion effects, affecting the simple volume loss method, as well as the loss of several small branches which were too close to the stem or other branches to be classified as initial potentially lost voxels therefore underestimating the true amount of structural loss with the voxel-based method.

The volume loss method difference among the low/medium relative quality combination point clouds was mostly accounted for by the moderate to significant occlusion effects, occurring more frequently in the initial scans, and the subsequent usage of the VPCR technique to minimize the resultant modelling error of the initial RTMs. Examining the two SDTs with the largest method difference, SDT18 and SDT29, the VPCR process resulted in systematic overestimation of volume along the stem and horizontal branches. By vertically-resampling the initial SDT point clouds to compensate for occlusion effects, the initial RTMs were essentially modelled in 5 cm thick horizontal slices with 5mm voxels, tending to overestimate stem volume in comparison to the final RTMs which were modelled without VPCR using 5 mm voxels.

If a tree's stem was a perfectly vertical circular cylinder, the VPCR process would theoretically not cause any modelling errors, however, as the trees' stems vary in diameter, shape, and relative orientation with respect to the ground, the vertical-resampling process overestimates stem volume by modelling each 5 cm slice as if the points contained in that slice were all in the same horizontal Z plane and thus modelling each 5mm slice as the largest possible 5 mm slice present in that 5 cm interval. The

volumes of branches which were nearly horizontal to the ground were also susceptible to being systematically overestimated as these were modelled in increments of 5 cm thickness, naturally overestimating the volume of branches which were less than 5 cm in diameter. While these modelling discrepancies resulted in structural loss estimation errors with the simple method, the voxel-based method was generally not affected by such minor RTM differences and provided more accurate structural loss estimations for the low/medium relative quality combination point clouds (Figure 26).

The voxel-based change detection approach provided a more accurate structural loss estimation in most cases as it was generally less susceptible to classifying modelling errors as volumetric loss. For example, if a portion of a SDT's stem was left hollow due to occlusion effects in the initial RTM but was correctly filled in the final RTM, this would cause an erroneous volumetric increase using the simple change detection method. However, the voxel-based method generally avoided this type of error as the final RTM would likely have some voxels present within the distance threshold of the poorly-modelled initial RTM section, thus correctly disregarding the apparent change in volume. The generalized set of models provided by the use of 5 cm voxels, while evaluating the 12 cm distance threshold, also reduced sensitivity to minor differences in the shape and size of branch or stem sections caused by noise points, scanner error, or modelling error.

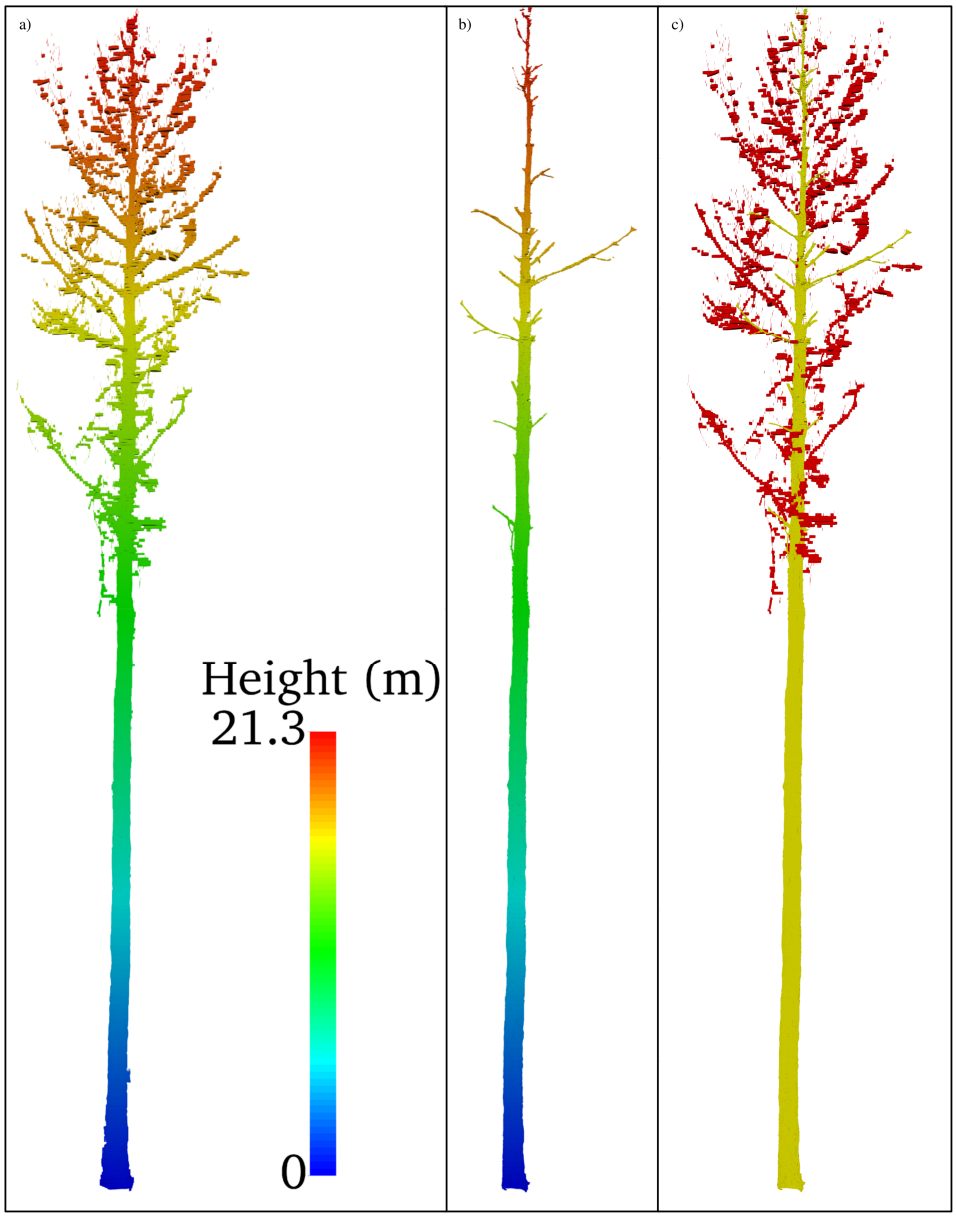

Figure 26: a) SDT18 initial RTM; b) SDT18 final RTM showing branch structural loss; c) dropped branches correctly identified while avoiding erroneous structural loss detections caused by model discrepancies; red – 5 mm voxels identified as structural losses using voxel-based method, yellow – SDT18 final RTM.

The voxel-based change detection method also allows for the identification of individual branches or stem sections that have been lost over time, which could be further analyzed in future studies, as opposed to the simple method which only estimates net volumetric loss. A hypothetical basic voxel-based method could function by directly comparing RTM pairs to identify particular voxels which were present in the initial model but absent in the final model, but in addition to an increased sensitivity to modelling error occurring with this hypothetical approach, this basic approach would also fail to account for the shifting positions of tree components as decay occurs over time. Three general forms of positional shifts were observed among the 29 SDTs: (1) branches sagging as decay progresses, (2) branch stubs rising in response to the loss of the branch's terminal end, and (3) stems leaning away from their original axis, occasionally in different directions in the case of a forked SDT. The ICP alignment procedures and associated metrics enabled the voxel-based change detection to generally avoid misclassifying shifted branches as having been lost (Figure 27).

Although the voxel-based method necessarily underestimates the volume of each lost branch in proportion to the distance threshold used, it is considered to provide a more accurate and consistent estimate in comparison to the hypothetical basic voxel-based approach which would only consider the presence or absence of each voxel without any spatial considerations.

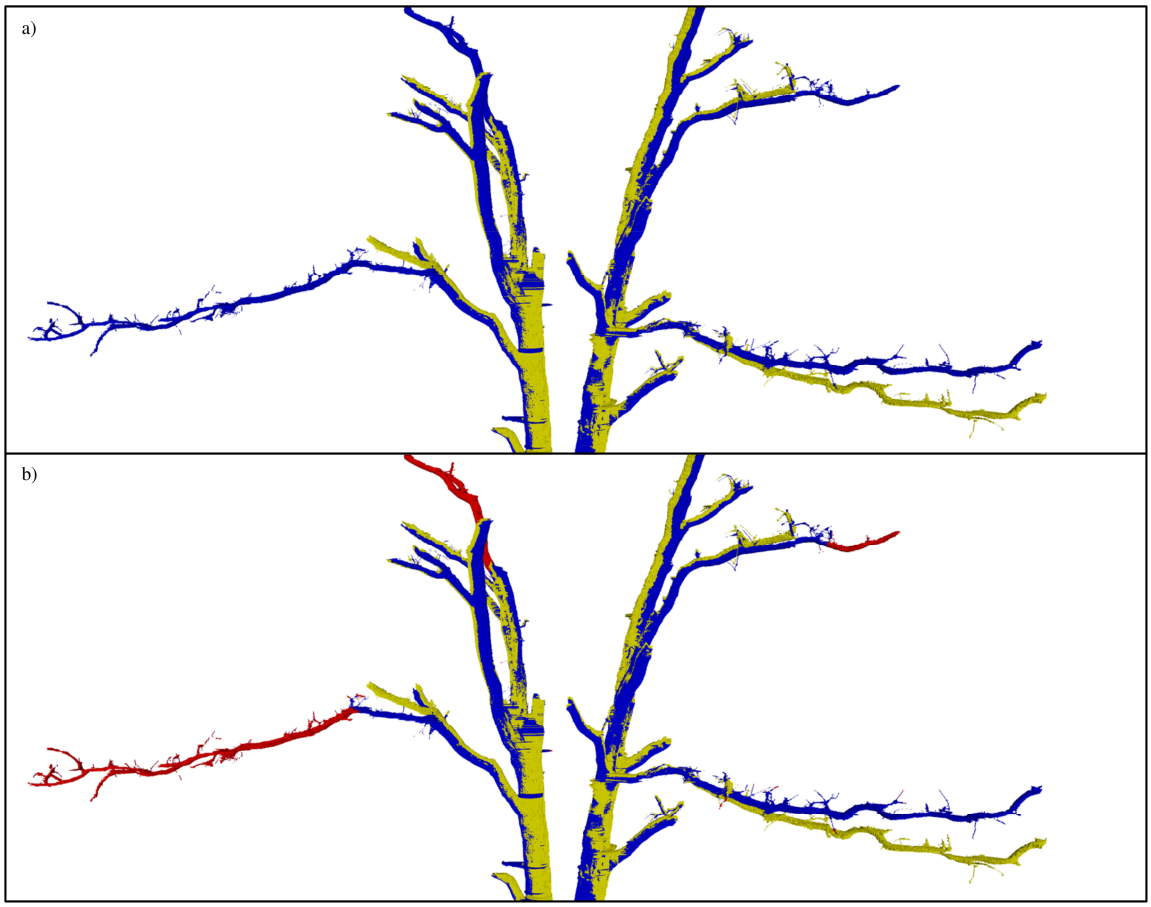

Figure 27: Example of shifting branch positions as decay progresses. a) detail of branches sagging and a branch stub rising after losing its terminal end; blue – initial RTM, yellow – final RTM; c) voxel-based structural loss method correctly identified lost branches, avoiding errors caused by branch shift; red – lost voxels.

Two oak trees, SDT6 and SDT13, did not experience any structural losses over their observation period and presented a chance to examine the repeatability of the volume estimation algorithm when applied to point clouds of structurally identical trees collected at different times. SDT6 was a medium/medium relative quality combination dataset, using the same FARO scanner for each observation with a time interval of 71

days and a net volume difference of 1.78 L and 0.0 L for the simple and voxel-based change detection methods, respectively. The erroneous volumetric increase detected using the simple method was due to occlusion effects and associated modelling errors at the base of the stem and represents a 0.29% deviation from the initial volume estimate, while the voxel-based method correctly determined that no structural losses had occurred. SDT13 was a low/medium relative quality combination dataset which was initially scanned with the Leica and finally scanned with the FARO with an elapsed time between observations of 753 days. An erroneous volume increase of 11.48 L, using the simple method, was estimated due to errors caused by minor occlusion effects and the generalizations resulting from vertically-resampling the initial point cloud, while the voxel-based method correctly estimated that no volumetric change had taken place.

The height bin analyses were aggregated by genus to investigate the potential of percentile height bins to identify and characterize structural loss patterns. The voxel-based structural loss height bins were used for analysis as they were found to provide more accurate change detection capability than the simple method. SDT5, an oak which lost approximately 85% of its volume over an elapsed time of 71 days due to a snapped stem near the ground, was excluded from the following height bin analysis as it was found to have a profound effect on the results when scaling its structural loss rate to an annual basis. It must be noted that due to the wide range of decay classes and sizes present in each genus' sample group, along with the small sample size of each genus, these height bin results are presented as an example of potential future applications of this study's methodologies. The focus of this study was the design and implementation

of detailed structural loss detection and quantification; the current height bin results are not yet considered suitable to be generalized for forestry applications until larger studies focused on this analysis may be conducted, although they offer a valuable opportunity to quantify and describe structural loss in a detailed manner. Figure 28 shows the average annual relative structural loss rate of pines and oaks in 5 % height bins, where the volume loss of each height bin was calculated as a percentage of the total volume of each SDT at the initial observation (e.g., if a particular height bin lost 10 L of volume over one year and the initial volume of the entire SDT was 800 L, this would be represented as an annual structural loss rate of 1.25% in that bin).

The average annual height bin structural loss rates are shown in Figure 29, where the volume loss of each height bin is represented as a percentage of the volume present in that same height bin as estimated in the initial RTMs (e.g., a particular height bin which had an initial volume of 100 L and a final volume of 20 L over a one year observation interval would result in an annual bin loss rate of 80%). The pines observed in this study had relative bin loss rates greater than oaks in each percentile height bin, with the exception of the 95 – 100% bin (Figure 29).

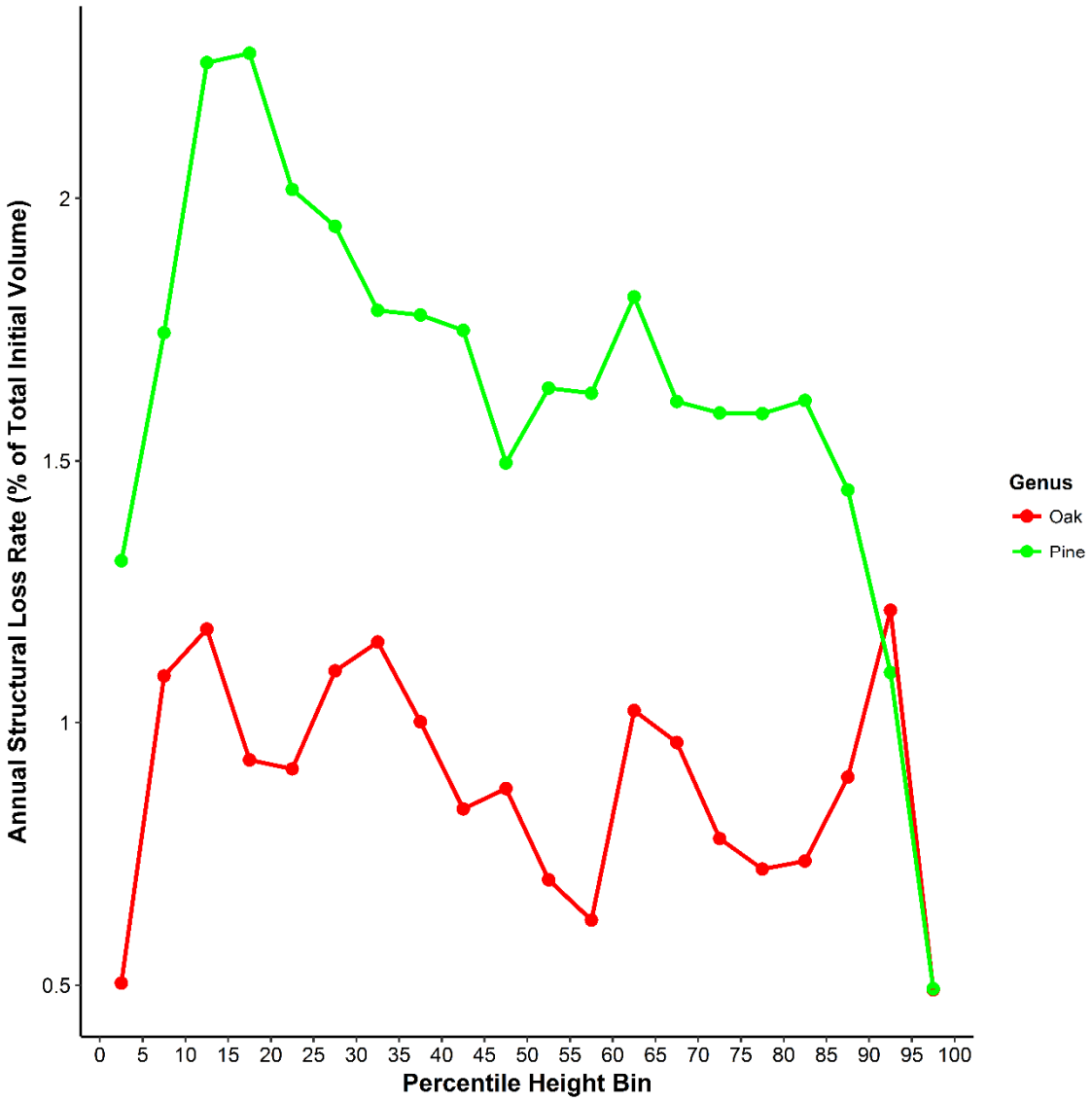

Figure 28: Average annual structural loss rates of oaks and pines detected using the voxel-based method; calculated as the mean percent volume loss in each height bin as a percentage of each tree's initial volume.

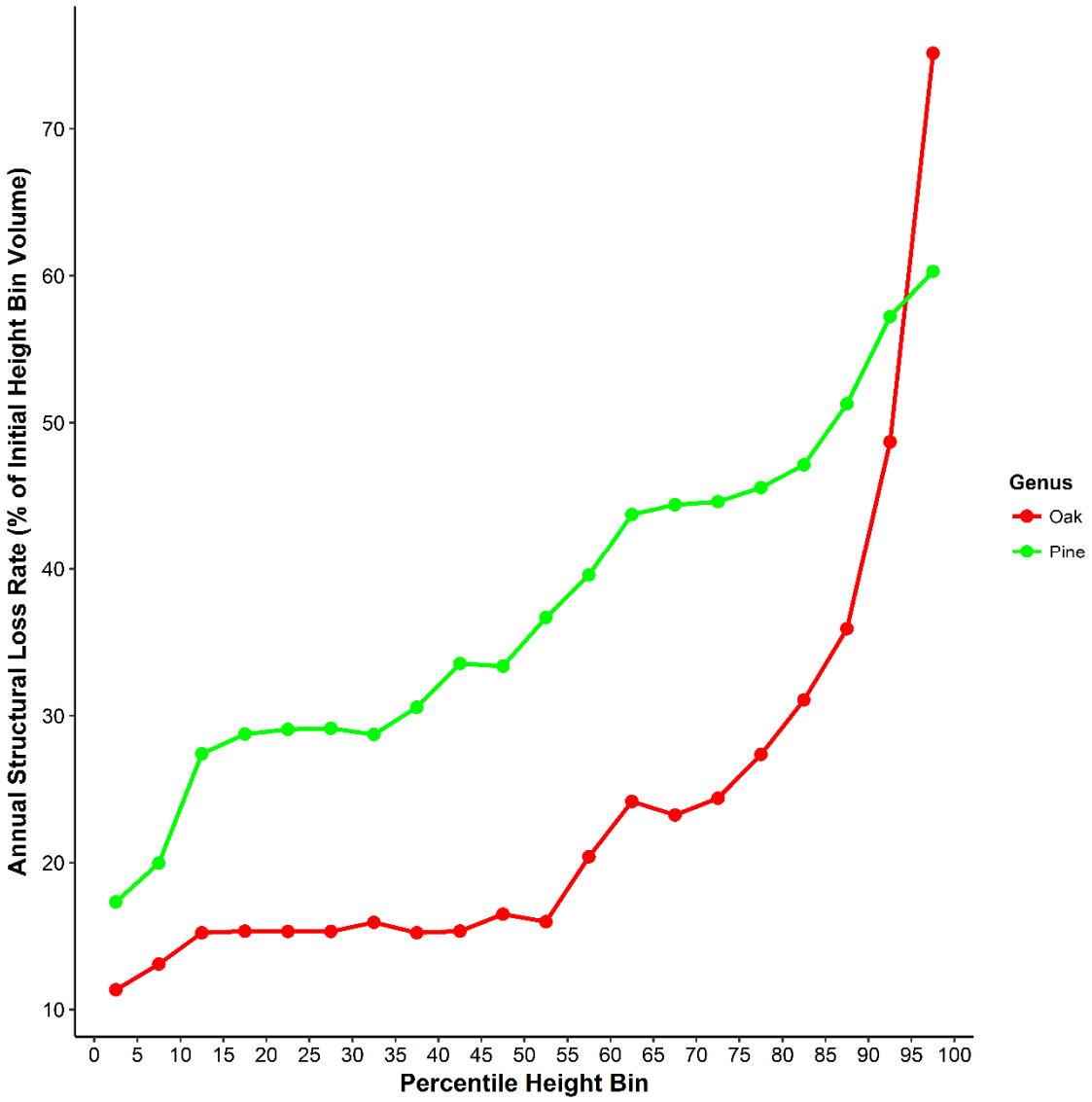

Figure 29: Average annual structural loss rates of oaks and pines detected using the voxel-based method; calculated as the mean percent volume loss in each height bin.

It is difficult to ascertain if this represents a regional trend, due to the aforementioned study limitations with regards to this height bin analysis, and may be potentially explained by a variety of factors such as the height and mass of large pines

making them more vulnerable to wind-induced stress and fragmentation, variation in site conditions between oaks and pines (e.g., soil moisture availability, occurrences of heavy storms), cause of mortality, time since mortality, variation in wood decay rates, and the effects of site conditions on tree morphology. Both oaks and pines show a generally increasing trend in the rate of relative bin structural loss with respect to increasing bin height, presumably due to branch drop in the upper crown and snapped stems. The relative bin structural loss rate of oaks tends to increase more rapidly than pines above the 70 – 75% bin, possibly due to the more complex branching structure generally observed among oaks in the upper crown area, which tend to drop prior to the tree being downed.

Based on the relative bin structural loss rates, pine and oak snags were estimated to have a mean longevity of approximately six years and nine years, respectively (Figure 30), as determined by loss rates of the lowest bin which, when completely lost, would signify a complete transition from SDT to downed woody debris. Alternatively, the longevity of each genus may be considered with respect to their observed average net structural loss rate. Pines and oaks were found to lose 32.8% and 17.7% of their initial volume per year, respectively, resulting in respective longevity estimates of 3.04 and 5.64 years.

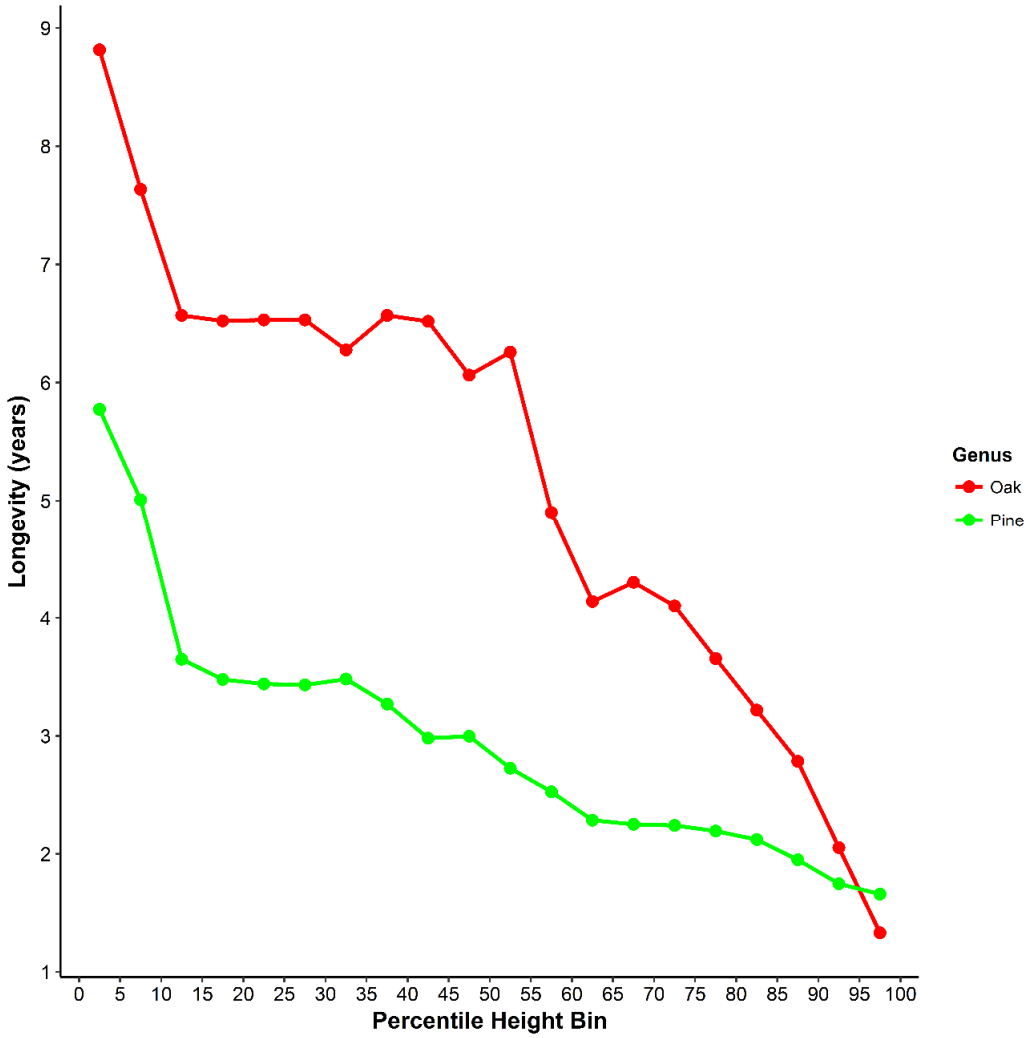

Figure 30: Average estimated longevity of oaks and pines SDTs in 5% height bins.

The discrepancy in longevity estimates was likely caused by short stumps remaining after a stem snapped near ground level, which were able to be scanned and still considered standing. A larger sample size in future studies would be needed to refine these longevity estimates. In previous studies, large loblolly pine snags (mean DBH of 49 cm) were found to have an average longevity of approximately six years in

eastern Texas (Conner and Saenz, 2005) with 15.4% of the snags still standing 10 years post-tree death. Hardwoods were found to have an average longevity of approximately five years in eastern Texas and Arkansas (Cain, 1996; Dickson et al., 1995). Harmon (1982) sampled fire-killed standing dead trees ranging from 5 – 15 cm DBH and found that *Quercus prinus* and *Quercus coccinea* both decayed more rapidly than *Pinus virginiana* and *Pinus rigida* in the southern Appalachian Mountains. The Harmon (1982) study used reductions in wood density over time to quantify rate of decay, but it is not clear if these trends in wood decay are consistent across various species and regions, nor if they are the primary driver of structural loss rates among standing dead trees. Bull and Partridge (1986) found that the longevity of *Pinus ponderosa* snags in eastern Oregon was related to the cause of mortality and Conner and Saenz (2005) observed that beetle-killed pine snags fell more rapidly than those killed by wind-snap. Although the snags observed in this study were believed to have been killed by drought stress, the severe drought conditions may have also facilitated other causes of death such as disease or insect damage (Moore et al., 2016), which may affect structural loss rates.

As the SDTs observed in this study were likely dead for three to four years prior to the initial scan, these longevity estimates are possibly underestimated since they had generally experienced structural losses prior to the first observation. Longevity estimates may also be biased depending on the true time of death for each tree as well as by survivor bias since some trees killed during the 2011 drought had likely been downed already and were thus unable to be included in this study.

Seen in Figure 28, pines in this study were observed to generally lose more volume, as a percentage of their initial total volume, in the lower height bins, while the oaks do not seem to follow a particular pattern. As softwoods tend to have a greater proportion of their volume contained in the stem, in comparison to hardwoods (Jenkins et al., 2003), the bulk of pine structural loss occurring in lower height bins is accounted for by snapped stems or downed trees, while the sporadic effect seen in the oaks may possibly be explained by variations in branching patterns among the oak sample group and the tendency for oak branches to represent a larger proportion of a tree's volume.

3.4 Conclusions

To the best of the author's knowledge, no prior studies have attempted to characterize the structural loss of SDTs in terms of quantified volumetric loss using terrestrial lidar. Several studies have investigated the longevity or transition dynamics of snags, sometimes including qualitative snag descriptions or height loss measurements (Aakala et al., 2008; Cain, 1996; Cline et al., 1980; Conner and Saenz, 2005; Corace et al., 2010; Dickson et al., 1983; Landram et al., 2002; Vanderwel et al., 2006) or estimated the decay rate of SDTs via reductions in wood density as decomposition occurs (Harmon, 1982; Krankina and Harmon, 1995) but the relationship of quantified structural loss rates to these studies is not well-documented. In this study, a novel methodology for detecting, quantifying, and characterizing the structural loss of standing dead trees was presented. Operating on voxelized reconstructed tree models created using the TreeVolX algorithm, a voxel-based change detection approach was able to provide generally more accurate change detection capabilities than simply comparing the

total volume of each respective reconstructed model pair. Height bin analyses found that pines tended to lose volume more rapidly than oaks, but significant variation among tree size and initial decay class, as well as a small sample size for each genus, make it difficult to determine if these findings may be generalized to broader forestry applications. Ideally, future studies focusing on applications of this, or similar, methodologies to estimate quantitative structural loss rates should design experiments which include larger sample sizes among DBH, height, and decay classes for each species or genus being studied and conduct multiple scans with a TLS from the time of initial mortality to a complete transition to downed woody debris. Even though successful volume and change detection estimates were possible for all combinations of relative point cloud quality in this study, future studies should strive to scan each tree from at least four positions at high resolution to maximize point cloud and RTM quality, although dense forest conditions can often make this challenging or even impossible.

The presented methodology could potentially be applied to future studies, at a species, genus, or broader level, with objectives of: estimating quantified structural loss rates, providing quantitative assessments of current qualitative decay class systems, deriving new quantitative decay class systems, assessing structural loss rates in response to various mortality events, providing precise estimates of carbon or nutrient fluxes as trees lose volume over time, assessing the effect of various environmental factors on structural loss rates, validating or implementing structural loss adjustments used in component ratio techniques for broad sampling schemes without relying on generalized allometric equations, and characterizing the morphological aspects of structural loss.

4. CONCLUSIONS

This study presents an automated voxel-based technique for accurately estimating the volume of standing dead trees with terrestrial lidar data. Using an adaptive contour interpolation approach, the method is capable of precisely modelling complex shapes with linear interpolation when a branch slice contains sufficiently dense point coverage as well as compensating for areas of occlusion or reduced point density by applying an elliptical contour generation. The incremental ellipse segmentation method offers an ability to more-accurately segment point clouds characterized by moderate, intermittent occlusion and the presented VPCR technique is capable of modelling point clouds with significant occlusion effects or consistently low point density. These features offer a robust solution to estimating the volume of standing dead trees as dense forest systems present a challenging scanning environment with respect to the objective of collecting very high quality point clouds.

Although this study focused on modelling standing dead trees, the volume estimation method is expected to provide similar results when applied to live trees scanned in leaf-off conditions. With the addition of a foliage filtering step, it could also presumably be applicable to live trees in leaf-on condition, although the presence of leaves may cause significant levels of occlusion with regards to laser returns from the tree's woody structure, leaving some branches difficult or impossible to model accurately and increasing the overall error of volume estimation. With the inclusion of density measurements or species-specific parameter estimates, accurate volume estimations could be used to estimate biomass, carbon content, or other biogeochemical

parameters of interest. The voxel-based modelling technique also facilitates accurate volume estimations of individual tree components, as branches or other areas of interest may be manually extracted from the reconstructed tree models and estimated by simply multiplying the number of voxels present by the volume of an individual voxel. Other potential applications of this modelling technique include evaluating or refining allometric equations, particularly with respect to standing dead trees in various states of decay, conducting change detection analysis to precisely monitor the decay or growth of individual trees over time, using TLS to validate or calibrate regional biomass estimations, and the automated estimation of morphological tree parameters.

Future volume estimation studies could focus on developing techniques to reduce the overall error of volume estimation, further refining methods intended to minimize errors caused by imperfect point clouds, testing the presented method on additional tree species, and investigating the potential to model individual tree point clouds derived from unmanned aerial systems lidar sensors or structure from motion techniques.

To the best of the author's knowledge, no prior studies have attempted to characterize the structural loss of SDTs in terms of quantified volumetric loss using terrestrial lidar. Several studies have investigated the longevity or transition dynamics of snags, sometimes including qualitative snag descriptions or height loss measurements (Aakala et al., 2008; Cain, 1996; Cline et al., 1980; Conner and Saenz, 2005; Corace et al., 2010; Dickson et al., 1983; Landram et al., 2002; Vanderwel et al., 2006) or estimated the decay rate of SDTs via reductions in wood density as decomposition occurs (Harmon, 1982; Krankina and Harmon, 1995) but the relationship of quantified

structural loss rates to these studies is not well-documented. In this study, a novel methodology for detecting, quantifying, and characterizing the structural loss of standing dead trees was presented. Operating on voxelized reconstructed tree models created using the TreeVolX algorithm, a voxel-based change detection approach was able to provide generally more accurate change detection capabilities than simply comparing the total volume of each respective reconstructed model pair. Height bin analyses found that pines tended to lose volume more rapidly than oaks, but significant variation among tree size and initial decay class, as well as a small sample size for each genus, make it difficult to determine if these findings may be generalized to broader forestry applications. Ideally, future studies focusing on applications of this, or similar, methodologies to estimate quantitative structural loss rates should design experiments which include larger sample sizes among DBH, height, and decay classes for each species or genus being studied and conduct multiple scans with a TLS from the time of initial mortality to a complete transition to downed woody debris. Even though successful volume and change detection estimates were possible for all combinations of relative point cloud quality in this study, future studies should strive to scan each tree from at least four positions at high resolution to maximize point cloud and RTM quality, although dense forest conditions can often make this challenging or even impossible.

The presented change detection methodology could potentially be applied to future studies, at a species, genus, or broader level, with objectives of: estimating quantified structural loss rates, providing quantitative assessments of current qualitative decay class systems, deriving new quantitative decay class systems, assessing structural

loss rates in response to various mortality events, providing precise estimates of carbon or nutrient fluxes as trees lose volume over time, assessing the effect of various environmental factors on structural loss rates, validating or implementing structural loss adjustments used in component ratio techniques for broad sampling schemes without relying on generalized allometric equations, and characterizing the morphological aspects of structural loss.

REFERENCES

Aakala, T., Kuuluvainen, T., Gauthier, S., & De Grandpré, L. (2008). Standing dead trees and their decay-class dynamics in the northeastern boreal old-growth forests of Quebec. *Forest Ecology and Management, 255*(3), 410-420.

Anderson, J. E., Plourde, L. C., Martin, M. E., Braswell, B. H., Smith, M.-L., Dubayah, R. O., . . . Blair, J. B. (2008). Integrating waveform lidar with hyperspectral imagery for inventory of a northern temperate forest. *Remote Sensing of Environment, 112*(4), 1856-1870.

Applied Imagery. (2009). Quick Terrain Modeler (Version 6.2) [computer software]. Chevy Chase, MD: Applied Imagery,.

Aschoff, T., Thies, M., & Spiecker, H. (2004). Describing forest stands using terrestrial laser-scanning. *International Archives of Photogrammetry, Remote Sensing and Spatial Information Sciences, 35*(5), 237-241.

Baddeley, A., Rubak, E., & Turner, R. (2015). Spatial Point Patterns: Methodology and Applications with R [Software]. London, England: Chapman and Hall/CRC Press. Available from http://www.crcpress.com/Spatial-Point-Patterns-Methodology-and-Applications-with-R/Baddeley-Rubak-Turner/9781482210200/.

Besl, P. J., & McKay, N. D. (1992). *Method for registration of 3-D shapes.* Paper presented at the Robotics-DL tentative.

Bienert, A., Hess, C., Maas, H., & von Oheimb, G. (2014). A voxel-based technique to estimate the volume of trees from terrestrial laser scanner data. *The International*

Archives of Photogrammetry, Remote Sensing and Spatial Information Sciences, 40(5), 101.

Brown, S., Gillespie, A. J., & Lugo, A. E. (1989). Biomass estimation methods for tropical forests with applications to forest inventory data. *Forest science, 35*(4), 881-902.

Bull, E. L., & Partridge, A. D. (1986). Methods of killing trees for use by cavity nesters. *Wildlife Society Bulletin (1973-2006), 14*(2), 142-146.

Cain, M. D. (1996). Hardwood snag fragmentation in a pine-oak forest of southeastern Arkansas. *American Midland Naturalist*, 72-83.

Cifuentes, R., Van der Zande, D., Salas, C., Farifteh, J., & Coppin, P. (2014). Correction of erroneous lidar measurements in artificial forest canopy experimental setups. *Forests, 5*(7), 1565-1583.

Cline, S. P., Berg, A. B., & Wight, H. M. (1980). Snag characteristics and dynamics in Douglas-fir forests, western Oregon. *The Journal of Wildlife Management*, 773-786.

Conner, R. N., & Saenz, D. (2005). The longevity of large pine snags in eastern Texas. *Wildlife Society Bulletin, 33*(2), 700-705.

Corace, R. G., Seefelt, N. E., Goebel, P. C., & Shaw, H. L. (2010). Snag longevity and decay class development in a recent jack pine clearcut in Michigan. *Northern Journal of Applied Forestry, 27*(4), 125-131.

Cornwell, W. K., Cornelissen, J. H., Allison, S. D., Bauhus, J., Eggleton, P., Preston, C. M., . . . Zanne, A. E. (2009). Plant traits and wood fates across the globe: rotted, burned, or consumed? *Global Change Biology, 15*(10), 2431-2449.

Côté, J.-F., Widlowski, J.-L., Fournier, R. A., & Verstraete, M. M. (2009). The structural and radiative consistency of three-dimensional tree reconstructions from terrestrial lidar. *Remote Sensing of Environment, 113*(5), 1067-1081.

Dassot, M., Colin, A., Santenoise, P., Fournier, M., & Constant, T. (2012). Terrestrial laser scanning for measuring the solid wood volume, including branches, of adult standing trees in the forest environment. *Computers and Electronics in Agriculture, 89*, 86-93.

Dassot, M., Constant, T., & Fournier, M. (2011). The use of terrestrial LiDAR technology in forest science: application fields, benefits and challenges. *Annals of Forest Science, 68*(5), 959-974.

Delagrange, S., & Rochon, P. (2011). Reconstruction and analysis of a deciduous sapling using digital photographs or terrestrial-LiDAR technology. *Annals of botany, 108*(6), 991-1000.

Dickson, J. G., Conner, R. N., & Williamson, J. H. (1983). Snag retention increases bird use of a clear-cut. *The Journal of Wildlife Management, 47*, 799-804.

Dickson, J. G., Williamson, J. H., & Conner, R. N. (1995). *Longevity and bird use of hardwood snags created by herbicides.* Paper presented at the Proceedings of the Annual Conference of the Southeastern Association of Fish and Wildlife Agencies.

Domke, G. M., Woodall, C. W., & Smith, J. E. (2011). Accounting for density reduction and structural loss in standing dead trees: Implications for forest biomass and carbon stock estimates in the United States. *Carbon Balance and Management, 6*(1), 14.

Dowle, M., & Srinivasan, A. (2017). data.table: Extension of `data.frame`. R package version 1.10.4 [Software]: Available from https://CRAN.R-project.org/package=data.table.

Drake, J. B., Dubayah, R. O., Clark, D. B., Knox, R. G., Blair, J. B., Hofton, M. A., . . . Prince, S. (2002). Estimation of tropical forest structural characteristics using large-footprint lidar. *Remote Sensing of Environment, 79*(2), 305-319.

FARO. (2013). FARO Laser Scanner Focus3D X 330^{3D} Product Specifications. Lake Mary, FL: FARO.

FARO. (2015). FARO Scene (Version 5.5) [computer software]. Lake Mary, FL: FARO.

Fitzgibbon, A., Pilu, M., & Fisher, R. B. (1999). Direct least square fitting of ellipses. *IEEE Transactions on pattern analysis and machine intelligence, 21*(5), 476-480.

Fraver, S., Milo, A. M., Bradford, J. B., D'Amato, A. W., Kenefic, L., Palik, B. J., . . . Brissette, J. (2013). Woody debris volume depletion through decay: implications for biomass and carbon accounting. *Ecosystems, 16*(7), 1262-1272.

Gama, J., & Chernov, N. (2015). conicfit: Algorithms for Fitting Circles, Ellipses and Conics Based on the work by Prof. Nikolai Chernov. R package version 1.0.4 [Software]: Available from https://CRAN.R-project.org/package=conicfit.

Garber, S. M., Brown, J. P., Wilson, D. S., Maguire, D. A., & Heath, L. S. (2005). Snag longevity under alternative silvicultural regimes in mixed-species forests of central Maine. *Canadian Journal of Forest Research, 35*(4), 787-796.

Girardeau-Montaut, D. (2016). CloudCompare (Version 2.8) [Software]. Available from http://www.cloudcompare.org.

Guo, Z., Chi, H., & Sun, G. (2010). Estimating forest aboveground biomass using HJ-1 Satellite CCD and ICESat GLAS waveform data. *Science China Earth Sciences, 53*, 16-25.

Hackenberg, J. (2015). *Group 1 Branches [Data file]*.

Hackenberg, J., Morhart, C., Sheppard, J., Spiecker, H., & Disney, M. (2014). Highly accurate tree models derived from terrestrial laser scan data: A method description. *Forests, 5*(5), 1069-1105.

Harmon, M. E. (1982). Decomposition of standing dead trees in the southern Appalachian Mountains. *Oecologia, 52*(2), 214-215.

Harmon, M. E., Cromack Jr, K., & Smith, B. G. (1987). Coarse woody debris in mixed-conifer forests, Sequoia National Park, California. *Canadian Journal of Forest Research, 17*(10), 1265-1272.

Hoerling, M., Kumar, A., Dole, R., Nielsen-Gammon, J. W., Eischeid, J., Perlwitz, J., . . . Chen, M. (2013). Anatomy of an extreme event. *Journal of Climate, 26*(9), 2811-2832.

Hopkinson, C., Chasmer, L., Young-Pow, C., & Treitz, P. (2004). Assessing forest metrics with a ground-based scanning lidar. *Canadian Journal of Forest Research, 34*(3), 573-583.

Hosoi, F., Nakai, Y., & Omasa, K. (2013). 3-D voxel-based solid modeling of a broad-leaved tree for accurate volume estimation using portable scanning lidar. *ISPRS Journal of photogrammetry and remote sensing, 82*, 41-48.

Hosoi, F., & Omasa, K. (2006). Voxel-based 3-D modeling of individual trees for estimating leaf area density using high-resolution portable scanning lidar. *IEEE transactions on geoscience and remote sensing, 44*(12), 3610-3618.

Hudak, A. T., Strand, E. K., Vierling, L. A., Byrne, J. C., Eitel, J. U., Martinuzzi, S., & Falkowski, M. J. (2012). Quantifying aboveground forest carbon pools and fluxes from repeat LiDAR surveys. *Remote Sensing of Environment, 123*, 25-40.

Hyyppä, J., Schardt, M., Haggrén, H., Koch, B., Lohr, U., Scherrer, H., . . . Hyyppä, H. (2001). HIGH-SCAN: The first European-wide attempt to derive single-tree information from laserscanner data. *The Photogrammetric Journal of Finland, 17*(2), 58-68.

Jenkins, J. C., Chojnacky, D. C., Heath, L. S., & Birdsey, R. A. (2003). National-scale biomass estimators for United States tree species. *Forest science, 49*(1), 12-35.

Kaasalainen, S., Hyyppä, J., Karjalainen, M., Krooks, A., Lyytikäinen-Saarenmaa, P., Holopainen, M., & Jaakkola, A. (2010). Comparison of terrestrial laser scanner and synthetic aperture radar data in the study of forest defoliation. *International*

Archives of Photogrammetry, Remote Sensing and Spatial Information Sciences, 38(7A), 82-87.

Kaasalainen, S., Krooks, A., Liski, J., Raumonen, P., Kaartinen, H., Kaasalainen, M., . . . Mäkipää, R. (2014). Change detection of tree biomass with terrestrial laser scanning and quantitative structure modelling. *Remote Sensing, 6*(5), 3906-3922.

Krankina, O. N., & Harmon, M. E. (1995). Dynamics of the dead wood carbon pool in northwestern Russian boreal forests. In M. J. Apps, D. T. Price, & J. Wisniewski (Eds.), *Boreal Forests and Global Change* (pp. 227-238). Dordrecht, Netherlands: Springer.

Ku, N.-W., Popescu, S. C., Ansley, R. J., Perotto-Baldivieso, H. L., & Filippi, A. M. (2012). Assessment of available rangeland woody plant biomass with a terrestrial LIDAR system. *Photogrammetric Engineering & Remote Sensing, 78*(4), 349-361.

Laiho, R., & Prescott, C. E. (2004). Decay and nutrient dynamics of coarse woody debris in northern coniferous forests: a synthesis. *Canadian Journal of Forest Research, 34*(4), 763-777.

Landram, F. M., Laudenslayer Jr, W. F., & Atzet, T. (2002). *Demography of snags in eastside pine forests of California.* (Gen. Tech. Rep. PSW-GTR-181). Albany, CA: U.S. Department of Agriculture, Forest Service, Pacific Southwest Research Station.

Lefsky, M., & McHale, M. (2008). Volume estimates of trees with complex architecture from terrestrial laser scanning. *Journal of Applied Remote Sensing, 2*(1), 023521.

Lefsky, M. A., Cohen, W. B., Parker, G. G., & Harding, D. J. (2002). Lidar remote sensing for ecosystem studies. *BioScience, 52*(1), 19-30.

Lefsky, M. A., Harding, D. J., Keller, M., Cohen, W. B., Carabajal, C. C., Del Bom Espirito-Santo, F., . . . de Oliveira, R. (2005). Estimates of forest canopy height and aboveground biomass using ICESat. *Geophysical research letters, 32*(22).

Leica Geosystems. (2006). Leica ScanStation 2 Product Specifications. Heerbrugg, Switzerland: Leica Geosystems.

Leica Geosystems. (2012). Leica Cyclone (Version 9.0) [computer software]. Heerbrugg, Switzerland: Leica Geosystems.

Litkey, P., Liang, X., Kaartinen, H., Hyyppä, J., Kukko, A., & Holopainen, M. (2008). Single-scan TLS methods for forest parameter retrieval. *Proceedings of SilviLaser, 2008*, 8th.

MacQueen, J. (1967). *Some methods for classification and analysis of multivariate observations.* Paper presented at the Proceedings of the fifth Berkeley symposium on mathematical statistics and probability.

McKinley, D. C., Ryan, M. G., Birdsey, R. A., Giardina, C. P., Harmon, M. E., Heath, L. S., . . . Murray, B. C. (2011). A synthesis of current knowledge on forests and carbon storage in the United States. *Ecological Applications, 21*(6), 1902-1924.

Moore, G. W., Edgar, C. B., Vogel, J. G., Washington-Allen, R. A., March, R. G., & Zehnder, R. (2016). Tree mortality from an exceptional drought spanning mesic to semiarid ecoregions. *Ecological Applications, 26*(2), 602-611.

Moskal, L. M., & Zheng, G. (2011). Retrieving forest inventory variables with terrestrial laser scanning (TLS) in urban heterogeneous forest. *Remote Sensing, 4*(1), 1-20.

Næsset, E. (1999). Decomposition rate constants of Picea abies logs in southeastern Norway. *Canadian Journal of Forest Research, 29*(3), 372-381.

Penman, J., Gytarsky, M., Hiraishi, T., Krug, T., Kruger, D., Pipatti, R., . . . Wagner, F. (Eds.). (2003). *Good practice guidance for land use, land-use change and forestry*. Kanagawa, Japan: IPCC National Greenhouse Gas Inventories Programme and Institute for Global Environmental Strategies. available at: http://www.ipcc-nggip.iges.or.jp/public/gpglulucf/gpglulucf_contents.htm.

Popescu, S. C. (2007). Estimating biomass of individual pine trees using airborne lidar. *Biomass and Bioenergy, 31*(9), 646-655.

Popescu, S. C., Wynne, R. H., & Nelson, R. F. (2003). Measuring individual tree crown diameter with lidar and assessing its influence on estimating forest volume and biomass. *Canadian journal of remote sensing, 29*(5), 564-577.

Pueschel, P. (2013). The influence of scanner parameters on the extraction of tree metrics from FARO Photon 120 terrestrial laser scans. *ISPRS Journal of photogrammetry and remote sensing, 78*, 58-68.

R Core Team. (2016). R: A language and environment for statistical computing. Vienna, Austria: R Foundation for Statistical Computing. Available from https://www.R-project.org/.

Raumonen, P., Kaasalainen, M., Åkerblom, M., Kaasalainen, S., Kaartinen, H., Vastaranta, M., . . . Lewis, P. (2013). Fast automatic precision tree models from terrestrial laser scanner data. *Remote Sensing, 5*(2), 491-520.

Russell, M. B., Fraver, S., Aakala, T., Gove, J. H., Woodall, C. W., D'Amato, A. W., & Ducey, M. J. (2015). Quantifying carbon stores and decomposition in dead wood: A review. *Forest Ecology and Management, 350*, 107-128.

Schlager, S. (2017). Morpho and Rvcg - Shape Analysis in R [Software]. In G. Zheng, S. Li, & G. Szekely (Eds.), *Statistical Shape and Deformation Analysis* (pp. 217-265). London, England: Academic Press.

Shan, J., & Toth, C. K. (Eds.). (2008). *Topographic laser ranging and scanning: principles and processing*. Boca Raton, FL: CRC press.

Sheridan, R. D., Popescu, S. C., Gatziolis, D., Morgan, C. L., & Ku, N.-W. (2014). Modeling forest aboveground biomass and volume using airborne LiDAR metrics and forest inventory and analysis data in the Pacific Northwest. *Remote Sensing, 7*(1), 229-255.

Simard, M., Pinto, N., Fisher, J. B., & Baccini, A. (2011). Mapping forest canopy height globally with spaceborne lidar. *Journal of Geophysical Research: Biogeosciences, 116*(G4).

Srinivasan, S., Popescu, S. C., Eriksson, M., Sheridan, R. D., & Ku, N.-W. (2014). Multi-temporal terrestrial laser scanning for modeling tree biomass change. *Forest Ecology and Management, 318*, 304-317.

Tansey, K., Selmes, N., Anstee, A., Tate, N., & Denniss, A. (2009). Estimating tree and stand variables in a Corsican Pine woodland from terrestrial laser scanner data. *International Journal of Remote Sensing, 30*(19), 5195-5209.

Trimble. (2010). Sunnyvale, CA: Trimble. available at: http://www.trimble.com.

Van Leeuwen, M., & Nieuwenhuis, M. (2010). Retrieval of forest structural parameters using LiDAR remote sensing. *European Journal of Forest Research, 129*(4), 749-770.

Vanderwel, M. C., Malcolm, J. R., & Smith, S. M. (2006). An integrated model for snag and downed woody debris decay class transitions. *Forest Ecology and Management, 234*(1), 48-59.

Vonderach, C., Voegtle, T., & Adler, P. (2012). Voxel-based approach for estimating urban tree volume from terrestrial laser scanning data. *International Archives of Photogrammetry, Remote Sensing and Spatial Information Sciences, 39*, 451-456.

Wehr, A., & Lohr, U. (1999). Airborne laser scanning—an introduction and overview. *ISPRS Journal of photogrammetry and remote sensing, 54*(2), 68-82.

Woudenberg, S. W., Conkling, B. L., O'Connell, B. M., LaPoint, E. B., Turner, J. A., & Waddell, K. L. (2010). *The Forest Inventory and Analysis Database: Database description and users manual version 4.0 for Phase 2*. (Gen. Tech. Rep. RMRSGTR-245). Fort Collins, CO: U.S. Department of Agriculture, Forest Service, Rocky Mountain Research Station.

Yao, T., Yang, X., Zhao, F., Wang, Z., Zhang, Q., Jupp, D., . . . Ni-Meister, W. (2011). Measuring forest structure and biomass in New England forest stands using Echidna ground-based lidar. *Remote Sensing of Environment, 115*(11), 2965-2974.

Zell, J., Kändler, G., & Hanewinkel, M. (2009). Predicting constant decay rates of coarse woody debris—a meta-analysis approach with a mixed model. *Ecological Modelling, 220*(7), 904-912.